In vivo Antimalarial Activity of the Hydroalcoholic Extract of Rhizomes of *Kniphofia foliosa* Hochst and *Kniphofia insignis* Rendle and their Constituents

BY: Yonatan Alebachew

Addis Ababa, Ethiopia

March, 2021

Addis Ababa University

School of Graduate Studies

This is to certify that the thesis prepared by Yonatan Alebachew, entitled: "*In vivo* Antimalarial Activity of the Hydroalcoholic Extract of Rhizomes of *Kniphofia foliosa* Hochst and *Kniphofia insignis* Rendle and their Constituents" and sub-mitted in partial fulfillment of the requirements for the Degree of Master of Science (Pharmacognosy) complies with the regulations of the University and meets the accepted standards with respect to originality and quality.

Signed by the Examining Committee:

External examiner: Dr. Workineh Shibeshi	Signature_____	Date_____
Internal examiner: Mr. Biniam Paulos	Signature_____	Date_____
Professor Kaleab Asres (Advisor)	Signature_____	Date_____
Dr. Daniel Bisrat (Advisor)	Signature_____	Date_____

Chair of Department or Graduate Program Coordinator

Abstract

***In vivo* Antimalarial Activity of the Hydroalcoholic Extract of Rhizomes of *Kniphofia foliosa* Hochst and *Kniphofia insignis* Rendle and their Constituents**

Yonatan Alebachew

Malaria is a major public health problem that affects millions of people. The widespread emergence of antimalarial drug-resistant *Plasmodium* strains especially the recent emergence of artemisinin resistance poses a great challenge in future prevention and control of malaria. As a result, there is an urgent need to discover new, safe, and effective antimalarial drugs with novel mechanisms of action. In this regard, traditional medicinal plants have paramount importance as seen in the discovery of the forefront antimalarials. *Kniphofia foliosa* Hochst and *Kniphofia insignis* Rendle are endemic Ethiopian plants traditionally used to treat malaria in different parts of the country. In the present study the 80% methanol rhizome extracts of both plants and some of their constituents were investigated for their antimalarial activity.

Fractionation of the hydroalcoholic extract of *K. foliosa* followed by preparative thin layer chromatography (PTLC) led to the isolation knipholone**,** dianellin, 10-knipholone gentibioside and 12-hydroxypentadec-9-en-1-yl methyl phthalate (HPMP) identified on the basis of spectroscopic (ESI-MS, 1D and 2D-NMR) data. Similarly, knipholone was isolated for the first time from crude phenolic fraction of *K. insignis*. The hydroalcoholic extracts of both plants, the phenolic fractions from *K. foliosa* and the compounds isolated thereof showed *in vivo* antiplasmodial activity ($p<0.001$) in Peters' 4-day suppressive test against *P. berghi* infected Swiss albino mice. Particularly, the hydroalcoholic extract of *K. foliosa* (400 mg/kg), 10-knipholone gentibioside (100 mg/kg) and knipholone (200 mg/kg) showed the highest activity with chemosuppression values of 61.52, 79.00 and 60.16%, respectively. From the dose-response

plot, the median effective (ED_{50}) doses of 10-knipholone gentibioside**,** knipholone and dianellin were determined to be 29.04, 81.25 and 92.31 mg/kg, respectively. Molecular docking study revealed that knipholone had a strong binding affinity to *Plasmodium falciparum* l-lactate dehydrogenase (pfLDH) target. Results of the current study showed that the extracts and compounds of the plants possess genuine *in vivo* antimalarial effect against *P. berghei* in mice, supporting their traditional use for the treatment of malaria.

Acknowledgments

First and foremost, I thank almighty God and our Mother of Perpetual help for being my strength.

My deepest gratitude go to my advisors Prof. Kaleab Asres and Dr. Daniel Bisrat for their invaluable advice, support, guidance throughout this work; and for facilitating the NMR and mass measurements of the compounds.

I would like to thank Dr. Solomon Tadesse and South Australia University for the NMR and mass data of YKFM-2; Prof. Sebsibe Demisew and Mr. Melaku Wondafrash for authentication of the expermental plants; Mr. Habtamu Kifle for allowing me to use a freeze drier and facilitating the NMR measurements; Mr. Solomon Tesfaye for initially showing the *in vivo* antimalarial assay techniques.

I would also like to acknowledge Addis Ababa University for sponsoring the study; Ethiopian Health Nutrition and Research Institute (EHNRI) for providing the donor mice and selling some of the experimental mice; and Rift Valley Health Science College for the kind gift of some of the experimental mice.

I would extend my heartfelt thanks to Mr. Hailemeskel Meshesha, Mrs. Hagere and Mr. Mola Wale.

Finally, I am also very much grateful to my family; friends; staff members of the Department of Pharmacognosy for all their assistance. The Department of Pharmaceutics and Social Pharmacy is also acknowledged for providing me with pure chloroquine.

Manuscript prepared and published in Malaria Journal.

Yonatan Alebachew, Daniel Bisrat, Solomon Tadesse, Kaleab Asres. *In vivo* anti-malarial activity of the hydroalcoholic extract of rhizomes of *Kniphofia foliosa* and its constituents. Malaria Journal. 2021;20:3.

Contents

Abstract……..……ii

Acknowledgments..... v

List of Figures..... x

List of Tables xiii

List of Acronyms xiv

1. Introduction..... 1

1.1 Malaria……...1

1.1.1 Malaria parasites and their transmission..... 1

1.1.2 Life cycle 3

1.1.3 Epidemiology..... 5

1.2 Natural products…….6

1.3 The genus *Kniphofia*……..8

1.3.1 Description..... 8

1.3.2 Distribution 9

1.3.3 Ethnobotanical use..... 9

1.3.4 Phytochemistry 10

1.3.5 Pharmacological activities..... 12

1.4 *Kniphofia foliosa* Hochst and *Kniphofia insignis* Rendle 13

1.4.1 Description and distribution..... 13

1.4.2 Ethnobotanical uses, chemistry, and pharmacological reports 14

1.5 Statement of the problem…….14

2 Objectives 16

2.1 General objective…….16

2.2 Specific objectives……...……16

3 Materials and methods 17

3.1 Materials……..17

3.1.1 Chemicals and reagents..... 17

3.1.2 Instruments..... 17

3.2 Methods……18

3.2.1 Plant collection..... 18

3.2.2 Extraction, fractionation and isolation..... 18

3.2.3 Experimental animals and rodent parasite 22

3.2.4 Acute oral toxicity testing..... 23

3.2.5 *In vivo* antimalarial assay..... 24

3.2.6 Molecular docking study..... 26

3.2.7 Statistical analysis..... 26

4 Results and Discussion 27

4.1 TLC chromatogram of the compounds…….....27

4.2 Structural elucidation compounds 1-4…….29

4.3 Structural elucidation compound 5……..38

4.4 Acute toxicity……...38

4.5 Antimalarial activity of the extracts of *K. folosia* and *K. insignis*……...39

4.6 Antimalarial activity of the phenol fractions and compounds isolated from *K. foliosa*……..41

4.7 Molecular docking study……..48

5 Conclusion 56

6 Recommendations..... 57

References..... 58

Appendices..... 74

Appendix I: ^{1}H, ^{13}C, DEPT and ESIMS of dianellin..... 74

Appendix II: ^{1}H, ^{13}C, DEPT and ESIMS of knipholone isolated from *K. foliosa* 78

Appendix III: ^{1}H and ESIMS of 10- knipholone gentibioside 83

Appendix IV: ^{1}H, ^{13}C, DEPT and ESIMS of 12-hydroxypentadec-9-en-1-yl methyl phthalate .. 87

Appendix V: ^{1}H and ESIMS of knipholone isolated from *K. insignis* 90

Appendix VI: Molecular docking supplementary figures 92

Appendix VII: A paper published ftom this thesis 106

List of Figures

Figure 1. Life cycle of the malaria parasite……5

Figure 2. Chemical structures of anti-malarial drugs (**1-3**) and compounds from the genus *Kniphofia* (**4-19**)……12

Figure 3. Isolation scheme of KFP-1, KFP-3 and KFP-5 from *Kniphofia foliosa*……20

Figure 4. Isolation scheme of YKFM-2 from *Kniphofia foliosa*……..……21

Figure 5. Isolation scheme of AL-1 from *Kniphofia insignis*……..…..22

Figure 6. TLC chromatogram of compound **1** (YKFM-2) applied as a spot; viewed under UV 254 (A) and 366 nm (B) light source with the solvent system BAW (butanol: acetic acid:water upper layer; 4:1:5): ethyl acetate (1:1)……..……..……...…27

Figure 7. TLC chromatogram of compound **2 (**KFP-1) and compound **5 (**AL-1**)** applied as a spot; viewed under UV 254 (A) and 366 nm (B) light source with the solvent system toluene: ethyl acetate (5:1)…….…...28

Figure 8. Normal and reversed phase TLC chromatogram of compound **3 (**KFP-3) applied as a spot. A and B are normal phase chromatograms viewed under UV 254 (A) and 366 nm (B) light source with the solvent system $CHCl_3$:MeOH:H_2O (40:10:1); and C and D are reversed phase chromatograms viewed under UV 254 (C) and 366 nm (D) light source with the solvent system MeOH:H_2O (4:1).…….…….28

Figure 9. TLC chromatogram of the compound **4** (KFP-5) applied as a spot; viewed under UV 254 (A) and 366 nm (B) light source with the solvent system hexane: ethyl acetate (3:1)..……...…...……29

Figure 10. Chemical structure of dianellin……..……..34

Figure 11. Chemical structure of knipholone……..……..……35

Figure 12. Negative mode mass fragmentation pattern of compound **3** …….….36

Figure 13. Positive mode mass fragmentation pattern of compound **3**…….….36

Figure 14. Chemical structure of 10-knipholone gentibioside…….……..37

Figure 15. Chemical structure of 12-hydroxypentadec-9-en-1-yl methyl phthalate …….……38

Figure 16. Percent chemosuppression effect of 80% rhizome extracts of *Kniphofia foliosa* *Kniphofia insignis* in mice infected with *P. berghei* in 4 day suppression test; Values are presented as mean ± SEM; n =5.....39

Figure 17. Antimalarial activity of knipholone, dianellin and 10-kniphplone gentibioside in mice infected with *Plasmodium berghei.* The ED_{50} was estimated from a plot of log dose against parasitaemia (expressed as a percentage of the control).……..……47

Figure 18. The binding modes of P2FE-400, knipholone, HPMP and chloroquine to plasmepsin II. A) Superimposition of redocked P2FE-400 (shown as a solid line) with its original position (shown in ball-stick model) as a complex (co-crystal) in the binding site of the crystal structure of plasmepsin II (PDB 4cku). B) Ribbon diagram of docked HPMP-plasmepsin II chain E subunit complex. C) Surface representation showing HPMP in the binding site of plasmepsin II. HPMP is shown in ball-stick model. D) Surface representation showing chloroquine in the binding site of plasmepsin II with lipophilicity coloring. White represent hydrophobic pockets and blue represent hydrophilic pockets. Chloroquine is shown in ball-stick model.……...….53

Figure 19. The binding modes of knipholone, HPMP and chloroquine to pfLDH binding site. A) Ribbon diagram of docked knipholone- pfLDH complex. Knipholone is shown in ball-stick model. B) A close-up view of diagram A. C) Surface representation showing knipholone in the binding site of pfLDH. Knipholone is shown in ball-stick model. D) Surface representation

showing HPMP in the binding site of pfLDH. HPMP is shown in ball-stick model. E) Binding interaction of knipholone with amino acid residues of pfLDH. F) Surface representation showing the superimposed compounds in the binding site of plasmodium falciparum l-lactate dehydrogenase (pfLDH) (PDB1ldg).……54

List of Tables

Table 1. ^{1}H and ^{13}C NMR data of compound **1** measured in deuterated methanol…….33

Table 2. ^{1}H and ^{13}C NMR data of compound **2** measured in deuterated chloroform……34

Table 3. ^{1}H NMR data of compound **3** measured in deuterated methanol.....35

Table 4. ^{1}H and ^{13}C NMR data of compound **4** measured in deuterated chloroform……37

Table 5. ^{1}H NMR data of compound **5** measured in deuterated chloroform ……..……..39

Table 6. Antimalarial activity of the 80 % rhizome extracts of *Kniphofia foliosa* and *Kniphofia insignis* in mice infected with *Plasmodium berghei*……..41

Table 7. Body weight of *Plasmodium berghei* infected mice before and after administration of the 80% rhizome extracts of *Kniphofia foliosa* and *Kniphofia insignis*……...…….42

Table 8. Antimalarial activity of the phenolic fractions of rhizome of *Kniphofia foliosa* in mice infected with *Plasmodium berghei* ……...……43

Table 9. Body weight of *Plasmodium berghei* infected mice before and after administration of the phenolic fractions of rhizome of *Kniphofia foliosa* ……..…..43

Table 10. Antimalarial activity of knipholone, dianellin and 10-kniphplone gentibioside in mice infected with *Plasmodium berghei* ……45

Table 11. Body weight of *Plasmodium berghei* infected mice before and after administration of knipholone, dianellin and 10- kniphplone gentibioside ……45

Table 12. Prediction of partition coefficient Log P, aqueous solubility Log S and partition coefficient for partially dissociated compounds Log D of the compounds, standard drugs and P2FE-400. ……..……...50

Table 13. Docking result of compounds on the crystal structure of plasmepsin II (4cku) and plasmodium falciparum l-lactate dehydrogenase (pfLDH) (PDB 1ldg) ……..….51

List of Acronyms

AAU	Addis Ababa University
ACTs	Artemisinin-based Combination Therapies
ANOVA	Analysis of Variance
CC	Column Chromatography
CDPK6	Calcium-Dependent Protein Kinase 6
$CHCl_3$	Chloroform
DEPT	Distortionless Enhancement by Polarization Transfer
ED_{50}	Effective dose that suppress 50 % of parasitaemia
EHNRI	Ethiopian Health Nutrition and Research Institute
ESIMS	Electrospray Ionization-Mass Spectrometry
EtOAc	Ethyl acetate
FT-NMR	Fourier Transform Nuclear Magnetic Resonance
HPMP	12-hydroxypentadec-9-en-1-yl methyl phthalate
HSPGs	Heparin sulfate proteoglycans
IISS	International Institute for Strategic Studies
MeOH	Methanol
MS	Mass Spectrometry
NMR	Nuclear Magnetic Resonance
OECD	Organization of Economic Cooperation and Development

PDB	Protein Data Bank
pfLDH	*Plasmodium falciparum* l-lactate dehydrogenase
PTLC	Preparative Thin Layer Chromatography
RNA	Ribonucleic acid
RPFCC	Reversed Phase Flash Column Chromatography
ROS	Reactive Oxygen Species
SoP	School of pharmacy
TLC	Thin-layer Chromatography
TMS	Tetramethylsilane
UV	Ultraviolet
WHO	World Health Organization
2D NMR	Two Dimensional Nuclear Magnetic Resonance

1. Introduction

1.1 Malaria

1.1.1 Malaria parasites and their transmission

Malaria continues to be one of the most serious life-threatening tropical infectious diseases. It is caused by protozoan parasite of the genus *Plasmodium* which comprises more than 200 single celled eukaryotic organisms under the phylum Apicomplexa**.** Among the 200 or more *Plasmodium* species, only five cause human malaria. These are *Plasmodium falciparum, P. vivax, P. malariae, P. ovale* and *P. knowlesi* (Cowman *et al.,* 2016; Barber *et al*., 2017). From the evolutionary aspect, *P. vivax, P. malariae* and *P. ovale* are closely related to a number of simian malarias**.** Based on small subunit ribosomal RNA gene sequence analysis, *P. vivax* appeared similar to *P. fragile,* a parasite of toque monkeys. Similarly, *P. malariae* was genetically indistinguishable from *P. brasilianum,* a parasite of New World monkeys (Waters *et al*., 1993; Ayala *et al*., 1999)**.** In fact, it has been suggested that *P. brasilianum* might have been *P. malariae* adapted to a new host over the last few hundred years (Tazi and Ayala, 2011). In general, it was estimated that these parasites most likely arose alongside the primate hosts about 30 million years ago. And recently, *P. falciparum* has been found to be derived from *P. praefalciparum,* a recent common ancestor of the gorilla parasite, some 40,000 years ago (Otto *et al*., 2018).

P. falciparum and *P. vivax* are responsible for the largest malaria public health burden. Particularly, *P. falciparum* malaria is most virulent and fatal due to the complication of cerebral malaria unless rapidly treated. In 2014, *P. falciparum* malaria killed approximately 1,200 African children less than 5 years of age each day (Smith *et al*., 2001; Maitland, 2016). Besides, it is associated with severe malaria complications in pregnancy. As relapsing malaria, *P. vivax* on its

part can survive in climatically unfavorable regions and can stay dormant in a hypnozoite form in human host liver for many years. As a result, *P. vivax* is majorly prevalent in Central and South America and in temperate climates (Alves *et al*., 2002). Moreover, many Africans who were negative for the Duffy antigen (also known as atypical chemokine receptor 1, required for red blood cell invasion) on the surface of red blood cells were found to be immune against *P. vivax* malaria (Miller *et al*., 2002). Now, *P. vivax* was isolated from Duffy negative patients. Unlike the other malaria parasites, for *P. falciparum* and *P. vivax* humans are the only mammalian hosts.

The less commonly transpired parasites *P. malariae* and *P. ovale* are found in Africa and Asia, but are especially prevalent in West Africa. *P. malariae* causes the mildest infections, although it has been associated with splenomegaly or renal damage upon chronic infection (Mueller *et al*., 2007; Alemu *et al.*, 2013). *P. knowlesi*, which was recently introduced and initially considered as a parasite of non-human primates, can also lead to severe and even fatal malaria complications (Singh *et al*., 2004; Tek Ng *et al*., 2008).

Human malaria parasites are transmitted from one person to another by female *Anopheles* mosquitoes. Male *Anopheles* mosquitoes do not transmit the disease. There are 400 different species of *Anopheles* mosquitos; around 40 exclusively transmit the disease (Sriwichai *et al.*, 2016). During *Anopheles* spp. mating, males transfer high levels of the steroid hormone 20-hydroxyecdysone to the females, and the presence of this hormone has been associated with favorable conditions for *Plasmodium* spp. development. Malaria competent *Anopheles* spp. are abundant and distributed all over the globe, including the Arctic. However, since the efficacy of malaria transmission depends on the vector species, it varies considerably worldwide; for example, in tropical Africa, *Anopheles gambiae* is a major and highly efficient vector (Sinka *et*

al., 2011, Mitchell *et al.,* 2015). Recently, *A. stephensi* was discovered as new vector in Ethiopia (Tadesse *et al*., 2021).

1.1.2 Life cycle

The complex life cycle of malaria parasites begins when a plasmodium infected female bites a human victim. As it bites, an infected *Anopheles* mosquito injects saliva containing sporozoites into the skin and blood. The highly motile sporozoites migrate to the liver by crossing through the sinusoidal barrier, which consists fenestrated endothelial cells and macrophage-like Kupffer cells and invade a small number of hepatocytes (Miller *et al*., 2013). Numerous specialized proteins are required for this traversal process. Broadly speaking, sporozoites injected into the dermis are in ‘‘migratory mode’’ and upon interaction with hepatocytes convert to ‘‘invasive mode.’’ One signal for this switch is recognition of hepatocytes through binding higher sulfated forms of heparin sulfate proteoglycans (HSPGs) activating calcium-dependent protein kinase 6 (CDPK6). The sporozoite and liver stages are collectively referred to as pre-erythrocytic parasites and do not cause physical signs or symptoms in the human host (Frevert *et al.,* 1993; Coppi *et al.,* 2007).

Each sporozoite-infected hepatocyte gives rise to tens of thousands of asexual parasites called merozoites. After a variable period of 5-16 days on average)**,** merozoites exit the liver into the bloodstream to begin a 48-hours cycle of erythrocytes invasion, replication, rupture, and merozoite release. Once inside a red cell, the merozoites develop first into ring form, then into trophozoite stage. During this period, the parasite feeds on the protein portion of hemoglobin and a waste product, hemozoin, accumulates in the host cell cytoplasm. The mature trophozoites (schizonts) again asexually divide to give 16-32 merozoites that egress when developed leading into the destruction of erythrocyte membrane and explosive release of the parasites to access new

host cells for invasion. The coordinated process of merozoite egress is tightly regulated and involves a number of protein kinases (Vaughan *et al*., 2012; Weiss *et al*., 2015; Cortes and Deitsch, 2017; Milner, 2017).

When the infected red blood cells (erythrocytes) rupture, clinical symptoms become evident. The symptoms include fever, headache, chills, sweats, vomiting, myalgias, and malaise. The severity of these symptoms has been correlated with parasite load. In the early stage of clinical manifestation, the fever attacks are periodic, every first day for *P. knowlesi*, every second day for benign tertian malaria, *P. vivax*; *P. ovale;* and subtertian malaria, *P. falciparum*; and every third day for quartan malaria, *P. malariae*, and this corresponds to release of a new generation of merozoites in the bloodstream. Again, the periodicity is regulated by human melatonin through a calcium-dependent pathway by increasing inositolpolyphosphate production in intraerythrocytic parasites (Mackintosh *et al*., 2004).

While a new generation of merozoites released during erythrocyte rupture will each potentially invade a new erythrocyte to continue the cycle, few of them will develop into male or female gametocytes which are dormant in human and may be ingested by a mosquito during a blood meal. Inside the mosquito mid gut, the male and female gametocyte fuse to form the zygote, at which time the parasite becomes diploid and homologous recombination can lead to significant genetic variability of progeny. Finally, they would become sporozoites that enter the mosquito salivary gland to complete the life cycle (Baker, 2010; Smith *et al*., 2014). Figure 1 (Phillips *et al*., 2016) presents a brief life cycle of the malaria parasite.

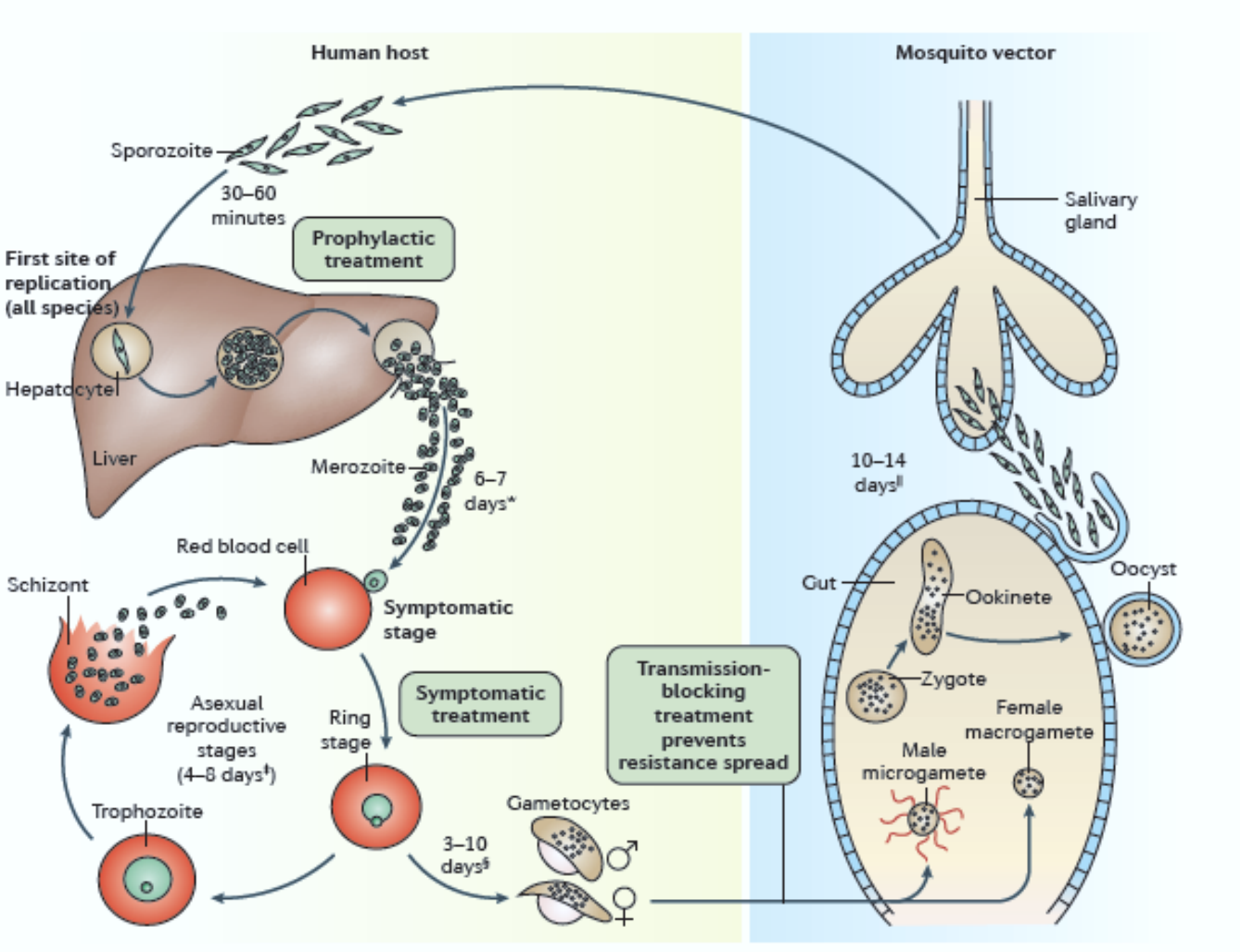

Figure 1. Life cycle of the malaria parasite. (Phillips *et al*., 2016).

1.1.3 Epidemiology

Malaria is one of the leading global public health challenges. There were an estimated 226 million cases of malaria and 405,000 deaths in 2018 (WHO, 2019). The number stands as 2.6 times as many deaths from armed conflicts in 2016, which were estimated to be 167,000 (IISS, 2016). It occurs mostly in poor tropical and subtropical areas of the world, where the Africa region accounted for 93% of all malaria cases and 93.8% of malaria deaths (WHO, 2019). Millions of people across Africa lack access to the preventive tools and chemoprevention drugs they needed. Most often, pregnant women and children under five years old are severely

affected. For instance, from the total deaths due to malaria in 2018, 67% or 272,000 were children under 5 years of age. That is nearly 745 children under age five daily or one child under five every two minutes dies of malaria in 2018 alone, and most of these deaths occurred in Sub-Saharan Africa (Snow *et al*., 2017; WHO, 2019). In addition to funding shortfalls and fragile health systems, the major contributor to malarial morbidity and mortality is almost certainly the increasing resistance of malaria parasites to available drugs (Farooq and Mahajan, 2004).

In Ethiopia, there has been success in the past recent years to reduce malaria burden. However, it is prevalent in 75% of the country putting over 40 million people at risk. It affected 4 to 5 million peoples and there were an estimated 621,345 new cases and 1561.7 deaths (WHO, 2017). The disease accounts for 7% of outpatient visits to health clinics and represents the third largest cause of morbidity (Girum *et al.,* 2019). In addition, 8% of global *P. vivax* malaria cases occur in Ethiopia (WHO, 2019). This was because most Ethiopians are Duffy antigen positive. The transmission of malaria in Ethiopia depends on altitude and rainfall with a lag time varying from a few weeks before the beginning of the rainy season to more than a month after the end of the rainy season (FMH, 2006; Adugna, 2009). Epidemics of malaria are common in Ethiopia involving even the highland or highland fringe areas (Kebede *et al*., 2005). Hence, the fight against malaria in Ethiopia remains a public health priority.

1.2 Natural products

Natural products from plants have played very significant role throughout history in the fight against malaria. For example, the aqueous extracts of cinchona bark had been an effective antimalarial preparation for more than 300 years. Later, quinine (**1**), the major active alkaloid of cinchona was isolated in the 1820s. Quinine had remained as the only available antimalarial

agent until the discovery of chloroquine (**2**) and other synthetic aminoquionlones. Some of these synthetic antimalarials were even designed based on the structure of quinine. Quinine is still used to today to treat some cases of chloroquine resistance strains (Meshnick and Dobson, 2001; Kaur *et al.*, 2009). Similarly, when the parasites become chloroquine resistant and the malaria burden was at stake in Southeast Asia, artemisinin was isolated from the cold ether extracts of the leaves of Chinese traditional medicinal herb, *Artemisia annua* in 1972 (White *et al*., 2015). Artemisinin was the greatest antimalarial compound for it was gameteocidal thereby limiting the transmission of malaria. *A. annua* or QingHao (green herb) has been used in Chinese traditional medicine as febrifuge for more than 4 hundreds years (Brossi *et al*., 1988; Cumming *et al*., 1996; White *et al*., 2015). Currently, the artemisinin-based combination therapies (ACTs) are first line treatments for uncomplicated falciparum malaria in all endemic countries (Mullard, 2018).

Inspired by the above success, different classes of antimalarial compounds were isolated from a variety of plant families. Although hundreds of potent antimalarial compounds were isolated from African traditional medicine, there hasn't been any clinically successful molecule (Saxena *et al*., 2003; Beroa *et al*., 2009; Ntie-Kang *et al*., 2014). To have a clinical candidate leads, more medicinal plant extracts, fractions, and compounds from African traditional medicine are supposed to be evaluated. In other words, African traditional medicine with its reach and majorly untouched ethnopharmacological resource has to be scientifically validated and standardized (Hostettmann *et al*., 2000; Pillay *et al*., 2003). For the particular case of antimalarial medicinal plant research in Ethiopia, there is an even more lucrative account of untouched or less-extensively investigated medicinal plant biodiversity. Therefore, in a continued search for lead antimalarial compounds from Ethiopian medicinal plants (Asamenew *et al*., 2014; Girma *et al*.,

2015), the rhizomes and constituents of *Kniphofia foliosa* Hochst and *Kniphofia insignis* Rendle have been investigated for their *in vivo* antimalarial activity against *Plasmodium berghei* in mice.

1.3 The genus *Kniphofia*

1.3.1 Description

The genus *Kniphofia* are members of the sub-family Asphodeloideae, family Asphodelaceae which comprises 70 species mainly confined to Africa (Dahlgren *et al*., 1985). Fifteen species have been recorded in Eastern Africa, of which seven of them occur in Ethiopia. Interestingly, five of the seven are endemic to Ethiopia. These are *K. foliosa, K. insignis, K. isoetifolia, K. schimperi* and *K. hildebrandtii* (Whitehouse, 2002; Demissew and Nordan, 2010). These plants grow from a thick rhizome in aggregates or solitarily, rarely with a thick, well developed woody stem. The leaves appearing at this non woody stem are arranged in basal rosettes, usually in 4 or 5 ranks, linear and tapering gradually to the apex. The inflorescence is simple, often subcapitate. The flowers produced thereof are most beautiful with varied flowers ranging from white to pink, yellow to red or brownish to various shades of red. Characteristically, the red color (pigment) is often more conspicuous at the apex, thus giving them a bicoloured appearance.Not only that they display these varied colours, they also display two different patterns of flower opening. In *K. isoetifolia* and *K. pumila*, the flowers open from top downwards (centrifugal), while in the other species the flowers open from base upwards (centripetal). Their flowers are sessile or with a short pedicel (Demissew and Nordan, 2010).

1.3.2 Distribution

Members of the genus are distributed in arid and mesic regions of the temperate, subtropical and tropical zones of the World, with the main center of diversity in southern Africa. Some of species are found to grow in grassland, grassy slopes, on steep hillsides and near streams in tall grass between 1220 and 2650 (–3150) m. Others grow on roadsides, on overgrazed areas with scattered trees, hillsides, on rock outcrops, and mountain plateaus between 2400 and 4000 m. Generally, most of the species usually prefer well drained soil, river banks, and in montane grassland. The plants also have a widespread occurrence in different regions of Ethiopia and Eritrea. They are found on steep grassy or rocky slopes, mountains of and marshy ground between 2400 and 3650 m in the Tigray, Gondar, Wollo, Shewa (Sululta), Arsi, Bale, Sidamo, and Harerge regions (Whitehouse, 2002; Demissew and Nordan, 2010).

1.3.3 Ethnobotanical use

In Ethiopia, the roots of *K. foliosa* are used for the treatment of abdominal cramps and for wound healing (Abate, 1989). The plant is also used to remove endoparasites in cattle. Likewise, plant infusions of *K. buchananii, K. parviflora, K. laxiflora,* and *K. rooperi* are used in South Africa as snake deterrents and for chest ailments. The genus *Kniphofia*, and to some extent also *Bulbine*, are included among several ornamental plants with economic potential. Inflorescences of members of the genus are sold as cut flowers, although mostly of South African species. Most importantly, the broad role of these plants in folk medicine suggests their feasible pharmacological potential (Hutchings *et al*., 1996).

1.3.4 Phytochemistry

The phytochemistry of species of the genus *Kniphofia* is not intensively investigated. Only some anthraquinones are reported from few members of the genus. A study on the chemotaxonomic significance of anthraquinones in the family Asphodelaceae have qualitatively identified some anthraquinones in 46 species of the genus *Kniphofia* and *Aloe* using analytical TLC and HPLC (van Wyk *et al*., 1995). Furthermore, two new anthraquinones, kniphofiones A and B (**4, 5**), together with other seven previously known monomeric and dimeric anthraquinones such as chrysophanol (**6**), aloe-emodin (**7**), asphodeline (**8**), microcarpin (**9**) were isolated from the whole parts of *K. ensifolia* (Dai *et al.,* 2013). Similarly, two new compounds, an indanone derivative kniphofiarindane (**10**) and a naphthalene derivative kniphofiarexine (**11**) together with other known compounds (**12**) were reported from the rhizomes of *K. reflexa* (Sema *et al*., 2018). Likewise, 3,5,8-trihydroxy-2-methylnaphthalene-1,4-dione (**13**) and dimeric anthraquinones (**8,14**) were reported from the roots of *K. isoetifolia* (Meshesha *et al*., 2017). Moreover, Dagne and Steglich (1984) isolated knipholone (**15**) as the first plant derived novel phenylanthraquinone from the roots of *K. foliosa*. Then other new knipholone derivatives; knipholone anthrone (**16**), knipholone cyclooxanthrone (**17**), and other anthraquinones, 10-methoxy- 10,7'-(chrysophanol anthrone)-chrysophanol (**18**), 10-(chrysophanol-7′-yl)-10-(β)-hydroxychrysophanol-9-anthrone (**13**), chryslandicin (**19**), and chrysophanol (**6**), were reported from the roots of *K. foliosa* (Dagne and Yenesew, 1993; Wube *et al*., 2005; Abdissa *et al*., 2013). In addition, miscellaneous compounds such as lectin-like proteins, shikimic acid and quinic acid were also reported from different species of genus *Kniphofia* (Ripperger *et al*., 1970).

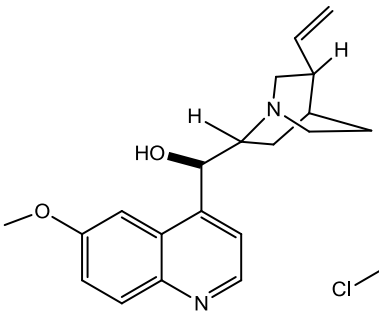

1

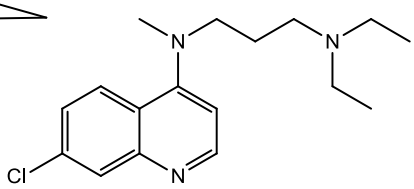

2

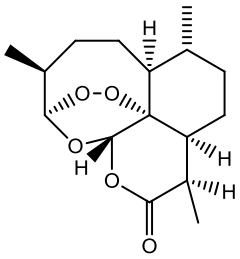

3

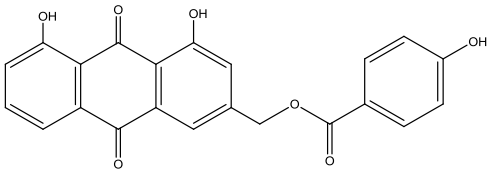

4

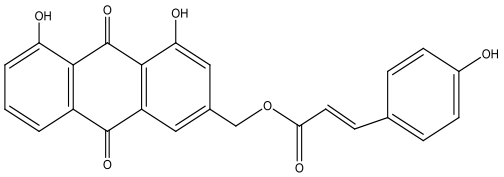

5

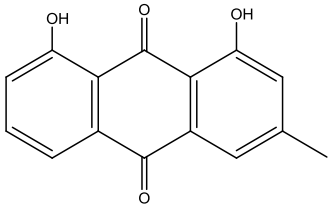

6

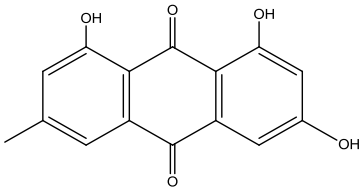

7

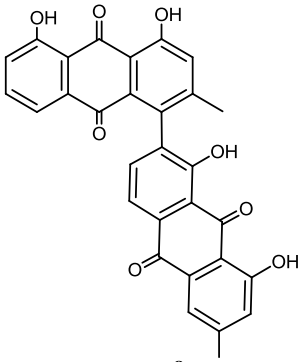

8

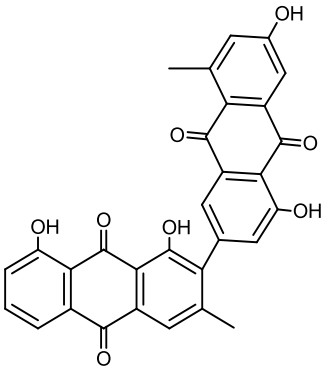

9

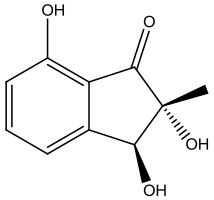

10

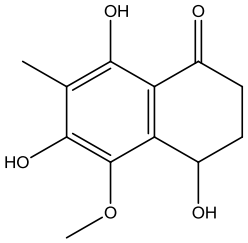

11

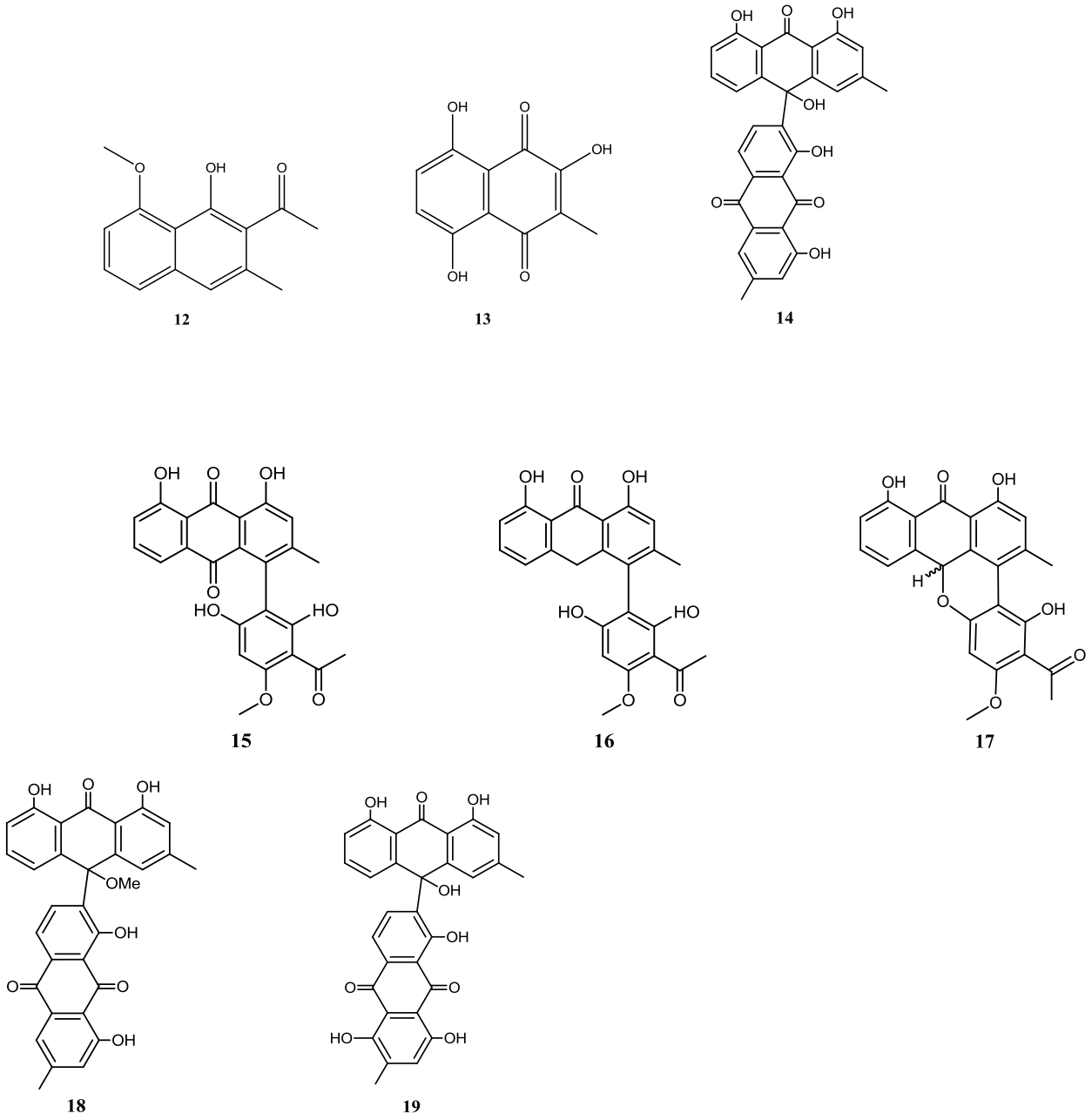

Figure 2. Chemical structures of anti-malarial drugs (**1-3**) and compounds from the genus *Kniphofia* (**4-19**).

1.3.5 Pharmacological activities

There are very few reports on *in vitro* antiplasomodial and anticancer activities of some species of *Kniphofia*. The dichloromethane and ethyl acetate extract of *K. foliosa* and the anthraquinons

isolated thereof have been reported to have *in vitro* antimalarial activity against the chloroquine-sensitive 3D7 strain of *Plasmodium falciparum*. 3,5,8-Trihydroxy-2-methylnaphthalene-1,4-dione (**13**) and the dimeric anthraquinones (**18**) were found to be the most active with IC_{50} values of 0.260 and 0.537 μg/ml respectively (Wube *et al*., 2005). Similarly, compounds isolated by *in vitro* antiplasmodial bioassay guided approach from the roots of *K. ensifolia* showed activity against chloroquine-resistant Dd2 strains *of P. falciparum*. Interestingly, (**13**) and (**18**) were the most active compounds with IC_{50} values of 0.4 and 0.2 μM, respectively (Dai *et al*., 2013). Compounds (**10)** and **(12**) isolated from *K. reflexa* displayed cytotoxic effect against kidney epithelial cell line (LLC-MK2), with the latter showing superior activity (CC_{50} = 4.44 μg/ml) than the former (Sema *et al.,* 2018). Similarly compounds (**8**) (**13**) and (**14**) isolated from the rhizomes of *K. isoetifolia* showed *in vitro* antibacterial activity against four bacterial strains (Meshesha *et al*., 2017). Furthermore, knipholone anthrone (**16**) exhibited rapid onset of cytotoxicity in leukaemic and melonocyte cancer cell lines with IC_{50} values ranging from 0.5 to 3.3 μM (Habtemariam, 2010).

1.4 *Kniphofia foliosa* Hochst and *Kniphofia insignis* Rendle

1.4.1 Description and distribution

Kniphofia foliosa is easily distinguished by the funnel shaped to tubular perianth, 18–27 mm long. Its flowers open from base upwards (centripetal). On the other hand, *K. insignis* is clearly distinguished from other species by the white perianth, which is unusual in the genus, and also by the fusiform roots. Whilst *K foliosa* grows on roadsides, on overgrazed areas with scattered trees, hillsides, on rock outcrops, and mountain plateaus, *K. insignis* often grows in water-logged or flooded meadows. *K. foliosa* is more widespread than *K. insignis*. The flowering period for *K.*

foliosa is from June to October, but it sometimes extends to December- January in wetter places and forest margins. On the other hand, the flowering period of *K. insignis* is from June to September (Whitehouse, 2002; Demissew and Nordan, 2010).

1.4.2 Ethnobotanical uses, chemistry, and pharmacological reports

The roots of *K. foliosa* and *K. insignis* are traditionally used for the treatment of abdominal cramps, malaria and wounds (Abate, 1989; Mothana *et al*., 2009). Previously, six anthraquinones, viz (**8**), (**15**), (**17**), (**14**), (**18**) and (**19**) were isolated from the roots of *K. foliosa* (Wube *et al*., 2001; Abdissa *et al*., (2013). All the the isolated compound showed *in vitro* antimalarial activity with varying activity levels. To date, there has not been any report concerning the phytochemistry and pharmacological activity of *K. insignis*.

1.5 Statement of the problem

Currently, malaria research has achieved an impressive success such as sequencing plasmodium genome, elucidating the pathobiology and drug resistance mechanisms of malaria, discovering new targets, and developing newer malaria bioassay techniques. Sadly, the disease still remains to be a public health challenge with worryingly high death toll especially in Africa. Besides lack of access to preventive tools and adequate treatment facilities in malaria endemic regions, by far the major cause of this daunting result has been the emergence of parasite drug resistance to available drugs (White, 1999; Wellems, 2002). Moreover, the recent emergence of resistance toward artemisinin combination therapy is the greatest future threat (Menard and Dondorp, 2017). Thus, there is undoubtedly an urgent need for novel, safe and effective antimalarial drugs.

Among the various drug discovery strategies, isolation of natural products from traditional medicinal plants stands strong as the history of antimalarial drug therapy is self-evident. It is often said that 80% the population in Ethiopia relies on traditional medicine for their primary health care. However, the vast proportion of medicinal plants has not been evaluated for their antimalarial activity. Thus, in the present study two traditionally used antimalarial plants namey, *Kniphofia foliosa* and *K. insignis* have been scientifically investigated for their *in vivo* antimalarial activities against *Plasmodium berghi* in mice.

2 Objectives

2.1 General objective

- To evaluate the antimalarial activity of the rhizomes of *Kniphofia foliosa* and *K. insignis* and the compounds isolated therefrom.

2.2 Specific objectives

- To evaluate antimalarial activity of the hydroalcoholic extracts of extracts *Kniphofia foliosa* and *K. insignis*;
- To fractionate the extract and isolate and compounds from the active fractions;
- To determine the antimalarial activity of the isolated compounds;
- To elucidate the structures of the isolated compounds; and
- To carry out molecular docking study of the isolated compounds

3 Materials and methods

3.1 Materials

3.1.1 Chemicals and reagents

Hexanes, chloroform, ethyl acetate, methanol (all from Sigma-Aldrich Co., MO, USA) and distilled water were the solvents used for extraction, fraction and isolation. Chromatographic separation was performed by analytical TLC on Silica gel 60 F254 (0.2 mm thick), column chromatography on Silica gel 60 (70 - 240 mesh) (Merck KGaA, Darmstadt, Germany) and solid phase separation on Isolute C_{18} columns (10 g; IST, Hengoed, UK). The following chemicals and drugs were used for the experiment: Trisodium citrate (BDH Chemicals Ltd, England), Geimsa (ESJAY Chemicals, Maharashtra, India), and pure chloroquine phosphate was supplied by Ethiopian Pharmaceutical Manufacturing Factory (EPHARM, Ethiopia).

3.1.2 Instruments

NMR spectra were recorded at 500 MHz for ^{1}H and 125 MHz for ^{13}C on a Bruker Avance DMX400 FT-NMR spectrometer (Bruker, Billerica, Massachusetts, USA) using tetramethylsilane (TMS) as internal standard. All spectra were measured in $CDCl_3$, except for compounds **1**, which was dissolved in CD_3OD. High resolution mass spectra (HRMS) were determined on a Shimadzu LC‐MS Advanced spectrometer (Shimadzu, Kyoto, Japan) in the positive and negative modes.

3.2 Methods

3.2.1 Plant collection

The rhizomes of *K. foliosa* were collected in February 2017 from mount Kundi near the city of Ankober in Shewa region of Central Ethiopia and identified by Professor Sebsibe Demisew at the National Herbarium, Addis Ababa University (AAU), Addis Ababa, Ethiopia, where voucher specimens were deposited (Collection number: YA01/2017). The rhizomes of *K. insignis* were collected in September 2018 from water-logged meadows of Sululta, in Oromiya region of Ethiopia and identified by Mr. Melaku Wondafrash, a senior botanist at the National Herbarium, College of Natural and Computational Sciences, AAU, where the voucher specimens were deposited (Collection number: YA001).

3.2.2 Extraction, fractionation and isolation

The air dried powdered rhizomes of both experimental plants were soaked in 80% methanol at room temperature for 4 days with occasional shaking. Removal of the organic solvent using rotary evaporator (BUCHI Rotavapor™ R-300, Switzerland) followed by freeze drying of the remaining water extract yielded a dark red gummy solid for *K. foliosa* and a red solid for *K. insignis*. Portion of the dried extracts were dissolved in 5% KOH solution and partitioned with chloroform to remove the nonphenolic components. The aqueous phase was acidified with 2% HCl and then further partitioned with chloroform. The chloroform layer was collected and concentrated in a rotary evaporator to give a dried solid designated crude phenolic fraction I. In addition, for *K. foliosa*, the reddish solid mass (methanol soluble) formed between the acidified aqueous and chloroform layers was collected as phenolic fraction II. Purification of phenolic fraction I of *K. foliosa* by preparative TLC and column chromatography, respectively gave

(Figure 3) KFP-1 and KFP-5. Likewise, phenolic fraction II gave (Figure 3) KFP-3 after purification using preparative TLC and solid phase extraction on Isolute C_{18} columns. Furthermore, portion of the hydroalcoholic extract of *K. foliosa* was fractionated on silicagel flash column chromatography to yield three fractions. Fraction 1 was eluted with 100% chloroform, fractions 2 and 3 with a mixture of chloroform and methanol (1:1), and fraction 4 with 100% methanol. Fraction 3 was concentrated and freeze dried to give viscous solid, which was further purified by sequential PTLC and solid phase extraction on Isolute C_{18} columns to give YKFM-2 (Figure 4). Also, purification of the phenol fraction of *K. insignis* by preparative TLC gave AL-1 (Figure 5).

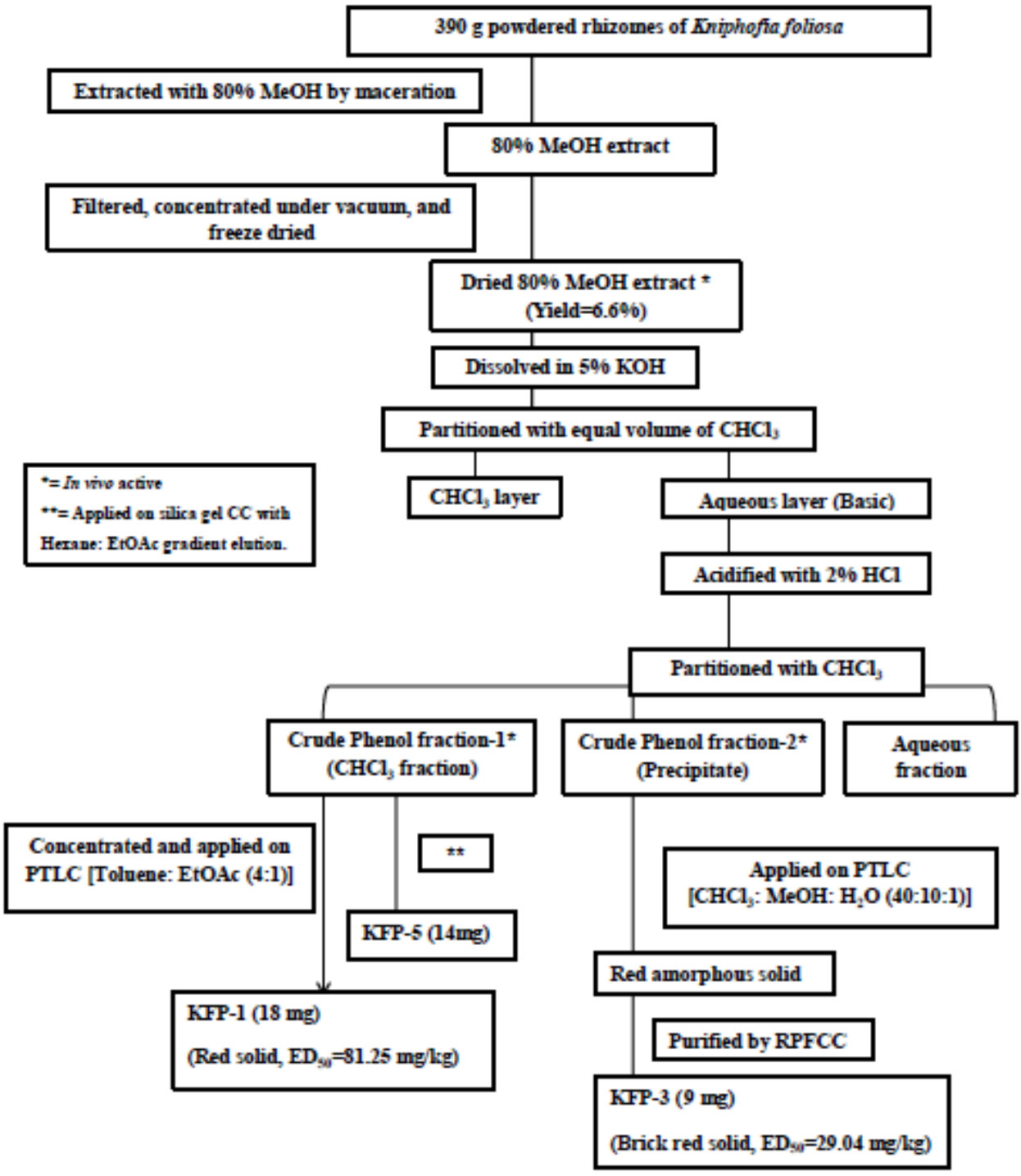

Figure 3. Isolation scheme of KFP-1, KFP-3 and KFP-5 from *Kniphofia foliosa*

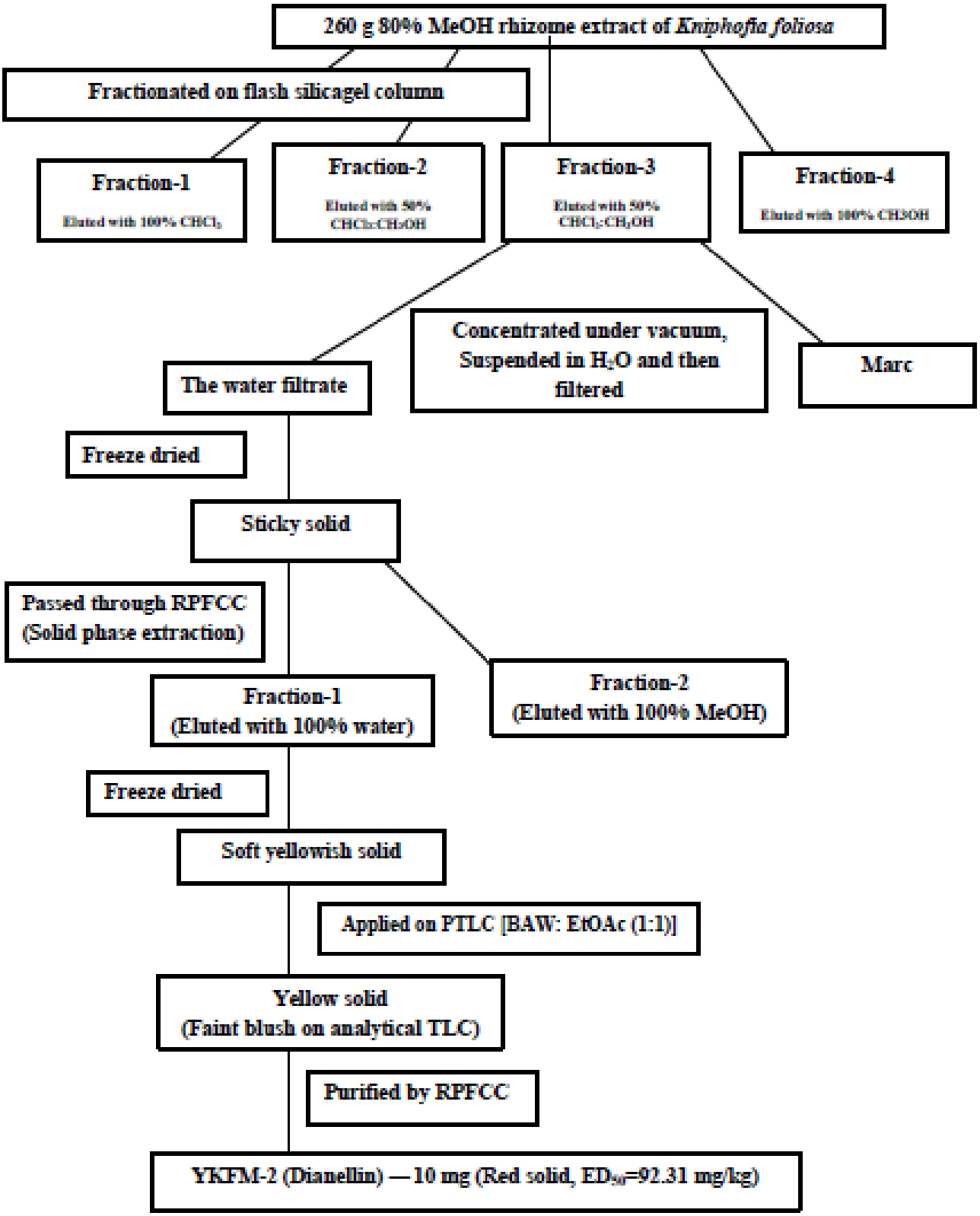

Figure 4. Isolation scheme of YKFM-2 from *Kniphofia foliosa*

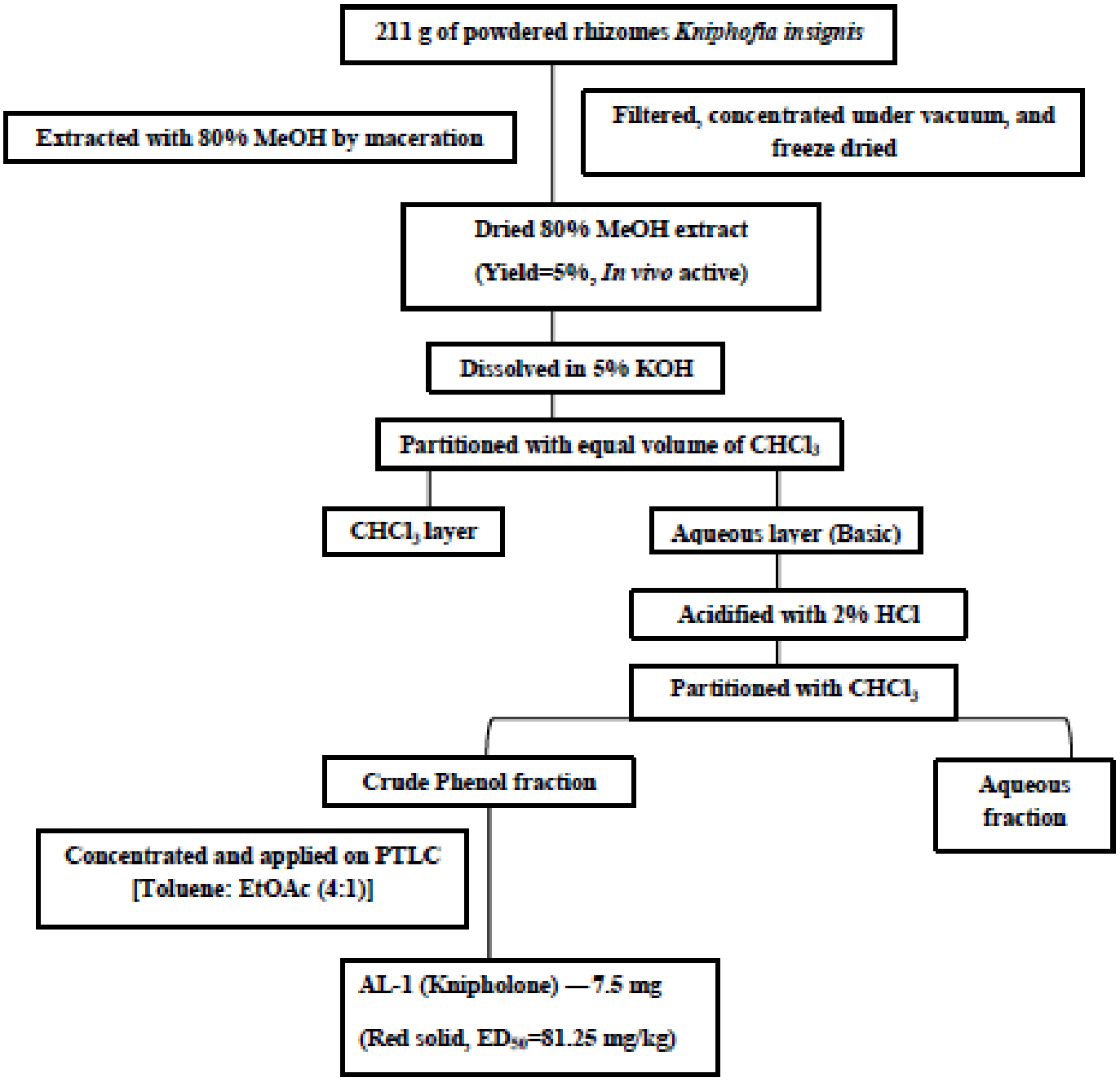

Figure 5. Isolation scheme of AL-1 from *Kniphofia insignis*

3.2.3 Experimental animals and rodent parasite

Healthy, 5-6 weeks old Swiss albino mice of either sex weighing 20-25 g were employed throughout the experiment. Most of the mice were obtained from the animal house of the School

of Pharmacy (SoP), AAU, and the rest were purchased or gifted, respectively, from the Ethiopian Health Nutrition and Research Institute (EHNRI) and Rift Valley Health Science College, Addis Ababa. The animals were held in stainless steel cages at room temperature and relative humidity for12 hour light-dark cycle. They were provided with food and water *ad libitum* in the animal house of the SoP, College of Health Sciences, AAU. They were acclimatized for one week before the experiment.

Chloroquine (CQ) sensitive *Plasmodium berghei* ANKA strain was used. The donor mice infected with the parasite was obtained from EHNRI. The parasites were maintained by serial blood passage from mouse to mouse at 5 days interval. All procedures followed were in accordance with the Guide for the Care and Use of Laboratory Animals (NIH Guidelines for Care and Use of Laboratory Animals, 1996) and were approved by the Ethical Review Board of the SoP, AAU.

3.2.4 Acute oral toxicity testing

Acute oral toxicity study was conducted as per the internationally accepted protocol of OECD Guideline 425 (OECD, 2008). Twenty healthy Swiss female albino mice weighing 20-25 g were randomly grouped into 4 each having 5 mice. Following 3-4 h of fasting (food only), one mouse from each group was orally administered 2000 mg/kg of the hydroalcoholic extract *K. foliosa*, *K. insignis*, KFP-1 and YKFM-2, consecutively. This was repeated on the remaining mice for the following four days. The mice were then observed individually for any physical or behavioral changes such as loss of appetite, ruffled fur, lacrimation, mortality, and other signs of toxicity for 4 h. The same procedure was followed for the remaining mice for the next five consecutive days and the results recorded. The follow-up observations were continued for all mice for 14 days.

3.2.5 *In vivo* antimalarial assay

3.2.5.1 Inoculation

Blood smear was prepared on microscope slides from blood films taken from the donor (infected) mouse tail. The smear was fixed with methanol and stained with Giemsa to determine parasitaemia level of the donor under a microscope (Primo Star, Carl Zeiss, Germany). The mice were then inoculated on day 0 with parasitized erythrocytes obtained from the donor by cardiac puncture using a sterile syringe when the parasitaemia level was 30-40%. The blood from the donor was collected on a Petri dish containing 2% trisodium citrate and was immediately diluted with uninfected mouse blood and normal saline in such way that the final volume contains 5×10^7 infected erythrocytes/ml of blood. The diluted blood (0.2 ml) was injected into all the experimental mice intraperitoneally (Waako *et al*., 2005; Hilou *et al.*, 2006).

3.2.5.2 4–Day suppressive test

The standard 4-day suppressive method was used for antimalarial evaluation of the test substances. The test was carried out in three phases. *K. foliosa* extract and its phenol fractions were evaluated in the first phase followed by KFP-1 and KFP-3 in the second phase, and YKFM-2 in the third phase respectively. During the first phase, 60 inoculated mice were randomly grouped into 12 groups each having five mice. Group 1 served as a negative control (distilled water,Vehicle1, 0.2 ml) for the extract and phenolic fraction 2 treated groups, while group 2 animals were used as a negative control (1% tween 80, Vehicle2, 0.2 ml) for phenolic fraction 1 treated group. The third group which served as a positive control was treated with standard pure chloroquine (25 mg/kg/day). The remaining nine groups were treatment groups and received 100, 200, and 400 mg/kg/day of the hydroalcoholic extract and the two phenol fractions.

Similarly, during evaluation of KPF-1 and KFP-3, 45 inoculated mice were randomly grouped into 9 groups, each containing five mice. The first two groups were negative controls (distilled water, Vehicle3, 0.2 ml) and positive controls (standard pure chloroquine, 25 mg/kg/day). The rest of the groups were treatment groups and received KFP-1(25, 50, 100 and 200 mg/kg/day) and KFP-3 (25, 50 and 100 mg/kg/day). During the third phase, a similar procedure was followed to test *K. insignis* extract and YKFM-2 on 40 inoculated mice at doses of 100, 200, and 400 mg/kg/day, and 25, 50, and 100 mg/kg/day, respectively. All the test substances were administered orally using oral gavage. Treatment was started 3 h post-infection on day 0 and continued daily for the next 3 days (i.e. from day 0 to day 3). On the fifth day (or day 4), two Giemsa-stained blood smears were prepared from the tail blood of each mice to count the number of parasites under the microscope with an oil immersion objective of 100x magnification power (Ancelin *et al*., 2003; Vennerstrom *et al*., 2004; Fentahun *et al*., 2017).

Mean percent parasitaemia and percent suppression were calculated using the following formula.

$$\%\ \text{Parasitemia} = \left(\frac{\text{Number of parasitized RBC}}{\text{Total number of RBC count}}\right) \text{X } 100$$

$$\%\ \text{suppression} = \left(\frac{\text{Mean parasitemia of negative control} - \text{Mean parasitemia of treated}}{\text{Mean parasitemia of negative control}}\right) \text{X } 100$$

3.2.5.3 Body weight and survival time measurement

Body weight and mean survival time were also used to evaluate the *in vivo* antimalarial activity of the test substances. Body weight of each mouse was measured on day 0 before infection and on day 4. Survival time was recorded from day 1 to day 28 post inoculation. Then, the mean body weight and mean survival time were calculated for each group (Teka *et al*., 2016).

3.2.6 Molecular docking study

Docking study was carried out on two crystal structures of plasmodium enzymes plasmepsin II (PDB: 4CKU) and l-lactate dehydrogenase (pfLDH) [PDB: 1LDG], using SeeSar10.0 software (BioSolveIT, Sankt Augustin, Germany). For plasmepsin II, the selected binding site was the binding pocket of a previously designed inhibitor P2FE-400, while for pfLDH, the cofactor NADH binding site was selected for docking. The HYDE score was used to estimate the binding affinity of the molecules (Schneider *et al*., 2012; Schneider *et al*., 2013).

3.2.7 Statistical analysis

Data analysis was carried out using IBM SPSS (Statistical Package for Social Sciences) Statistics for Windows, Version 20.0. Armonk, NY: IBM Corp. Results were expressed as mean ± standard error of mean (M ± SEM). Statistical significance was determined by one-way ANOVA followed by Tukey post hoc test to compare percent suppression (activity), mean survival time and percent changes in body weight of the *P. berghei* infected mice among the treatment and control groups. $P < 0.05$ were considered significant.

4 Results and Discussion

4.1 TLC chromatogram of the compounds

As illustrated in section 3.2.2, phytochemical investigation of the rhizome extracts of *K. foliosa* over silica gel column and PTLC resulted in the isolation of four compounds (**1-4**). The TLC chromatograms of these compounds are shown in Figures 6-9. Similarly the the rhizome extract of *K. insignis* afforded compound **5** (Figure 7).

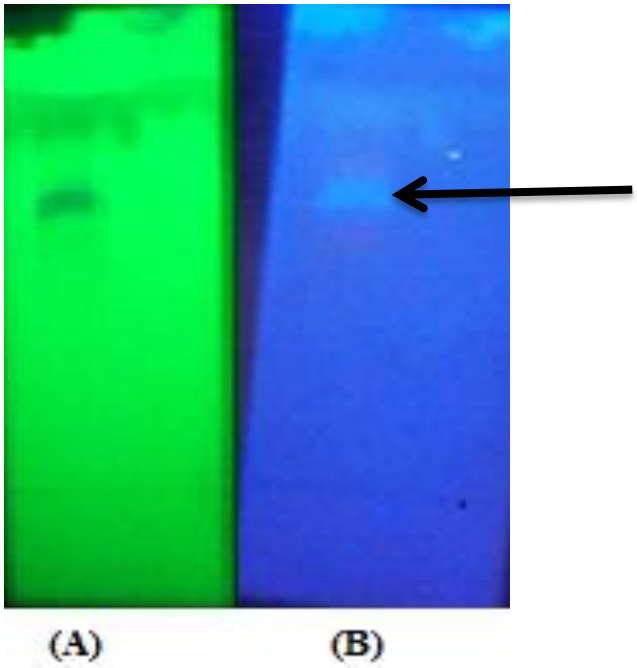

Figure 6. TLC chromatogram of compound **1** (YKFM-2) applied as a spot; viewed under UV 254 (A) and 366 nm (B) light source with the solvent system BAW (butanol: acetic acid:water upper layer; 4:1:5): ethyl acetate (1:1).

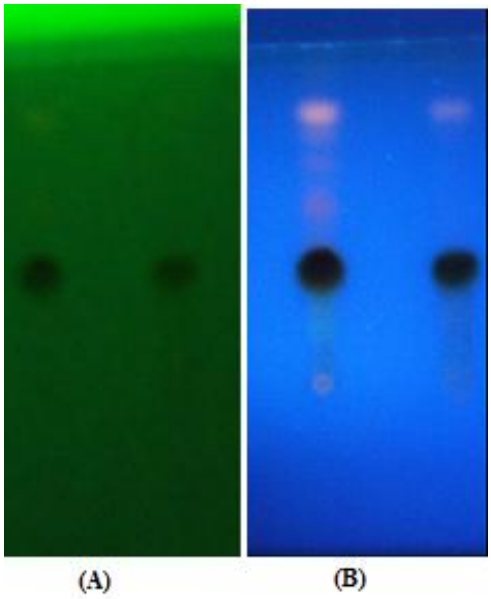

Figure 7. TLC chromatogram of compound **2 (**KFP-1) and compound **5 (**AL-1**)** applied as a spot; viewed under UV 254 (A) and 366 nm (B) light source with the solvent system toluene: ethyl acetate (5:1)**.**

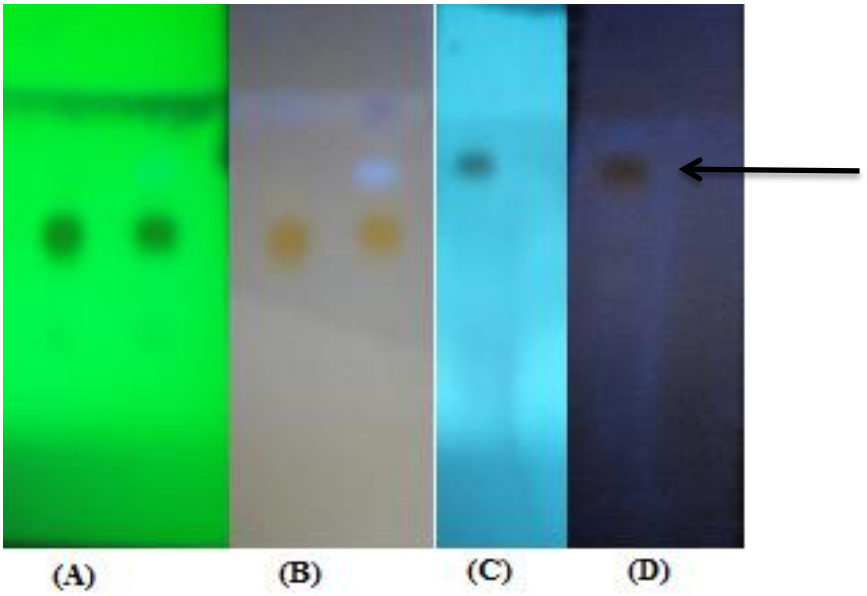

Figure 8. Normal and reversed phase TLC chromatogram of compound **3 (**KFP-3) applied as a spot. A and B are normal phase chromatograms viewed under UV 254 (A) and 366 nm (B) light source with the solvent system $CHCl_3$:MeOH:H_2O (40:10:1); and C and D are reversed phase chromatograms viewed under UV 254 (C) and 366 nm (D) light source with the solvent system MeOH:H_2O (4:1).

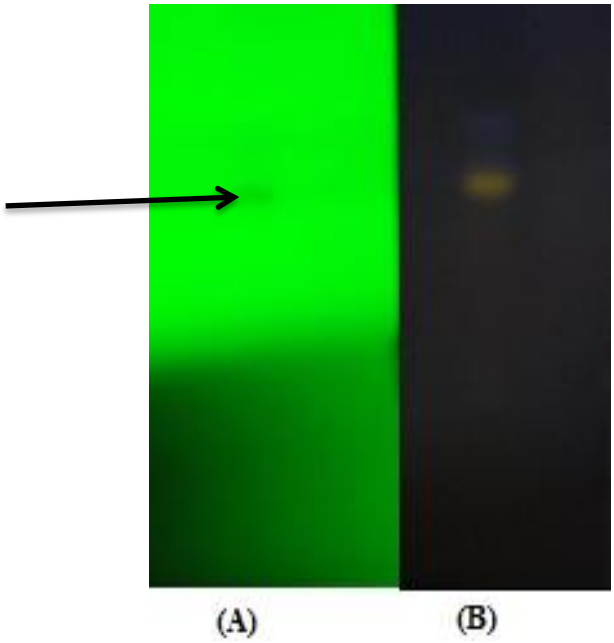

Figure 9. TLC chromatogram of the compound **4** (KFP-5) applied as a spot; viewed under UV 254 (A) and 366 nm (B) light source with the solvent system hexane: ethyl acetate (3:1).

4.2 Structural elucidation compounds 1-4

Compound **1** was obtained as a light red amorphous solid. The positive high resolution-ESI mass spectrum gave a pseudomolecular ion at *m/z* 547.1619 $[M+Na]^+$ (calcd. *m/z* 547.1791 $[M+Na]^+$, corresponding to a molecular formula $C_{25}H_{32}O_{12}$. In the ^1H NMR spectrum, four proton signals which resonated at δ 7.12 (*s*, H-4), 7.28 (1H, *dd*, *J* = 1.3, 7.3 Hz, H-7), 7.36 (1H, *d*, *J* = 8.2 Hz, H-6) and 7.40 (1H, *dd*, *J* = 1.3, 8.2 Hz, H-5) indicated the presence of aromatic ring moiety. Three of these proton signals which are multiplets imply that they are found in close proximity (or are adjacent) and the fourth singlet aromatic proton peak at δ 7.12 (*s*, H-4) provides clues for the presence of a fused aromatic ring system. The presence of a disaccharide unit in compound **1** was revealed by the typical anomeric proton signals at δ 3.31 (1H, *m*, H-4′′) and 5.05 (1H, *d*, *J* = 7.9 Hz, H-1′). The proton peaks from δ 5.05 to 2.91 further justify the presence of a disaccharide moiety. The ^{13}C spectrum region from δ 76.82 to 66.59 also confirmed that the compound

contains a disaccharide moiety. In addition, the two elevated ^{13}C sugar signals at δ 102.84 and 100.86 indicate that the sugar units are linked through acetal bond. Furthermore, the absence of one CH signal in the sugar region (δ 76.82 - δ 66.59) suggests that one of the sugar units is rhamnose. And this was found to be in good agreement with ^{13}C NMR reports of similar glycosides (Cichewicz and Nair, 2002; Dias *et al*., 2009). Hence, the disaccharide moiety was confirmed to be rhamnose-glucose 1,6 linkage. In addition, the presence of 10 ^{13}C signals from δ 154.71 to δ 110.5 implies that the fused aromatic ring system is naphthalene. Six of these carbon signals are absent from DEPT spectrum indicating that they are quaternary aromatic carbons. Besides, two of them are elevated (δ 154.71 and δ 151.49) suggesting that they are oxygenated quaternary aromatic carbons. On the other hand, the two less elevated (δ 136.74 and δ 113.54) quaternary aromatic carbons are the bridgehead carbons of the fused aromatic system (Dias *et al*., 2009). The remaining two quaternary aromatic carbon signals resonated at δ 124.73 (C-2) and δ 133.30 (C-3). Lastly, the ^{13}C signals at 207.7 and 41.3 are the carbonyl carbon and its acetyl methyl. Therefore, based on the above evidence and in comparison with ^{1}H and ^{13}C NMR data of the same and related compounds (Cichewicz *et al*., 2002; Dias *et al*., 2009), compound **1** was characterized as dianellin or 1-(1-hydroxy-3-methyl-8-(((2S,3R,4S,5S,6R)3,4,5-trihydroxy-6-((((2S,3S,4S,5S,6R)3,4,5-trihydroxy-6-methyltetrahydro-2H-pyran-2-yl)oxy) methyl)tetrahydro-2H-pyran-2yl)oxy)naphthalen-2-yl) ethanone (Figure 10). Table 1 summerizes NMR data of compound **1**.

Compound **2** was isolated as an orange colored amorphous solid. The molecular formula was determined as $C_{24}H_{18}O_8$ by positive-ion ESI-MS spectrometry (*m/z* 458.21 $[M+Na]^+$), which was also consistent with ^{1}H and ^{13}C NMR spectral data. The chelated hydroxyl protons shown as singlet peaks at δ 12.6 (1H, *s*, -OH, H-1) and 11.9 (1H, *s*, -OH, H-8) and the typical ABC pattern

of the proton peaks at δ 7.57 (1H, *dd*, *J* = 8, 7 Hz, H-6), 7.55 (1H, *dd*, *J* = 7, 1.5 Hz, H-5), 7.21 (1H, *dd*, *J* = 8, 1.5 Hz, H-7) indicate the presence of chrysophanol moiety. Besides, the singlet aromatic proton signal present at δ 7.28 suggests that it is found adjacent to substituted aromatic carbon. The ^{13}C and DEPT spectrum of compound **2** also supports the presence of chrysophanol moiety (Dagne and Steglich, 1984; Bezabih and Abegaz, 1998). Moreover, from the ^{13}C spectrum, additional aromatic carbon signals at δ 152.44, 132.72, 125.75, 125.31, and 120.11 together with the ^{1}H peaks at 14.3 (*s*, OH), 6.19 (*s*, aromatic H), 5.70 (*s* (*br*), OH) and 3.91 (*s*, OCH_3) indicate the attachment of methyl etherified acetylphloroglucinol moiety to the chrysophanol. These data in comparison with the reported ^{1}H and ^{13}C NMR results identified compound 2 as knipholone (Figure 11). Table 2 summerizes the NMR data of compound **2**.

Compound **3** was obtained as a red solid. The negative-ion ESI-MS of KFP-3 showed molecular ion peak at *m/z* 760.36 $[M]^-$ and its positive-ion ESIMS showed a pseudomolecular peak ion at *m/z* 784.30 $[MH+Na]^+$ (Molecular weight:760.69). This together with the ^{1}H NMR data determined the chemical formula of compound **3** as $C_{36}H_{40}O_{18}$. The fragment ion peak at 325.40 on negative-ion ESIMS (Figure 12) indicates the presence of gentiobiose disaccharide moiety. The fragment ion peak at 717.31 $[M - COCH_3]^-$ on negative-ion ESIMS further infers the compound as a knipholone gentiobioside (Qhotsokoane-Lusunzi and Karuso, 2001a). Giving additional proof was the fragment ion peak at 581.54 [M – acetylphloroglucinol] $^+$ on positive-ion ESIMS (Figure 13). From ^{1}H NMR spectrum, the anomeric protons at δ 5.21 and δ 4.43 and the CH sugar proton peaks from δ 3.1 to 4.5 support presence of gentiobiose moiety. There are five typical knipholone type aromatic proton signals at δ 7.71 (1H, *dd*, *J* = 7.5, 8.4 Hz, H-6), δ 7.6 (1H, *d*, *J* = 6.8 Hz, H-5), δ 7.31 (1H, *s*, H-2), δ 6.9 (1H, *dd*, *J* = 1.1, 8.3 Hz, H-7) and δ 6.14 (1H, *s*, H-5') indicating chrysophanol unit. The singlet aromatic proton at δ 6.14 (*s*, H5′), the

OCH_3 protons at δ 3.89, the acetyl methyl protons at δ 2.52 and hydroxyl protons at δ 4.51 and δ 8.51 prove that the acetylphloroglucinol unit is attached to chrysophanol. Furthermore, the remaining proton signal at δ 2.12 clearly identifies the aglycone to be knipholone (Qhotsokoane-Lusunzi and Karuso, 2001a; Qhotsokoane-Lusunzi and Karuso, 2001b; Abegaz *et al.,* 2002). Therefore, combining these results and in comparison with ^{1}H NMR and ^{13}C NMR data of similar compounds, compound **3** was characterized 10-knipholone gentiobioside or 4-(3-acetyl-2,6-dihydroxy-4-methoxyphenyl)-1,8-dihydroxy-3-methyl-10-(((3R,4S,5S,6R)-3,4,5-trihydroxy-6-((((2S,3R,4S,5S,6R)-3,4,5-trihydroxy-6-(hydroxymethyl)tetrahydro-2H-pyran-2-yl)oxy) methyl)tetrahydro-2H-pyran-2-yl)oxy)anthracen-9(10H)-one (Figure 14). Table 3 summerizes NMR data of compound **3**.

Compound **4** was isolated as a yellow amorphous solid. It exhibited a pseudomolecular ion peak at *m/z* 427 $[M+Na]^+$ on the positive-ion ESI-MS spectrum suggesting its molecular weight to be 404.54. The chemical formula $C_{24}H_{36}O_5$ was deduced for Compound **3** on the basis of ESI-MS and NMR data. In the ^{1}H NMR spectrum, the four distinct aromatic proton signals (at δ 7.85, δ 7.69, δ 7.3, δ 7.12) denote the presence of a disubstituted aromatic ring. The peak at δ 3.7 is indicative of the presence of OCH_3 protons. The broad peak at δ 5.5 CH (SP^2) establishes the presence of double bond. In addition, there is an indication for OCH_2 (at δ 4.35a, 4.15b) and OH proton (at δ 5.13). The proton peak at δ 2.8 affirms the presence of OCH proton (also supported by ^{13}C). The other proton peaks in the upfield region between δ 2.3 and δ 0.89 are congested CH_2 peaks with the one at the end being CH_3 (δ 0.89). In the ^{13}C NMR spectrum, there are 8 signals between δ 135.17 and δ 127.09 in two sets, 6 of them are aromatic ring carbons and two are CH (SP^2) double bond carbons. Furthermore, the two carbonyl carbon peaks shown at δ 174.30 and δ 172.83 suggest the occurrence of esterified OCH_3 and long-chain alkane. This is clearly

supported by the DEPT spectrum which shows a single OCH_2 peak at δ 62.08 and OCH_3 peak at δ 51.42, and the rest of the congested CH_2 carbon peaks are aligned as expected from δ 34.04 to δ 14.12 with peak at δ 14.12 assigned to CH_3 (Peakall, 1975; Amade *et al*., 1994; Sastry and Rao, 1995; Lee *et al*., 2000; Chatterjee and Dutta, 2003). Hence, based on the above data and in comparison with the ^{1}H NMR and ^{13}C NMR of related compounds, the structure of compound **4** was determined to be 12-hydroxypentadec-9-en-1-yl methyl phthalate (HPMP) (Figure 15). Table 4 summerizes NMR data of compound **4**.

Table 1.^{1}H and ^{13}C NMR data of compound **1** measured in deuterated methanol

Present data			Reference data (Cichewicz *et al*., 2002)	
Position	δ_C (ppm)	δ_H (ppm)	δ_C (ppm)	δ_H (ppm)
1	151.49	-	150.2	-
2	124.73	-	125.2	-
3	133.30	-	132.8	-
4	119.58	7.12 (1H, *s*)	119.4	7.21 (1H, *s*)
5	122.58	7.40 (1H, *dd*, *J* = 1.3, 8.2 Hz)	122.3	7.47 (1H, *dd*, *J* = 1.0, 8.0 Hz)
6	127.20	7.36 (1H, *d*, *J* = 8.2 Hz)	127.3	7.40 (1H, *dd*, *J* = 8.0, 8.0 Hz)
7	110.51	7.28 (1H, *dd*, *J* = 1.3, 7.3, Hz)	110.7	7.30 (1H, *dd*, *J* = 1.0, 8.0 Hz)
8	154.71	-	154.2	-
9	113.54	-	113.2	-
10	136.74	-	135.7	-
1′	102.84	5.05 (1H, *d*, *J* = 7.9 Hz)	102.6	5.04 (1H, *d*, *J* = 7.5 Hz)
2′	73.57	3.46 (1H, *t*, *J* = 8.8 Hz)	73.3	3.39 (1H, *m*)
3′	76.82	3.37 (1H, *m*)	76.2	3.36 (1H, *m*)
4′	70.13	2.91 (1H, *m*)	70.1	3.18 (1H, *m*)
5′	76.10	3.68 (1H, *m*)	76.0	3.59 (1H, *m*)
6	66.59	4.05 (1H, *d*, *J* = 8.9 Hz); 3.63 (1H, *m*)	66.6	3.93 (1H, *dd*, *J* = 1.5, 11.0 Hz); 3.50 (2H, *m*)
1″	100.86	4.71 (1H, *d*, *J* = 1.4 Hz)	100.7	4.62 (1H, *d*, *J* = 1.5 Hz)
2″	70.84	3.84 (1H, *dd*, *J* = 1.6, 3.4 Hz)	70.4	3.68 (1H, *m*)
3″	71.03	3.63 (1H, *m*)	70.7	3.50 (2H, *m*)
4″	72.59	3.31 (1H, *m*)	71.9	3.20 (1H, *m*)
5″	68.55	3.52 (1H, *m*)	68.4	3.49 (1H, *m*)
6″	16.55	1.17 (3H, *d*, *J* = 6.2 Hz)	17.7	1.12 (3H, *d*, *J* = 6.0 Hz)
Ar$\underline{CH_3}$	18.49	2.25 (3H, *s*)	19.0	2.25 (3H, *s*)
CO$\underline{CH_3}$	41.3	2.97 (3H, *s*)	31.9	2.52 (3H, *s*)
$\underline{C}OCH_3$	207.07	-	204.4	-

s = singlet, *d* = Doublet, *dd* = Doublet of doublets, *t* = Triplet, *m* = Multiplet.

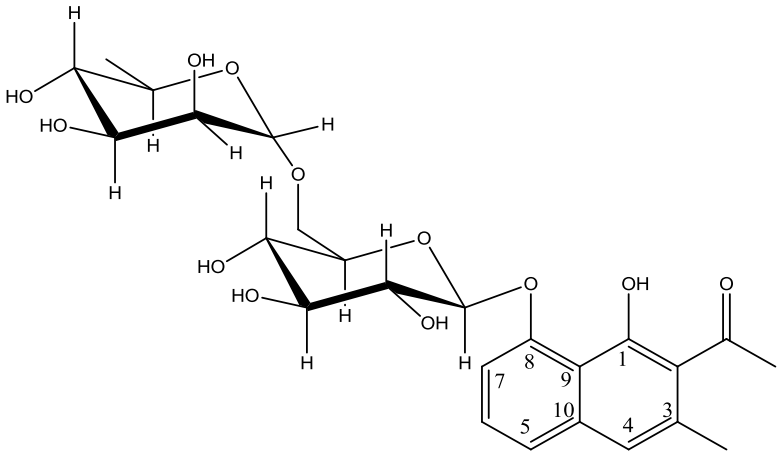

Figure 10. Chemical structure of dianellin

Table 2. ^{1}H and ^{13}C NMR data of compound **2** measured in deuterated chloroform

Present data			Reference data (Bezabih and Abegaz, 1998)	
Position	δ_C (ppm)	δ_H (ppm)	δ_C (ppm)	δ_H (ppm)
1	161.69	12.6 (1H, *s* , -OH)	161.7	12.53 (1H, *s*, -OH)
1a	115.22	-	114.7	-
2	125.31	7.28 (1H, *s*)	124.6	7.32 (1H, *q*, *J* = 0.7 Hz)
3	152.44	-	151.6	
4	125.75	-	128.5	
4a	132.72	-	131.6	
5	120.11	7.55 (1H, *dd*, *J* = 1.5, 7 Hz)	119.3	7.56 (1H, *dd*, *J* = 1.5, 7 Hz)
5a	134.27	-	134.4	
6	137.12	7.57 (1H, *dd*, *J* = 7, 8 Hz)	137.4	7.75 (1H, *dd*, *J* = 7, 8 Hz)
7	123.85	7.21 (1H, *dd*, *J* = 1.5, 8 Hz)	123.3	7.30 (1H, *dd*, *J* = 1.5, 8 Hz)
8	159.51	11.9 (1H, *s*, -OH)	161.1	12.0 (1H, *s*, -OH)
8a	115.37	-	115.5	-
9	192.68	-	192.5	-
10	182.66	-	181.9	-
1′	106.07	-	104.7	-
2′	163.27	5.7 (1H, *s* (*br*), -OH)	163.3	8.95 (1H, *s* (*br*), -OH)
3′	107.14	-	107.3	-
4′	163.07	-	162.4	-
5′	90.61	6.19 (1H, *s*)	91.2	6.24 (1H, *s*)
6′	162.85	14.3 (1H, *s*, -OH)	161.9	-
$ArCH_3$	21.02	2..21 (3H, *s*)	20.4	2.17 (3H, *d*, *J* = 0.7 Hz)
OCH_3	55.56	3.91 (3H, *s*)	55.6	3.98 (3H, *s*)
$CO\underline{CH_3}$	33.14	2.70 (3H, *s*)	32.6	2.62 (3H, *s*)
$\underline{C}OCH_3$	202.3	-	202.3	-

s = singlet, *d* = Doublet, *dd* = Doublet of doublets, *q* = Quartet, *m* = Multiplet, *br* = Broad.

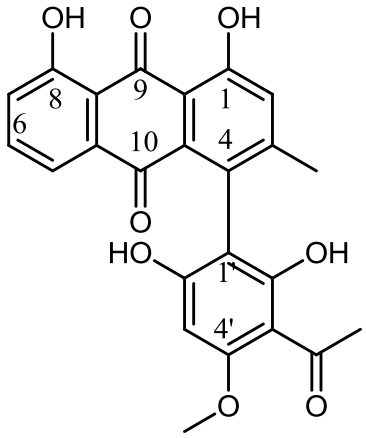

Figure 11. Chemical structure of knipholone

Table 3. ^{1}H NMR data of compound **3** measured in deuterated methanol

Position	δ_H (ppm)	Position	δ_H (ppm)
1	-	5′	6.14 (1H, *s*)
1a	-	6′	8.52 (1H, *s*, -OH)
2	7.31 (1H, *s*)	$ArCH_3$	1.91(3H, *s*)
3	-	OCH_3	3.89 (3H, *s*)
4	-	$CO\underline{CH_3}$	2.52 (3H, *s*)
4a	-	$\underline{C}OCH_3$	-
5	7.6 (1H, *d*, *J* = 6.8 Hz)	1″	5.21 (1H, *d*, *J* = 7.9)
5a	-	2″	3.57-3.66 (1H, *m*)
6	7.71 (1H, *dd*, *J* = 7.5, 8.4 Hz)	3″	3.50-3.53 (1H, *m*)
7	6.9 (1H, *dd*, *J* = 1.1, 8.3 Hz)	4″	3.42-3.47 (1H, *m*)
8	-	5″	3.42-3.47 (1H, *m*)
8a	-	6″	3.83 (1H, *m*, a), 4.54 (1H, *m*, b)
9	-	1‴	4.43(1H, *m*)
10	-	2‴	3.15 (1H, *m*,1H)
1′	-	3 ‴	3.19 - 3.24 (1H, *m*)
2′	4.51 (1H, *s* (*br*), -OH)	4‴	3.50-3.53 (1H, *m*)
3′	-	5‴	3.57-3.66 (1H, *m*)
4′	-	6‴	4.19 (1H, *m*, a), 33.57-3.66 (1H, *m*, b)

s = singlet, *d* = Doublet, *dd* = Doublet of doublets, *m* = Multiplet, *br* = Broad.

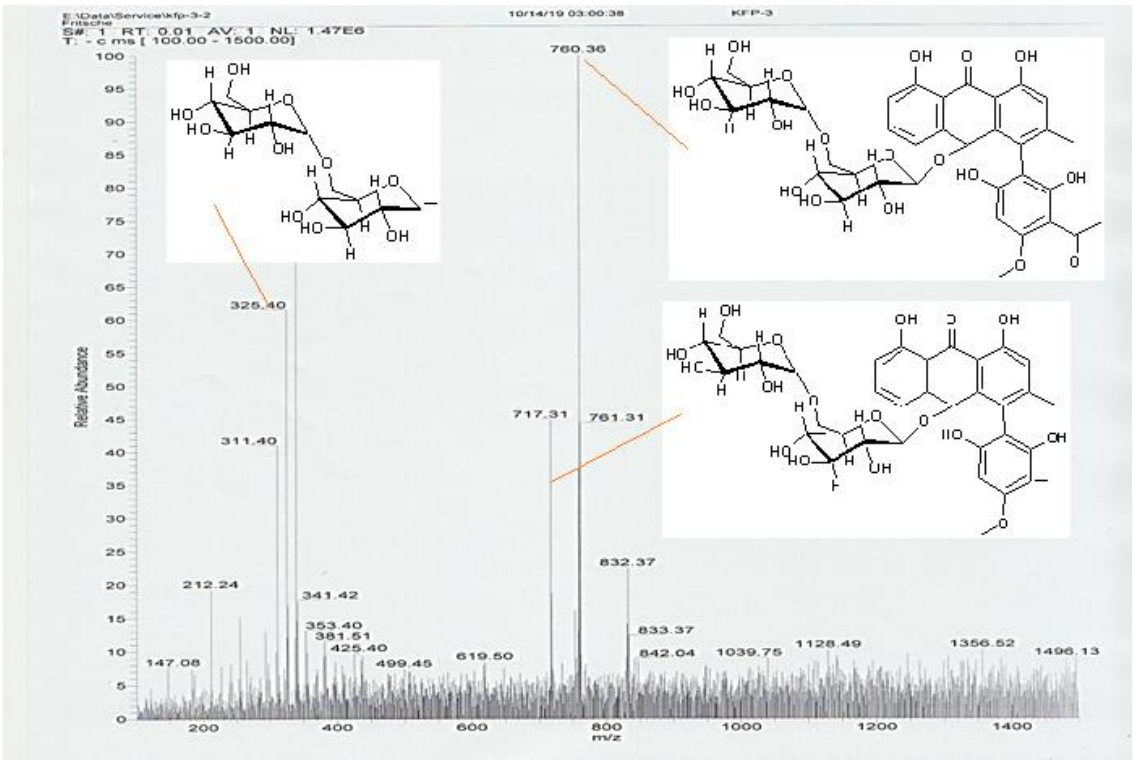

Figure 12. : Negative mode mass fragmentation pattern of compound **3**

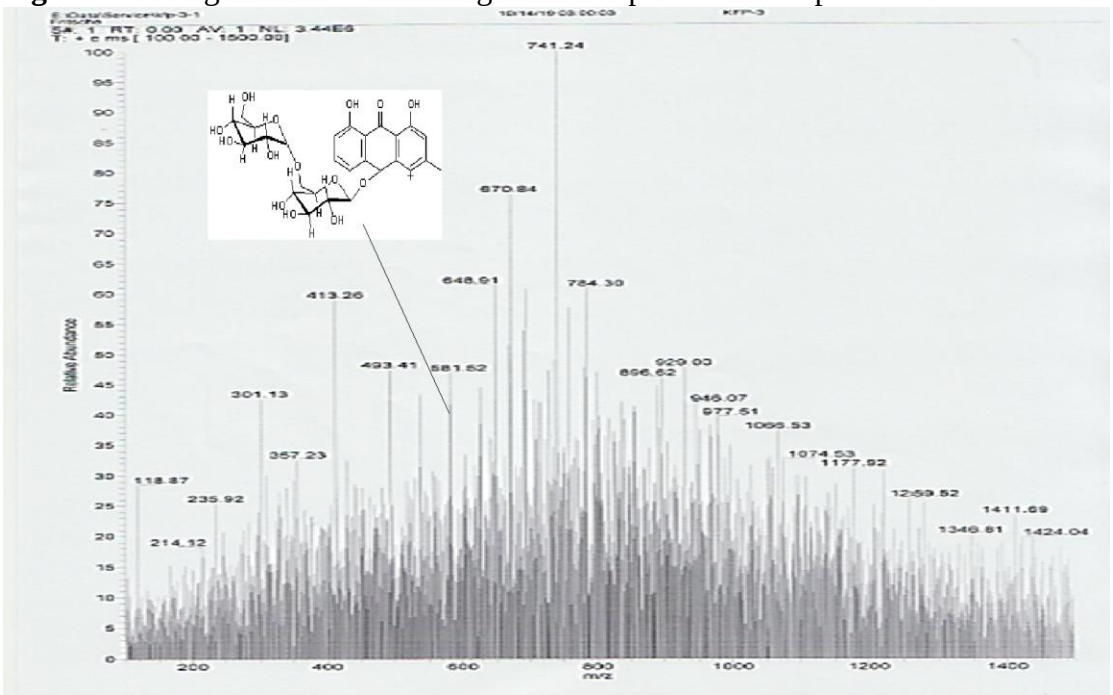

Figure 13. : Positive mode mass fragmentation pattern of compound **3**

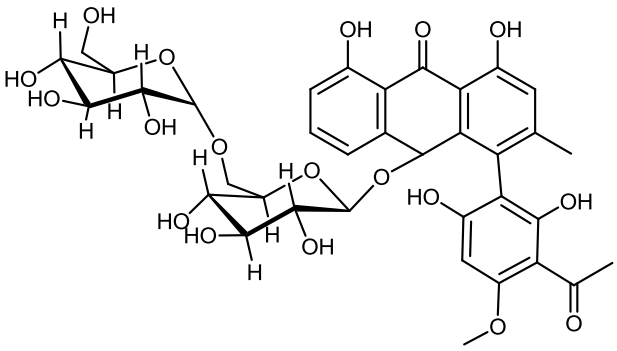

Figure 14. Chemical structure of 10-knipholone gentiobioside

Table 4. ^{1}H and ^{13}C NMR data of compound **4** measured in deuterated chloroform

Position	δ_C (ppm)	δ_H(ppm)
1	14.12	0.89 (3H, *s*)
2	22.58	1.20-1.40 (2H, *m* (*br*))
3	34.09	1.20-1.40 (2H, *m* (*br*))
4	68.86	2.80 (1H, *br*)
5	39.72	2.30 (2H, *s*)
6	129.88	5.50 (1H, *br*)
7	129.72	5.50 (1H, *br*)
8	32.19	2.11 (2H, *s*)
9	29.27	1.20-1.40 (2H, *m* (*br*)))
10	29.16	1.20-1.40 (2H, *m* (*br*))
11	29.27	1.20-1.40 (2H, *m* (*br*))
12	26.39	1.20-1.40 (2H, *m* (*br*))
13	25.61	1.20-1.40 (2H, *m* (*br*))
14	27.19	1.60 (2H, *s*)
15	62.86	4.35 (1H, a), 4.15 (1H, b)
1	135.17	-
2	129.07	-
3	128.26	7.85 (1H, *m*)
4	130.01	7.30 (1H, *m*)
5	130.18	7.12 (1H, *m*)
6	128.02	7.69 (1H, *m*)
CO<u>CH$_3$</u>	51.42	3.70 (3H, *s*)
<u>C</u>OCH$_3$	174.30	-
<u>C</u>OO	173.26	-

s = singlet, *m* = Multiplet, *br* = Broad.

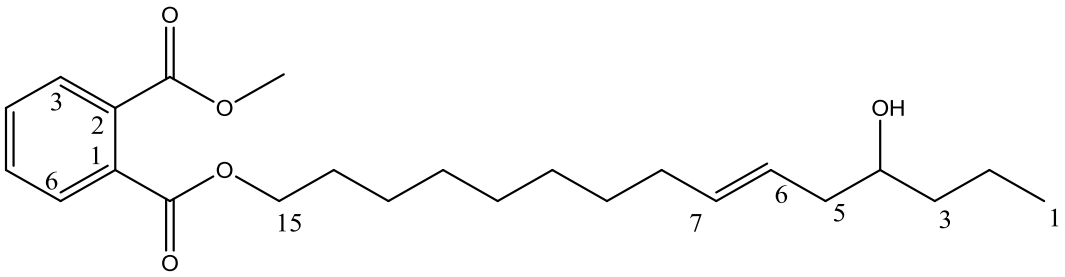

Figure 15. Chemical structure of 12-hydroxypentadec-9-en-1-yl methyl phthalate

4.3 Structural elucidation compound 5

Compound 5 was isolated from the rhzome extract of *K. insignis* as a red solid. The ESI-MS spectrum of compound **5** displayed a molecular ion peak $[M]^+$ at *m/z* 434 (calcd. *m/z* 434.39 $[M]^+$), this in conjuction with HNMR data detrmined the chemical formula to be $C_{24}H_{18}O_8$. It showed similar ^{1}H NMR spectrum with compound **2** and reported results of knipholone. Therefore, based on ESIMS and ^{1}H NMR spectra and by analytical co-TLC with compound **2**, the chemical structure of compound **5** was found to be that of knipholone (Figure 11). This was the first report of knipholone from *K. insignis.* Table 5 summerizes NMR data of compound **5**.

4.4 Acute toxicity

The acute toxicity test results of this study documented that the 80% methanol extracts of *K. foliosa* and *K. insignis*, knipholone and dianellin were safe by oral route at a dose of 2000 mg/kg (OECD, 2008; Gereziher *et al.*, 2014). After 72 h, the animals tolerated the administered dose although immediate mild toxicity sings such as ruffled fur, loss of appetite and slight sleepiness, which disappeared few hours after administration were observed. Also, there was no mortality within 14 days of observations which entails that the LD_{50} of the extracts knipholone and dianellin was above 2000 mg/kg.

Table 5. ^{1}H NMR data of compound **5** measured in deuterated chloroform

Present data		Refernce data (Bezabih and Abegaz, 1998)
Position	δ_H (ppm)	δ_H (ppm)
1	12.1 (1H, *s* (*br*), -OH)	12.53 (1H, *s*, -OH)
1a	-	-
2	7.31 (1H, *s*)	7.32 (1H, *q*, *J* = 0.7 Hz)
3	-	
4	-	
4a	-	
5	7.65 (1H, *dd*, *J* = 1.5, 7 Hz)	7.56 (1H, *dd*, *J* = 1.5, 7 Hz)
5a	-	
6	7.74 (1H, *dd*, *J* = 7, 8 Hz)	7.75 (1H, *dd*, *J* = 7, 8 Hz)
7	7.12 (1H, *dd*, *J* = 1.5, 8 Hz)	7.30 (1H, *dd*, *J* = 1.5, 8 Hz)
8	11.55 (1H, *s*, -OH)	12.0 (1H, *s*, -OH)
8a	-	-
9	-	-
10	-	-
1’	-	-
2’	-	8.95 (1H, *s* (*br*), -OH)
3’	-	-
4’	-	-
5’	6.18 (1H, *s*)	6.24 (1H, *s*)
6’	14.3 (1H, *s*, -OH)	-
$ArCH_3$	2.28 (3H, *s*)	2.17 (3H, *d*, *J* = 0.7 Hz)
OCH_3	3.9 (3H, *s*)	3.98 (3H, *s*)
$CO\underline{CH_3}$	2.7 (3H, *s*)	2.62 (3H, *s*)
$\underline{C}OCH_3$	-	-

s = singlet, *dd* = Doublet of doublets, *q* = Quartet, *br* = Broad.

4.5 Antimalarial activity of the extracts of *K. folosia* and *K. insignis*

The 80% methanol extracts of *K. foliosa* and *K. insignis* showed chemosuppressive effect against *P. berghei* in mice (Figure 16). At all dose level tested, both extracts exhibited a statistically significant ($p<0.001$) dose dependent effect (Table 6). However, the 80% extract of *K. folosia* was found to have higher activity than *K. insignis* with 61 and 50 % suppression at 200 and 400 mg/kg, respectively. Moreover, the extract of *K. folosia* significantly extended the survival days

of treated groups at 200 and 400 mg/kg compared with the negative controls, indicating that the extract has the capacity to lower the overall pathologic effect of the parasite in mice. *K. insignis* extract did not show a significant prolongation of mean survival days. In both plant extracts, there was no significant difference in percent change in weight (before and after the treatment) among groups compared with the positive control (Table 7).

According to Deharo *et al.* (2001), the 80 % extract of *K. folosia* can be regarded as good in its antimalarial activity since it showed greater than 50% suppression at a dose of 200 mg/kg. Likewise, the 80% extract of *K. insignis* was considered moderate as it showed greater than 50% activity at a dose of 400 mg/kg. Previous studies demonstrated that medicinal plants rich in anthraquinones such as aloes and senna possess notable *in vivo* antimalarial activity (Abosi and Raseroka, 2003; Kaou *et al*., 2008; Biruk *et al*., 2020). Hence, the antimalarial activity of the two extracts could be mainly due to the anthaquniones —including the phenylanthaquniones like knipholone and its glycosides —together with other constituents present in them. This study is the first account of *in vivo* antimalarial report of both plants and the genus *Kniphofia* as well.

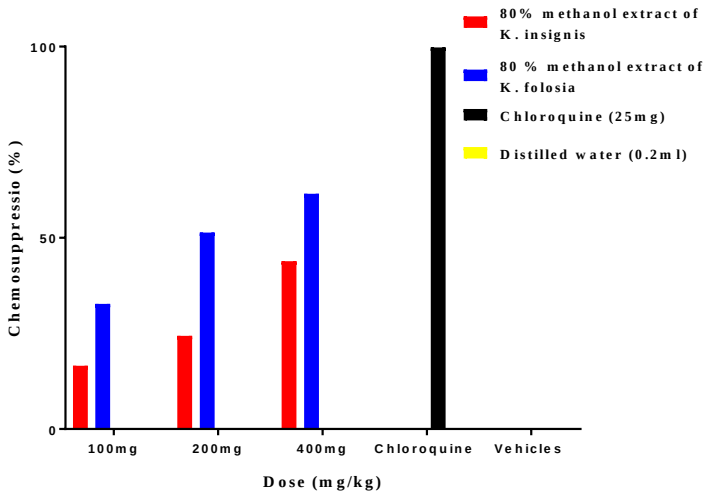

Figure 16. Percent chemosuppression effect of 80% rhizome extracts of *Kniphofia foliosa* and *Kniphofia insignis* in mice infected with *P. berghei* in 4 day suppression test; Values are presented as mean ± SEM; n =5.

Table 6. Antimalarial activity of the 80 % rhizome extracts of *Kniphofia foliosa* and *Kniphofia insignis* in mice infected with *Plasmodium berghei*.

Test substances	Dose (mg/kg/day)	Percent parasitaemia	Percent Suppression	Mean survival time (in days)
Vehicle1	0.2ml	35.9860±1.22034	0.0000	6.0000±.31623
KF100	100	24.2100±1.18037	32.7200^{a*d**e*i*}	9.4000±0.50990^{a**i*}
KF200	200	17.4920±0.67964	51.3900^{a*c**i*}	9.6000±0.92736^{a*i*}
KF400	400	13.8480±0.76024	61.5200^{a*c*i*}	8.4000±0.24495^{i*}
Vehicle4	0.2ml	41.0760±1.36009	0.0000	5.8000±.58310
KI100	100	34.2680±1.27062	16.5700^{e*h*i*}	7.6000±0.24495^{i*}
KI200	200	31.0720±.99973	24.3500^{e*h*i*}	8.0000±0.00000^{i*}
KI400	400	23.0560±.93552	43.8700^{e*f*g*i*}	8.2000±0.66332^{i*}
Chloroquine	25	.0140±.00600	99.8000^{a-h*}	27.2000±.58310^{a*b*c*d*e*f*8*h*}

Values are presented as mean ± SEM; n = 5; a = compared to vehicle1 (distilled water), b = compared to KF100, c = compared to KF200, d = compared to KF400, e = compared to vehicle4 (distilled water), f = compared to KI-100mg, g = compared to KI200, h = compared to KI400, i= compared to chloroquine; * ($p < 0.001$); **($p < 0.01$); KF= 80 % methanol extract of *K. foliosa*, KI= 80% methanol extract of *K. insignis*; numbers refer to doses in mg/kg/day.

4.6 Antimalarial activity of the phenol fractions and compounds isolated from *K. foliosa*

The two phenolic fractions of *K. folosia* were also found to have activity against *P. berghei* in mice (Table 8). Compared to their respective negative controls, both factions possessed significant suppressive activity at all dose levels tested. They showed the highest activity at 400 mg/kg with fraction 1 and fraction 2 causing 46.32% and 47.53% suppression, respectively. Both fractions prolonged the mean survival days of the treatment groups by 2 days relative to their negative controls although it was not statistically significant. No significant difference in percent change in weight was noted in the treatment groups when compared with the positive controls (Table 9). Therefore, it can be deduced that the phenolic fractions of *K. folosia* are moderate in

their *in vivo* antimalarial activity, congruent with earlier reports that extracts containing phenolic compounds and their glycosides have modest levels of antiplasmodial activity (Liu *et al.,* 2007; Bankole *et al.,* 2015; Alson *et al.,* 2018). Furthermore, owing to the antioxidant nature of many phenolic compounds, the suppressive action of the fractions could in part be as a result of inhibition of the oxidative damage caused by the parasite on infected erythrocytes (Miyachi *et al*., 1986; Kling *et al*., 2014).

Table 7: Body weight of *Plasmodium berghei* infected mice before and after administration of the 80% rhizome extracts of *Kniphofia foliosa* and *Kniphofia insignis*

Test substances	Dose (mg/kg/day)	Pretreatment body weight	Post treatment body weight	Percentage change %
Vehicle1	0.2ml	22.5280± 0.64006	22.9340±1.57639	1.8071±6.48589^{h**}
KF100	100mg	23.2720±0.42033	22.2280±.88663	-4.3152±4.54610^{h*}
KF200	200mg	24.4620±.63663	22.6660±.70278	-7.3684±1.10718^{h*}
KF400	400mg	23.0960±.56001	22.6580±1.25293	-1.2013±7.85001^{h*}
Vehicle4	0.2ml	22.7940±0.87239	19.8260±0.58504	--12.7886±2.30362^{h*}
KI100	100mg	26.1920±0.67468	24.1560±.70728	-7.8079± 0.33696^{h*}
KI200	200mg	26.9440±0.53491	25.9740±.58891	-3.6216±.27929^{h*}
KI400	400mg	26.5140±0.34460	24.9860±.49836	-5.7131±2.09832^{h*}
Chloroquine	25mg	22.7060±0.64006	27.5960±.65512	21.9779±3.36183^{a*b*c*d*e*f*g*}

Values are presented as mean ± SEM; n = 5; a = compared to vehicle1 (distilled water), b = compared to KF100, c = compared to KF200, d = compared to KF400, e = compared to vehicle4 (distilled water), f = compared to KI-100mg, g = compared to KI200, h = compared to KI400, i= compared to chloroquine; * ($p < 0.001$); **($p < 0.01$); KF= 80 % methanol extract of *K. foliosa,* KI= 80% methanol extract of *K. insignis*; numbers refer to doses in mg/kg/day.

Although all the compounds showed significant suppression at all dose levels tested (Table 10), 10-knipholone gentiobioside displayed superior activity with percent suppression values of 55.38

and 79.34% at doses of 50 and 100 mg/kg, respectively. Knipholone also revealed a percent suppression value of 55.4% and 60.16% at 100 mg/kg and 200 mg/kg doses, respectively. Moreover, it significantly prolonged the mean survival days of the treatment groups (Table 10). The dose-response plot (Figure 17) disclosed that the ED_{50} values of 10-knipholone gentiobioside, knipholone and dianellin were 29.04, 81.25 and 92.31 mg/kg, respectively. However, none of the compounds caused significant difference in percent change of weight among the treated groups (Table 11).

Table 8. Antimalarial activity of the phenolic fractions of rhizome of *Kniphofia foliosa* in mice infected with *Plasmodium berghei*

Test substances	Dose (mg/kg/day)	Percent Parasitaemia	Percent suppression	Mean survival time (in days)
Vehicle1	0.2ml	38.25400±0.61845	0.0000	6.0000±0.70711
P-F1	100	26.5120±1.24295	30.3500^{a*i*}	7.8000±1.30384^{i*}
P-F1	200	24.1000±1.27770	37.0700^{a*i*}	8.2000±1.64317^{i*}
P-F1	400	20.6240±1.56333	46.3200^{a*i*}	8.2000±1.09545^{i*}
Vehicle2	0.2ml	35.9860±1.22034	0.0000	6.0000±.31623
P-F2	100	26.2020±1.35847	27.1900^{a**h**i*}	8.2000±1.09545^{i*}
P-F2	200	21.9360±1.75275	39.0400^{a*i*}	7.6000±1.14018^{i*}
P-F2	400	18.8820±.98484	47.5300^{a*f**i*}	8.2000±0.83666^{i*}
Chloroquine	25	0.0140±.00600	99.8000^{a*}	27.2000±.58310^{a*b*c*d*e*f*g*h*}

Values are presented as mean ± SEM; n = 5; a = compared to vehicle-1 (1% tween 80), b = compared to P-F1 100mg, c = compared to P-F1 200 mg, d = compared to P-F1 400 mg, e = compared to vehicle-2 (distilled water), f = compared to P-F2 100 mg, g = compared to P-F2 200 mg, h = compared to P-F2 400 mg, i= compared to chloroquine, * ($p < 0.001$); **($p < 0.01$); PF-1 = phenol fraction-1 of *K. foliosa*, PF-2 = phenol fraction-2 of *K. folosia*; numbers refer to doses in mg/kg/day.

Table 9: Body weight of *Plasmodium berghei* infected mice before and after administration of the phenolic fractions of rhizome of *Kniphofia foliosa*

Test substances	Dose (mg/kg/day)	Pretreatment body weight	Post treatment body weight	Percentage change %
Vehicle1	0.2ml	25.2800±0.80381	20.1900±0 .34663	-6.9917±1.60266i*
P-F1	100	23.7420±0.44124	21.0380±0.15519	-9.4485±2.16900^{i}*
P-F1	200	24.9480±0.46938	23.9980±1.08998	-11.7442±3.66979^{i*}
P-F1	400	22.2880±0.70354	23.1760±0.86142	-4.5356±6.11778^{i*}
Vehicle2	0.2ml	22.5280±0.64006	22.9340±1.57639	1.8071±6.48589^{i*}
P-F2	100	26.0260±0.97783	21.3100±0.17714	-14.3463±3.80786^{i8}
P-F2	200	25.5600±0.36778	22.9800±0.80603	-16.9997±3.11504^{e***i*}
P-F2	400	25.1780±0.76047	21.9020±0.25958	-13.2048±1.66398^{i*}
Chloroquine	25	22.7060±0.91185	27.5960±0.65512	21.9779±3.36183^{a*b*c*d*e*f*g*h*}

Values are presented as mean ± SEM; n = 5; a = compared to vehicle-1 (1% tween 80), b = compared to P-F1 100 mg, c = compared to P-F1 200 mg, d = compared to P-F1 400 mg, e = compared to vehicle-2 (distilled water), f = compared to P-F2 100 mg, g = compared to P-F2 200 mg, h = compared to P-F2 400mg, i = compared to chloroquine, * ($p < 0.001$); **($p < 0.01$); PF-1 = phenol fraction-1 of *K. folosia* , PF-2 = phenol fraction-2 of *K. folosia*; numbers refer to doses in mg/kg/day.

Previously, the methanol and dichloromethane extracts of *K. folosia* as well as dimeric anthraquinones and knipholone isolated therefrom have been shown to have *in vitro* activity against chloroquine-resistant 3D7 strains of *P. falciparum*. The ED_{50} of knipholone against 3D7 strains was 1.49 ug/ml (Wube *et al*., 2005). In addition, knipholone isolated from *Bulbine capitata* and *Bulbine frutescens* has been reported to possess *in vitro* activity against chloroquine-resistant (K1) and chloroquine-sensitive (NF54) strains with IC_{50} values of 1.06 and 1.7 µM, respectively (Bringmann *et al*., 1999; Abegaz *et al*., 2002). In this study the acute toxicity as well as the *in vivo* antiplasmodial activities of the various extracts of *K. folosia* and their major constituents together with the 80% extract of *K. insignis* were evaluated against *P.*

berghei in mice. Since members of the genus *Kniphofia* have been documented to produce anthraquinones and related phenols (Dai *et al*., 2014; Sema *et al*., 2018), the total extract was further fractionated into phenolic and nonphenolic fractions. Results of the current study demonstrated that the hydroalcoholic extracts, the fractions as well as the isolated compounds significantly suppressed parasitemia indicating that they possesses blood schizonticidal activity on early infection of mice with *P. berghei*.

Table 10. Antimalarial activity of knipholone, dianellin and 10-kniphplone gentibioside in mice infected with *Plasmodium berghei*

Test substances	Dose (mg/kg/day)	Percent parasitaemia	Percent suppression	Mean survival time (in days)
Vehicle3	0.2ml	46.3560±1.46925	0.0000	6.4000±0.50990
Knipholone	25	30.5440±1.45634	34.1200^{a*d*e*g*h*m*}	8.8000±0.37417^{m*}
	50	26.2640±1.80001	42.6400^{a*e**h*m*}	9.0000±0.54772^{m*}
	100	20.7940±0.91475	55.1400^{a*b*f**e**h*m*}	9.2000±0.73485^{a***m*}
	200	18.4680±0.97391	60.1600^{a*b*c**f*h*m*}	9.4000±0.24495^{a**m*}
KFP-3	25	28.6680±0.84123	38.1600^{a*d**e*g**h*m*}	8.8000±0.37417^{m*}
	50	20.8900±0.55842	55.3800^{a*b*f**h*m*}	8.4000±0.60000^{m*}
	100	9.5780±0.31091	79.3400^{a*b*c*d*f*g*m*}	9.0000±0.44721^{m*}
Vehicle4	0.2ml	41.0760±1.36009	0.0000	5.8000±0.58310
Dianellin	25	28.8220±0.96771	29.8300^{i*k*l*m*}	7.6000±0.24495^{m*}
	50	22.9860±0.77243	44.0400^{i*j*l*m*}	8.2000±0.37417^{m*}
	100	18.9900±0.84156	53.7700^{i*j*k*m*}	8.2000±0.37417^{m}
Chloroquine	25	0.0140±0.00600	99.8000$^{a–l\ *}$	27.4000±.400000$^{a–l*}$

Values are presented as mean ± SEM; n = 5; a = compared to vehicle3 (distilled water), b = compared to knipholone 25 mg, c = compared to knipholone 50 mg, d = compared to knipholone 100 mg, e = compared to knipholone 200 mg, f = compared to KFP-3 25 mg, g = compared to KFP-3 50 mg, h = compared to KFP-3 100mg, i = compared to vehicle4 (distilled water), j= compared to dianellin 25 mg, k = compared to dianellin 50 mg, l = compared to dianellin 100 mg, m = compared to chloroquine; * ($p < 0.001$); **($p < 0.01$); ***($p < 0.05$); KPF-3 = 10-kniphoplone gentibioside; numbers refer to doses in mg/kg/day.

Table 11. Body weight of *Plasmodium berghei* infected mice before and after administration of knipholone, dianellin and 10- kniphplone gentibioside

Test substances	Dose (mg/kg/day)	Pretreatment body weight	Post treatment body weight	Percentage change %
Vehicle3	0.2ml	23.3500±0.80061	20.1900±0.34663	-3.1600±0.73963 ^{m*}
Knipholone	25	22.8100±0.73340	21.0380±0.15519	-1.7720±0.58177 ^{m*}
	50	24.9940±0.81215	23.9980±1.08998	-0.9960±0.28351 ^{m*}
	100	25.1600±0.72600	23.1760±0.86142	-1.9840±0.15914 ^{m*}
	200	25.9820±0.10322	23.4680±0.75774	-2.5140±0.66363 ^{m*}
KFP-3	25	25.5160±0.21551	25.8240±0.36601	0.3080±0.49318m**
	50	24.1060±0.83333	24.6820±0.50201	0.5760±0.38132m**
	100	23.9060±0.51124	22.5260±0.17589	-1.3800±0.33685^{m*}
Vehicle4	0.2ml	22.7940±0.87239	19.8260±.58504	-2.9680±0.63845 ^{m*}
Dianellin	25	23.4100±0.40104	21.3100±0.17714	-2.1000±0.35937 ^{m*}
	50	25.5000±0.36742	22.9800±0.80603	-2.5200±0.56096 ^{m*}
	100	22.4060±0.77152	21.9020±0.25958	-0.5040±0.71583 ^{m*}
Chloroquine	25	22.7060±0.91185	27.5960±0.65512	4.8900±0.63426$^{a–e*f**g**h–l*}$

Values are presented as mean ± SEM; n = 5; a = compared to vehicle3 (distilled water), b = compared to knipholone 25 mg, c = compared to knipholone 50 mg, d = compared to knipholone 100 mg, e = compared to knipholone 200 mg, f = compared to KFP-3 25 mg, g = compared to KFP-3 50 mg, h = compared to KFP-3 100 mg, i = compared to vehicle4 (distilled water), j= compared to dianellin 25mg, k = compared to dianellin 50 mg, l = compared to dianellin 100 mg, m = compared to chloroquine; * ($p < 0.001$); **($p < 0.01$); ***($p < 0.05$); KPF-3 = 10-kniphplone gentiobioside; numbers refer to doses in mg/kg/day.

The results also revealed that the *in vivo* ED_{50} values of knipholone (81.25 mg/kg) correlate well with its reported *in vitro* activities. After 4 days of treatment with different doses of knipholone, 10-knipholone gentiobioside and dianellin, there were significant differences in percent parasite suppression among the treatment groups. However, there was no significant change in mean survival time among mice administered with different doses of knipholone, 10-knipholone

gentiobioside and dianellin except that the animals which received 100 and 200 mg/kg of knipholone survived longer than those given 25 mg/kg of the compound. This is an indication that the different doses of the test compounds have the same effect on overall pathologic effect of the parasite in mice concurrent with previous results obtained for the crude extract and solvent fractions of *Strychnos mitis* leaves (Fentahun *et al*., 2017). To the best of our knowledge, this is the first report on acute toxicity and *in vivo* antimalarial evaluation of *K. folosia*, *K. insignis* and their constituents.

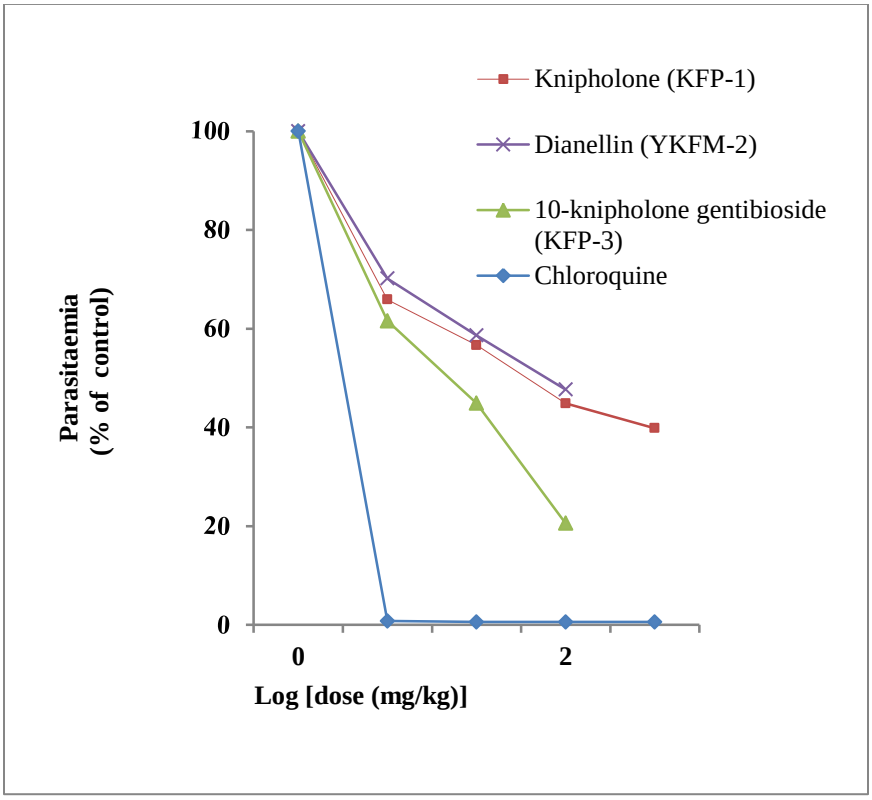

Figure 17. Antimalarial activity of knipholone, dianellin and 10-kniphplone gentiobioside in mice infected with *Plasmodium berghei.* The ED_{50} was estimated from a plot of log dose against parasitaemia (expressed as a percentage of the control); Values are presented as mean ± SEM; n = 5.

Perusal of literature reveals that a number of promising anthraquinones and preanthraquinones leads such as visimione, rufigallol, uveoside, aloin and phenyl anthraquinones have been isolated and/or synthesized (Winter *et al*., 1996; François *et al*., 1999; Hernández-Medel and Pereda-Miranda, 2002; Wube *et al*., 2005; Asamenew *et al*., 2014). These compounds are considered as oxidants like artemisinins and 4-aminoquinolines. More importantly, they are catalytic oxidants that enhance the production of reactive oxygen species (ROS) inside parasitized erythrocytes or increase these cells' susceptibility to oxygen radicals. The free oxygen radicals formed interact with heme or other biomolecular targets inhibiting its tetramerazition to the insoluble hemozoin (malaria pigment) (Ignatushchenkoa *et al*., 1997; Ziegler *et al*., 2002). Knipholone, being an anthraquinone derivative, is anticipated to undergo one-electron oxidation and subsequently interact with heme (or other biomolecular targets) thereby inhibiting its tetramerzation (or detoxification of heme). Similarly, because of the structural similarity of dianellin with phlorizin, a monoglucosidechalcone, its antimalarial mechanism of action could be due to inhibition of the solute transporter of the host cell membrane induced by the parasite invasion (Kutner *et al*., 1987; Ehrenkranz *et al*., 2005).

4.7 Molecular docking study

To get further insight on the mechanism of action of the isolated compounds and to study their binding interaction and identify hypothetical binding motifs, a docking study of knipholone**,** dianellin, HPMP, 10 knipholone gentiobioside and the standard antimalarial drugs chloroquine and artemisinin were carried out on two crystal structures of enzymes. The two *Plasmodium* enzymes were plasmepsin II (PDB code 4cku) involved in haemoglobin metabolism by the parasite, and *P. falciparum* l-lactate dehydrogenase (pfLDH) (PDB code 1ldg) involved in

glycolysis (or glucose metabolism of the parasite) (Bazik *et al*., 1993; Silva *et al*., 1996; Noteberg *et al*., 2003). There is a strong suggestion that haemoglobin digesting enzymes found in the food vacuole of the plasmodium and pfLDH are potential antimalarial chemothaputic targets for chloroquine and related aminoquionlones, anthraquinones and other oxidative phenolic compounds (Slater, 1993; Ignatushchenkoa *et al*., 1997; Haque *et al*., 1999; Pagola *et al*., 2000; Choi *et al*., 2007; Alessandro *et al*., 2013; Tiwari *et al*., 2017; Cheuka *et al*., 2020; de Sousa *et al*., 2020). Gossypol and other phenolic compounds were also found to be pfLDH inhibitors (Conners *et al*., 2005; Megnassan *et al*., 2012). Besides, chloroquine has been found to bind to the cofactor (NADH) binding site of pfLDH acting as a competitive inhibitor (Read *et al*., 1999). Table 12 shows *in silico* prediction of the physicochemical properties; partition coefficient (Log P), aqueous solubility (Log S), and partition coefficient for partially dissociated compounds (Log D) of the isolated compounds and P2FE-400, a designed inhibitor of plasmepsin II.

The binding modes of P2FE-400, knipholone, HPMP and chloroquine to plasmepsin II are shown in Figure 18. P2FE-400 showed the highest and strongest affinity for the aspartic protease, plasmepsin II, with the HYDE score of -38.3 KJ/mol (Table 13). The aspartic protease plasmepsin II has two aspartic acid residues Asp34 and Asp214 (the catalytic dyad) that serve as proton donors and acceptors, respectively, in the amide hydrolysis of peptide bonds in proteins. As shown in the current study and also describebed by Jaudzems *et al*. (2014), P2FE-400 forms four hydrogen bonds with the catalytic dyad (Asp34 and Asp214), Val78 and Ser218 amino acid residues. Chloroquine and HPMP showed a comparable binding affinity with an estimated HYDE score of -19.7 and -19.2 KJ/mol, respectively. The Cl substituent of chloroquine was found to be unsuitable for binding in the hydrophobic cavity of plasmepsin II. Chloroquine forms

hydrogen bonds with Gly36 and Val78 amino acid residues. Similarly, HPMP forms a single hydrogen bond with Ser118. Its methoxyl group and adjacent carbonyl oxygen to the methoxyl group are not favored in the hydrophobic region of the binding pocket. Knipholone and dianellin showed weak binding interaction with HYDE score of -6 and -4.2 KJ/mol, respectively. Nonetheless, knipholone forms two hydrogen bonds with one of the catalytic dyad (Asp214) and Val78 amino acid residues.

The binding modes of knipholone, HPMP and chloroquine to pfLDH binding site are shown in Figure 19. Knipholone (-29.1 KJ/mol) and HPMP (-26.6 KJ/mol) showed stronger binding interaction with pfLDH than chloroquine (-24.7 KJ/mol) (Table 13). Knipholone forms hydrogen bonds with Ile54 and Val98 amino acid residues. Its carbonyl oxygen (at C-9) and hydroxyl group in ring A (at C-1) of the anthraquinone moiety, and the carbonyl oxygen (at C-3′) of the phloroglucinol moiety together with the *ortho* and *para* hydroxyl groups (at C-1′ and C-4′) are not favorable for binding. For HPMP, the methoxyl group and double bond in the long aliphatic chain are not suited for binding in the hydrophobic region. It also forms four hydrogen bonds with Ile54, Gly99, Phe100 and Asn140 amino acid residues with unique thermodynamically stable conformation. Interestingly, the two hydrogen bonds that HPMP forms with Gly99 and Asn149 are similar to two of the five hydrogen bond interactions seen in docking of NADH cofactor. From the experimental data, there were seven hydrogen bonds in pfLDH-NADH complex, of which four are observed in this study (Chaikuad *et al*., 2005). Chloroquine on its part showed two hydrogen bonds with Asp53 and Gly99 amino acid residues. One of the N-ethyl groups of chloroquine is not needed in the hydrophilic binding sites. Moreover, the actual pfLDH-chloroquine complex also showed two hydrogen bonds with Glu122 and Gly99 (Read *et al*., 1999). In contrast, dianellin did not show binding interaction with pfLDH.

Table 12. Prediction of partition coefficient Log P, aqueous solubility Log S and partition coefficient for partially dissociated compounds Log D of the compounds, standard drugs and P2FE-400. .

Compounds	Structure	Log P	Log S	Log D
Knipholone ZINC000004098683	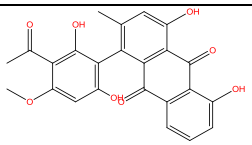	3.47	0	3.253
Dianellin	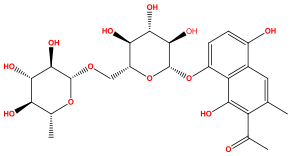	-2.75	3.391	-1.468
HPMP	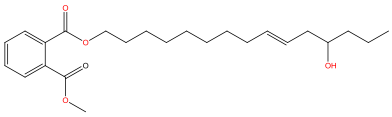	5.47	1.321	5.866
10-knipholone gentiobioside	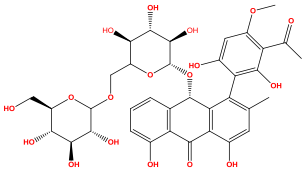	-0.603	1.03	2.928
Chloroquine	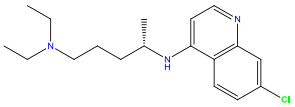	2.64	2.780	2.287
Artemisinin	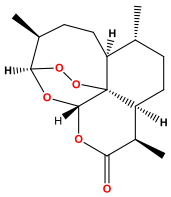	2.64	2.232	3.042
P2FE-400	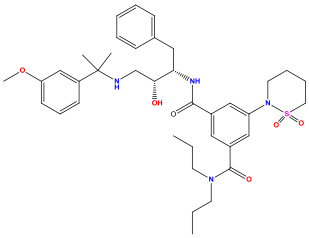	4.74	0.439	1.954
Anthraquinone dimer	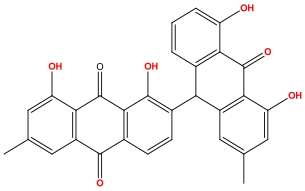	4.63	-1.528	4.565

Table 13. Docking result of compounds on the crystal structure of plasmepsin II (4cku) and plasmodium falciparum l-lactate dehydrogenase (pfLDH) (PDB 1ldg)

Plasmepsin II (4cku)		*Plasmodium falciparum* l-lactate dehydrogenase (pfLDH) (PDB 1ldg).	
Compounds	HYDE score ΔG_{HYDE} (kj/mol)	Compounds	HYDE score ΔG_{HYDE} (kj/mol)
P2FE-400	-38.3	Knipholone ZINC000004098683	-29.1
Chloroquine	-19.7	HPMP	-26.6
HPMP	-19.2	Chloroquine	-24.7
Anthraquinone dimer	-18.6	Anthraquinone dimer	-22.8
Artemisinin	-10.1	Artemisinin	-10.4
Knipholone ZINC000004098683	-6.5		
Dianellin	-4.2		

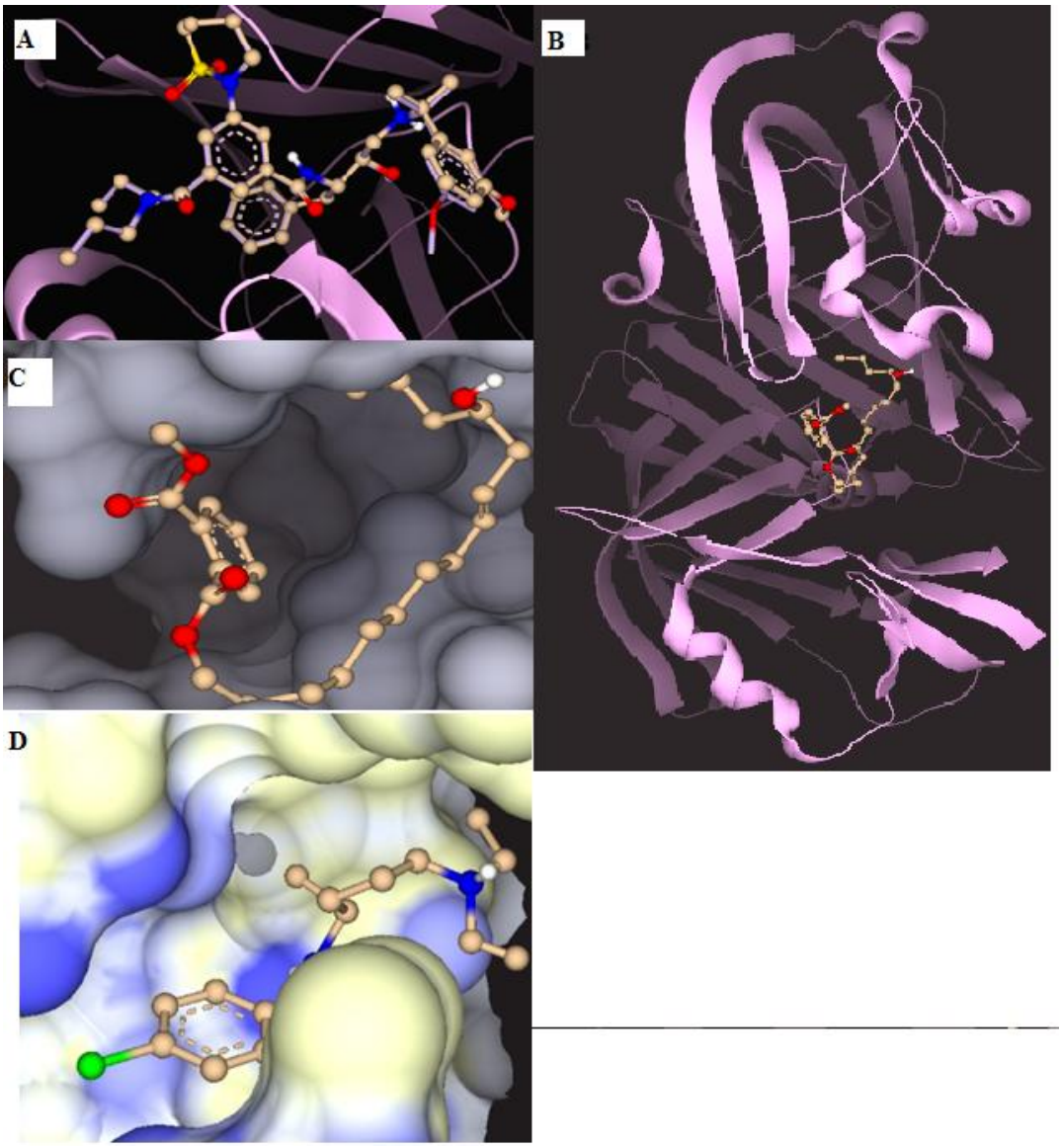

Figure 18. The binding modes of P2FE-400, knipholone, HPMP and chloroquine to plasmepsin II. A) Superimposition of redocked P2FE-400 (shown as a solid line) with its original position (shown in ball-stick model) as a complex (co-crystal) in the binding site of the crystal structure of plasmepsin II (PDB 4cku). B) Ribbon diagram of docked compound **4** -plasmepsin II chain E subunit complex. C) Surface representation showing HPMP in the binding site of plasmepsin II. HPMP is shown in ball-stick model. D) Surface representation showing chloroquine in the binding site of plasmepsin II with lipophilicity coloring. White represent hydrophobic pockets and blue represent hydrophilic pockets. Chloroquine is shown in ball-stick model.

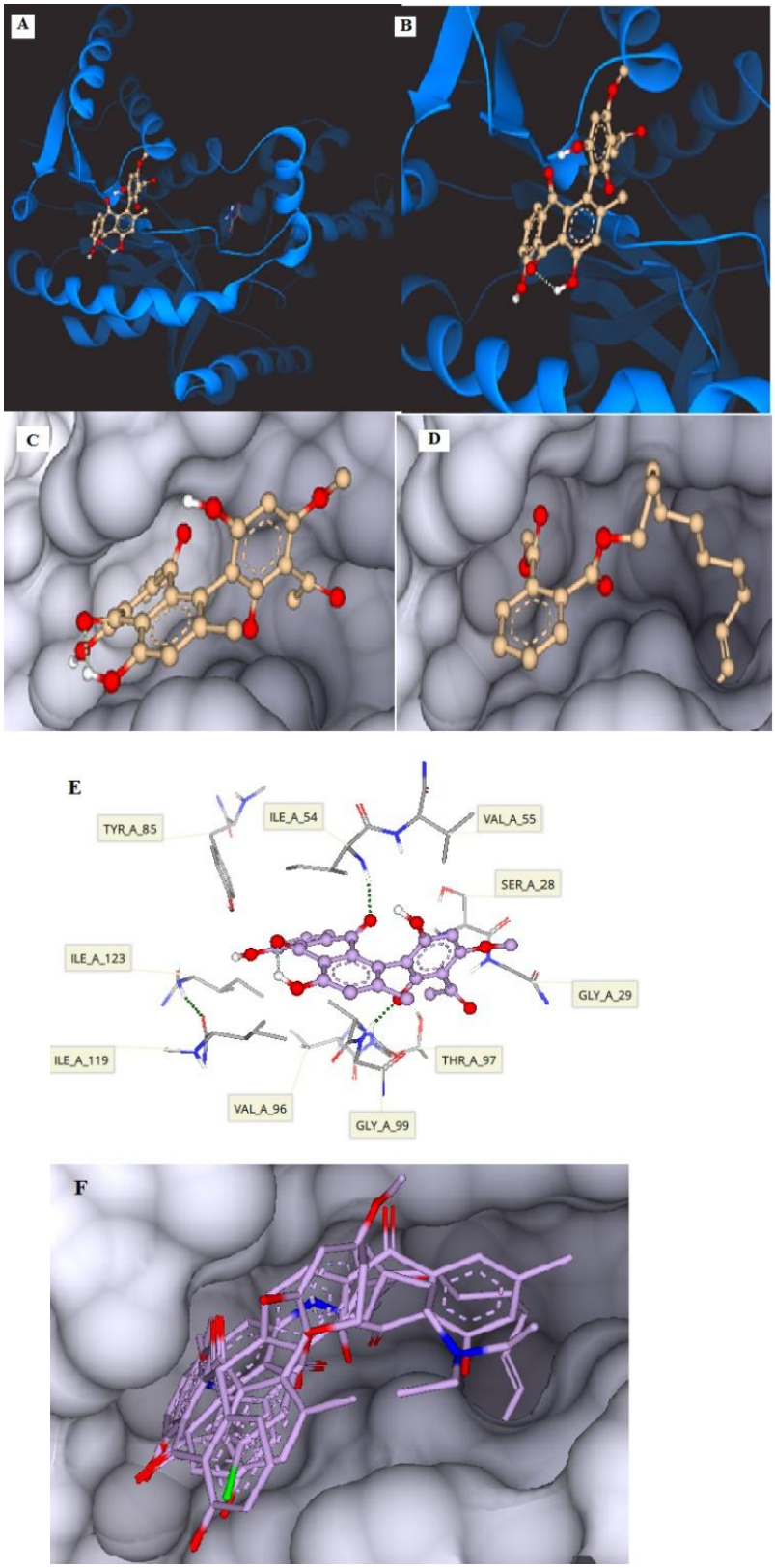

Figure 19. The binding modes of knipholone, HPMP and chloroquine to pfLDH binding site. A) Ribbon diagram of docked knipholone- pfLDH complex. Knipholone is shown in ball-stick

model. B) A close-up view of diagram A. C) Surface representation showing knipholone in the binding site of pfLDH. Knipholone is shown in ball-stick model. D) Surface representation showing HPMP in the binding site of pfLDH. HPMP is shown in ball-stick model. E) Binding interaction of knipholone with amino acid residues of pfLDH. F) Surface representation showing the superimposed compounds in the binding site of plasmodium falciparum l-lactate dehydrogenase (pfLDH) (PDB1ldg).

5 Conclusion

The present study revealed that *K. foliosa* and *K. insignis* possess genuine *in vivo* antimalarial effect against *P. berghei* in mice. The results further revealed that the antimalarial activities of the plants are attributed, in part or in full, to the presence of anthrone and naphthalene derivatives. This finding in conjunction with the safety profile obtained from the acute oral toxicity results support the traditional use of the plants for the treatment of malaria. The current molecular docking study also identified the binding motifs of the isolated compounds showing that knipholone and HPMP interact with important amino acid residues in the binding site of the target enzymes.

6 Recommendations

- Further phytochemical investigations to isolate the undiscovered polar constituents of both plants are needed.
- *In vitro* and *in vivo* mechanism of action study of knipholone and its semisynthestic dervatives (structural analogs) on pfLDH are recommended to be done.

References

Abate G (1989). *Etse Debdabe: Ethiopian Traditional Medicine*. In: Demissew S. (Ed.). Addis Ababa University Press, Addis Ababa, p 99-183.

Abegaz BM, Bezabih M, MsutaT, Brun R, Menche D, Mühlbacher J, Bringmann G (2002). Gaboroquinones A and B and 4′-*O*-Demethylknipholone-4′-*O*-*β*-D-glucopyranoside, phenylanthraquinones from the roots of *Bulbine frutescens. J Nat Prod* 65, 1117-1121.

Abdissa N, Akala HM, Heydenreich M, Midiwo JO, Ndakala A, Yenesew A (2013). Knipholone cyclooxanthrone and an anthraquinone dimer with antiplasmodial activities from the roots of *Kniphofia foliosa*. *Phytochem Lett* 6, 241-245.

Abosi AO, Raseroka BH (2003). *In vivo* antimalarial activity of *Vernonia amygdalina. Br J Biomed Sci* 60, 89-91.

Adugna A (2009). Malaria in Ethiopia. www.Ethio DemographyAnd Health.Org. Accessed on 03-26-2019.

Alemu A, Fuehrer HP, Getnet G, Tessema B, Noedl H (2013). *Plasmodium ovalecurtisi* and *Plasmodium ovalewallikeri* in North-West Ethiopia. *Malar J* 12, 346.

Alson SG, Jansen O, Cieckiewicz E, Rakotoarimanana H, Rafatro H, Degotte G, Francotte P, Frederich M (2018). *In vitro* and *in vivo* antimalarial activity of caffeic acid and some of its derivatives. *J Pharm Pharmacol* 70, 1349-1356.

Alves FP, Durlacher RR, Menezes MJ, Krieger H, Silva LH, Camargo EP (2002). High prevalence of asymptomatic *Plasmodium vivax* and *Plasmodium falciparum* infections in native Amazonian populations. *Am J Trop Med Hyg* 66, 641-648.

Amade P, Mallea M, Bouaicha N (1994). Isolation, structural identification and biological activity of two metabolites produced by *Penicillium olsonii* Bainier and Sartory. *J Antibiot* (Tokyo) 47, 201-207.

Ancelin ML, Calas ML, Bonhoure A, Herbute S, Vial HJ (2003). *In vivo* antimalarial activities of mono-and bis quaternary ammonium salts interfering with *Plasmodium* phospholipid metabolism. *Antimicrob Agents Chemother* 47, 2598-2605.

Asamenew G, Bisrat D, Mazumder A, Asres K (2011). *In vitro* antimicrobial and antioxidant activities of anthrone and chromone from the latex of *Aloe harlana* Reynolds. *Phytother Res* 25, 1756-1760.

Ayala FJ, Escalante AA, Rich SM (1999). Evolution of *Plasmodium* and the recent origin of the world populations of *Plasmodium falciparum*. *Parassitologia* 41, 55-68.

Baker DA (2010). Malaria gametocytogenesis. *Mol Biochem Parasitol* 172, 57–65.

Bankole AE, Adekunlel AA, Sowemimo AA, Umebese CE, Abiodun O, Gbotosho GO (2016). Phytochemical screening and *in vivo* antimalarial activity of extracts from three medicinal plants used in malaria treatment in Nigeria. *Parasitol Res* 115, 299-305.

Barber BE, Rajahram GS, Grigg MJ, William T, Anstey NM (2017). World Malaria Report: time to acknowledge *Plasmodium knowlesi* malaria. *Malar J* 16, 135.

Bazik DJ, Fox BA, Gonyer K (1993). Expression of *Plasmodium falciparum* lactate dehydrogenase in *Escherichia coli*. *Mol Biochem Parasitol* 59, 155-166.

Bero J, Frédérich M, Quetin-Leclercq J (2009). Antimalarial compounds isolated from plants used in traditional medicine. *J Pharm Pharmacol* 61, 1401-1433.

Bezabih M, Abegaz BM (1998). 4′-Demethyl knipholone from aerial parts of *Bulbine capitata*. *Phytochemistry* 48, 1071-1073.

Biruk H, Sentayehu B, Alebachew Y, Tamiru W, Ejigu A, Assefa S (2020). *In vivo* antimalarial activity of 80% methanol and aqueous bark extracts of *Terminalia brownii* Fresen. (Combretaceae) against *Plasmodium berghei* in mice. *Biochem Res Int* 2020, 9749410.

Brossi A, Venugopalan B, Gerpe LD, Yeh HJC, Flippen-Anderson JL, Buchs P, Luo XD, Milhous W, Peters W (1988). Arteether, a new antimalarial drug: synthesis and antimalarial properties. *J Med Chem* 31, 645-650.

Chatterjee S, Dutta TK (2003). Metabolism of butyl benzyl phthalate by *Gordonia* sp. strain MTCC 4818. *Biochem Biophys Res Commun* 309, 36-43.

Cheuka PM, Dziwornu G, Okombo J, Chibale K (2020). Plasmepsin inhibitors in antimalarial drug discovery: medicinal chemistry and target validation (2000 to present). *J Med Chem* 63, 4445-4467.

Choi S, Pradhan A, Hammond NL, Chittiboyina AG, Tekwani BL, Avery MA (2007). Design, synthesis, and biological evaluation of *plasmodium falciparum* lactate dehydrogenase inhibitors. *J Med Chem* 50, 3841-3850.

Cichewicz RH, Lim K-C, McKerrow JH, Nair MG (2002). Kwanzoquinones A – G and other constituents of *Hemerocallis fulva* 'Kwanzo' roots and their activity against the human pathogenic trematode *Schistosoma mansoni*. *Tetrahedron* 58, 8597-8606.

Cichewicz RH, Nair MG (2002). Isolation and characterization of stelladerol, a new antioxidant naphthalene glycoside, and other antioxidant glycosides from edible daylily (*Hemerocallis*) flowers. *J Agric Food Chem* 50, 87−91.

Conners R, Schambach F, Read J, Cameron A, Sessions RB, Vivas L, Easton A, Croft SL, Brady RL (2005). Mapping the binding site for gossypol-like inhibitors of *Plasmodium falciparum* lactate dehydrogenase. *Mol Biochem Parasitol* 142, 137-148.

Coppi A, Tewari R, Bishop JR, Bennett BL, Lawrence R, Esko JD, Billker O, Sinnis P (2007). Heparansulfate proteoglycans provide a signal to *Plasmodium* sporozoites to stop migrating and productively invade host cells. *Cell Host Microbe* 2, 316-327.

Corte´s A, Deitsch KW (2017). Malaria epigenetics. *Cold Spring Harb Perspect Med* 7, a025528.

Cowman AF, Healer J, Marapana D, Marsh K (2016). Malaria: biology and disease. *Cell* 167, 610-624.

Cumming JN, Ploypradith P, Posner GH (1997). Antimalarial activity of artemisinin (Qinghaosu) and related trioxanes: mechanism (s) of action. *Adv Pharmacol* 37, 253-297.

Dagne E, Steglich W (1984). Knipholone: a unique anthraquinone derivative from *Kniphofia foliosa*. *Phytochemistry* 23, 1729-1731.

Dagne E, Yenesew A (1993). Knipholone anthrone from *kniphofia foliosa*. *Phytochemistry* 34, 1440-1441.

Dahlgren RMT, Clifford HT, Yeo PF (1985). *The Families of the Monocotyledons*. Springer-Verlag, Berlin.

Dai Y, Harinantenaina L, Bowman JD, Da Fonseca IO, Brodie PJ, Goetz M, Cassera MB, Kingston DG (2014). Isolation of antiplasmodial anthraquinones from *Kniphofia ensifolia,* and synthesis and structure-activity relationships of related compounds. *BioOrg Med Chem* 22, 269-276.

D'Alessandro S, Silvestrini F, Dechering K, Corbett Y, Parapini S, Timmerman M, Galastri L, Basilico N, Sauerwein R, Alano P, Taramelli D (2013). A *Plasmodium falciparum* screening assay for anti-gametocyte drugs based on parasite lactate dehydrogenase detection. *J Antimicrob Chemother* 68, 2048-2058.

Deharo E, Bourdy G, Quenevo C, Muñoz V, Ruiz G, Sauvain M (2001). A search for natural bioactive compounds in Bolivia through a multidisciplinary approach. Part V. Evaluation of the antimalarial activity of plants used by the Tacana Indians. *J Ethnopharmacol* 77, 91–98.

Demissew S, Nordan I (2010). *Aloes and Lilies of Ethiopia and Eritrea*. Shama Books, Addis Ababa, p 113-125.

de Sousa ACC, Combrinck JM, Maepa K, Egan TJ (2020). Virtual screening as a tool to discover new β-haematin inhibitors with activity against malaria parasites. *Sci Rep* 10, 3374.

Dias DA, Silva CA, Urban S (2009). Naphthalene aglycones and glycosides from the Australian medicinal plant, *Dianella callicarpa*. *Planta Med* 75, 1442–1447.

Ehrenkranz JRL, Lewis NG, Kahn CR, Roth J (2005). Phlorizin: a review. *Diabetes Metab Res Rev* 21, 31-38.

Farooq U, Mahajan RC (2004). Drug resistance in malaria. *J Vector Borne Dis* 41, 45–53.

Fentahun S, Makonnen E, Awas T, Giday M (2017). *In vivo* antimalarial activity of crude extracts and solvent fractions of leaves of *Strychnos mitis* in *Plasmodium berghei* infected mice. *BMC Complement Altern Med* 17, 13.

François G, Steenackers T, Assi LA, Steglich W, Lamottke K, Holenz J, Bringmann G (1999). Vismione H and structurally related anthranoid compounds of natural and synthetic origin as promising drugs against the human malaria parasite *Plasmodium falciparum*: structure-activity relationships. *Parasitol Res* 85, 582-588.

Frevert U, Sinnis P, Cerami C, Shreffler W, Takacs B, Nussenzweig V (1993). Malaria circumsporozoite protein binds to heparan sulfate proteoglycans associated with the surface membrane of hepatocytes. *J Exp Med.* 177, 1287-1298.

Geremedhin G, Bisrat D, Asres K (2014). Isolation, characterization and *in vivo* antimalarial evaluation of anthrones from the leaf latex of *Aloe percrassa* Todaro. *J Nat Remedies* 14, 119-125.

Girma B, Bisrat D, Asres K (2015). Antimalarial evaluation of the leaf latex of *Aloe citrina* and its major constituent. *Anc Sci Life* 34, 142-146.

Gomez MS, Piper RC, Hunsaker LA, Royer RE, Deck LM, Makler MT, Vander Jagt DL (1997). Substrate and cofactor specificity and selective inhibition of lactate dehydrogenase from the malarial parasite *P. falciparum. Mol Biochem Parasitol* 90, 235-246.

Habtemariam S (2010). Knipholone anthrone from *Kniphofia foliosa* induces a rapid onset of necrotic cell death in cancer cells. *Fitoterapia* 81, 1013–1019.

Haque TS, Skillman AG, Lee CE, Habashita H, Gluzman IY, Ewing TJA, Goldberg DE, Kuntz ID, Ellman JA (1999). Potent, low-molecular-weight non-peptide inhibitors of malarial aspartyl protease plasmepsin II. *J Med Chem* 42, 1428-1440.

Hilou A, Nacoulma OG, Guiguemde TR (2006). *In vivo* antimalarial activities of extracts from *Amaranthus spinosus* L. and *Boerhaavia erecta* L. in mice. *J Ethnopharmacol* 103, 236–240.

Hostettmann K, Marston A, Ndjoko K, Wolfender JL (2000). The potential of African plants as a source of drugs. *Curr Org Chem* 4, 973-1010.

Hernández-Medel MR, Pereda-Miranda R (2002). Cytotoxic anthraquinones *Picramnia antidesma*. *Planta Med* 68, 556-558.

Hutchings A (1996). *Zulu medicinal plants*. University of Natal Press, Pietermaritzburg, p 27-31.

Ignatushchenkoa MV, Winter RW, Bächinger HP, Hinrichs DJ, Riscoe MK (1997). Xanthones as antimalarial agents; studies of a possible mode of action. *FEBS Lett* 409, 67-73.

IISS (2016). The IISS armed conflict survey 2016: The worldwide review of political, military and humanitarian trends in current conflicts. International institute for strategic studies, Routledge.

Jaudzems K, Tars K, Maurops G, Ivdra N, Otikovs M, Leitans J, Kanepe-Lapsa I, Domraceva I, Mutule I, Trapencieris P, Blackman MJ, Jirgensons A (2014). *Plasmepsin* inhibitory activity and structure-guided optimization of a potent hydroxyethylamine-based antimalarial hit. *ACS Med Chem Lett* 5, 373-377.

Kaou AM, Mahiou-Leddet V, Hutter S, Aïnouddine S, Hassani S, Yahaya I, Azas N, Ollivier E (2008). Antimalarial activity of crude extracts from nine African medicinal plants. *J Ethnopharmacol* 116, 74-83.

Kaur K, Jain M, Kaur T, Jain R (2009). Antimalarials from nature. *Bio Org Med Chem* 17, 3229-3256.

Kebede A, Mccann JC, Kiszewski AE, Ye-ebiyo Y (2005). New evidence of the effects of agro-ecologic change on malaria transmission. *Am J Trop Med Hyg* 73, 676-680.

Kling B, Bücherl D, Palatzky P, Matysik FM, Decker M, Wegener J, Heilmann J (2014). Flavonoids, flavonoid metabolites, and phenolic acids inhibit oxidative stress in the neuronal cell line HT-22 monitored by ECIS and MTT assay: a comparative study. *J Nat Prod* 77, 446-454.

Kutner S, Breuer WV, Ginsburg H, Cabantchik ZI (1987). On the mode of action of phlorizin as an antimalarial agent in *in vitro* cultures of *Plasmodium falciparum. Biochem Pharmacol* 36, 123-129.

Lee HJ, Georgiadou A, Otto TD, Levin M, Coin LJ, Conway DJ, Cunnington AJ (2018). Transcriptomic studies of malaria: a paradigm for Investigation of systemic host-pathogen interactions. *Microbiol Mol Biol Rev* 82, e00071-17.

Liu Y, Murakami N, Ji H, Abreu P, Zhang S (2007). Antimalarial flavonol glycosides from *Euphorbia hirta*. *Pharm Biol* 45, 278–281.

Mackintosh CL, Beeson JG, Marsh K (2004). Clinical features and pathogenesis of severe malaria. *Trends Parasitol* 20, 597–603.

Maitland K (2016). Severe malaria in African children — the need for continuing investment. *N Engl J Med* 375, 2416–2417.

Megnassan E, Keita M, Bieri C, Esmel A, Frecer V, Miertus S (2012). Design of novel dihydroxynaphthoic acid inhibitors of *Plasmodium falciparum* lactate dehydrogenase. *Med Chem* 8, 970-984.

Menard D, Dondorp A (2017). Antimalarial drug resistance: A threat to malaria elimination. *Cold Spring Harb Perspect Med* 7, a025619.

Meshesha M, Deyou T, Tedla A, Abdissa N (2017). Chemical constituents of the roots of *Kniphofia isoetifolia* Hochst. And evaluation for antibacterial activity. *J Pharm Pharmacogn Res* 5, 345-353.

Meshnick SR, Dobson MJ (2001). *The History of Antimalarial Drugs Antimalarial Chemotherapy: Mechanisms of Action, Resistance, and New Directions in Drug* Discovery. In: Rosenthal PJ. (Ed.). Humana Press Inc, Totowa.

Miller LH, Mason SJ, Clyde DF, Mc Ginniss MH (1976). The resistance factor to *Plasmodium vivax* in blacks. The Duffy-blood-group genotype, *FyFy*. *N Engl J Med* 295, 302–304.

Milner DA Jr (2018). Malaria pathogenesis. *Cold Spring Harb Perspect Med* 8, a025569.

Mitchell SN, Kakani EG, South A, Howell PI, Waterhouse RM, Catteruccia F (2015). Mosquito biology. Evolution of sexual traits influencing vectorial capacity in anopheline mosquitoes. *Science* 347, 985-988.

Miyachi Y, Yoshioka A, Imamura S, Niwa Y (1986). Antioxidant action of antimalarials. *Ann Rheum Dis* 45, 244-248.

Mueller I, Zimmerman PA, Reeder JC. *Plasmodium malariae* and *Plasmodium ovale* – the 'bashful' malaria parasites. *Trends Parasitol* 23, 278-283.

Mullard A (2018). Malaria medicine box expands. *Nat Rev Drug Discov* 17, 693-695.

National Institute of Health Guidelines for the Care and Use of Laboratory Animals and National Institutes of Health, Office of Science and Health Reports (1996). Guide for care and use of laboratory animals 83-23. Office of Science and Health Reports, Department of Health and Human Services, Bethesda, Md, USA.

Ng OT, Ooi EE, Lee CC, Lee PJ, Ng LC, Pei SW, Tu TM, Loh JP, Leo YS (2008). Naturally acquired human *Plasmodium knowlesi* infection, Singapor. *Emerg Infect Dis* 14, 814-816.

Ntie-Kang F, Onguéné PA, Lifongo1 LL, Ndom JC, Sippl W, Mbaze LM (2014). The potential of antimalarial compounds derived from African medicinal plants, part II: a pharmacological evaluation of non-alkaloids and non-terpenoids. *Malar J* 13, 81.

Nöteberg D, Hamelink E, Hultén J, Wahlgren M, Vrang L, Samuelsson B, Hallberg A (2003). Design and synthesis of plasmepsin I and plasmepsin II inhibitors with activity in *Plasmodium falciparum*-infected cultured human erythrocytes. *J Med Chem* 46, 734-746.

OECD (2008). The Organization of Economic Co-operation and Development. Guidelines for testing of chemicals. Guideline 425: Acute oral toxicity. Paris, France.

Otto TD, Gilabert A, Crellen T, Böhme U, Arnathau C, Sanders M, Oyola SO, Okouga AP, Boundenga L, Willaume E, Ngoubangoye B, Moukodoum ND, Paupy C, Durand P, Rougeron V, Ollomo B, Renaud F, Newbold C, Berriman M, Prugnolle F (2018). Genomes of all known members of a *Plasmodium* subgenus reveal paths to virulent human malaria. *Nat Microbiol* 3, 687-697.

Pagola S, Stephens PW, Bohle DS, Kosar AD, Madsen SK (2000). The structure of malaria pigment beta-haematin. *Nature* 404, 307-310.

Peakall DB (1975). *Phthalate esters: Occurrence and Biological Effects*. *Section of Ecology and Systematics*. Langmuir laboratory, Cornell University, Ithaca, New York 14850.

Phillips MA, Burrows JN, Manyando C, van Huijsduijnen RH, Van Voorhis WC, Wells TNC (2017). Malaria. *Nat Rev Dis Primers* 3, 17050.

Pillay P, Maharaj VJ, Smith PJ (2008). Investigating South African plants as a source of new antimalarial drugs. *J Ethnopharmacol* 119, 438–454.

Qhotsokoane-Lusunzi MA, Karuso P (2001a). Secondary metabolites from Basotho medicinal plants. I. *Bulbine narcissifolia. J Nat Prod* 64, 1368-1372.

Qhotsokoane-Lusunzi MA, Karuso P (2001b). Secondary metabolites from Basotho medicinal mlants. II* *Bulbine capitata. Aust J Chem* 54, 427–430.

Read JA, Wilkinson KW, Tranter R, Sessions RB, Brady RL (1999). Chloroquine binds in the cofactor binding site of *Plasmodium falciparum* lactate dehydrogenase. *J Biol Chem* 274, 10213-10218.

Sastry VMVS, Rao GRK (1995). Dioctyl phthalate, and antibacterial compound from the marine brown alga—*Sargassum wightii. J Appl Phycol* 7, 185-186.

Saxena S, Pant N, Jain DC, Bhakuni RS (2003). Antimalarial agents from plant sources. *Curr Sci* 85, 1314-1329.

Sema DK, Lannang AM, Tatsimo SJ, Yousuf S, Zoufoud D, Iqbal U, Wansi JD, Sewald N, Choudhary MI (2018). New indane and naphthalene derivatives from the rhizomes of *Kniphofia reflexa* Hutchinson ex Codd. *Phytochem Lett* 26, 78-82.

Singh B, Kim Sung L, Matusop A, Radhakrishnan A, Shamsul SS, Cox-Singh J, Thomas A, Conway DJ (2004). A large focus of naturally acquired *Plasmodium knowlesi* infections in human beings. *Lancet* 363, 1017-1024.

Sinka ME, Bangs MJ, Manguin S, Chareonviriyaphap T, Patil AP, Temperley WH, Gething PW, ElyazarIqbal RF, Kabaria6 CW, Harbach RE, Hay S (2011). The dominant Anopheles vectors of human malaria in the Asia-Pacific region: Occurrence data, distribution maps and bionomic précis. *Parasit Vectors* 4, 89.

Smith RC, Vega-Rodríguez J, Jacobs-Lorena M (2014). The *Plasmodium* bottleneck: malaria parasite losses in the mosquito vector. *Mem Inst Oswaldo Cruz* 109, 644-661.

Smith TA, Leuenberger R, Lengeler C (2001). Child mortality and malaria transmission intensity in Africa. *Trends Parasitol* 17, 145-149.

Snow RW, Sartorius B, Kyalo D, Maina J, Amratia P, Mundia CW, Bejon P, Noor AM (2017). The prevalence of *Plasmodium falciparum* in sub-Saharan Africa since 1900. *Nature* 550, 515-518.

Sriwichai P, Samung Y, Sumruayphol S, Kiattibut K, Kumpitak C, Payakkapol A, Kaewkungwal J, Yan G, Cui L, Sattabongkot J (2016). Natural human *Plasmodium* infections in major Anopheles mosquitoes in western Thailand. *Parasit Vectors* 9, 17.

Sturm A**,** Amino Rogerio, Sand van de C, Regen T, Retzlaff S, Rennenberg A, Krueger A, Pollok JM, Menard R, Heussler VT (2006). Manipulation of host hepatocytes by the malaria parasite for delivery into liver sinusoids. *Science* 313, 1287-1290.

Tadesse FG, Ashine T, Teka H, Esayas E, Messenger LA, Chali W, Meerstein-Kessel L, Walker T, Wolde Behaksra S, Lanke K, Heutink R, Jeffries CL, Mekonnen DA, Hailemeskel E, Tebeje SK, Tafesse T, Gashaw A, Tsegaye T, Emiru T, Simon K, Bogale EA, Yohannes G, Kedir S,

Shumie G, Sabir SA, Mumba P, Dengela D, Kolaczinski JH, Wilson A, Churcher TS, Chibsa S, Murphy M, Balkew M, Irish S, Drakeley C, Gadisa E, Bousema T (2021). Anopheles stephensi Mosquitoes as Vectors of Plasmodium vivax and falciparum, Horn of Africa, 2019. *Emerg Infect Dis* 27, 603-607.

Tazi L, Ayala FJ (2011). Unresolved direction of host transfer of *Plasmodium vivax* v. *P. simium* and *P. malariae* v. *P. brasilianum*. *Infect Genet Evol* 11, 209-221.

Teka T, Bisrat D, Yeshak MY, Asres K (2016**)**. Antimalarial activity of the chemical constituents of the leaf latex of *Aloe pulcherrima* Gilbert and Sebsebe. *Molecules* 21, 1415.

Tiwari HK, Kumar P, Jatana N, Kumar K, Garg S, Narayanan L, Sijwali PS, Pandey KC, Gorobets NY, Dunn BM, Parmar VS (2017). *In vitro* antimalarial evaluation of piperidine- and piperazine-based chalcones: inhibition of falcipain-2 and plasmepsin II hemoglobinases activities from *Plasmodium falciparum*. *ChemistrySelect* 2, 7684-7690.

van Wyk BE, Yenesew A, Dagne E (1995). Chemotaxonomic significance of anthraquinones in the roots of Asphodeloideae (Asphodelaceae). *Biochem Syst Ecol* 23, 277-281.

Vaughan AM, Mikolajczak SA, Wilson EM, Grompe M, Kaushansky A, Camargo N, Bial J, Ploss A, Kappe SH (2012). Complete *Plasmodium falciparum* liver- stage development in liver-chimericmice. *J Clin Invest* 122, 3618-3628.

Vennerstrom JL, Arbe-Barnes S, Brun R, Charman SA, Chiu FC, Chollet J, Dong Y, Dorn A, Hunziker D, Matile H, McIntosh K, Padmanilayam M, Santo Tomas J, Scheurer C, Scorneaux B,

Tang Y, Urwyler H, Wittlin S, Charman WN (2004). Identification of an antimalarial synthetic trioxolane drug development candidate. *Nature* 430, 900-904.

Waako PJ, Gumede B, Smith P, Folb PI (2005). The *in vitro* and *in vivo* antimalarial activity of *Cardiospermum halicacabum* L. and *Momordica foetida* Schumch. Et Thonn. *J Ethnopharmacol* 99, 137-143.

Waters AP, Higgins DG, McCutchan TF (1993). The phylogeny of malaria: A useful study. *Parasitol Res* 9, 246-250.

Weiss GE, Gilson PR, Taechalertpaisarn T, Tham WH, de Jong NW, Harvey KL, Fowkes FJ, Barlow PN, Rayner JC, Wright GJ, Cowman AF, Crabb BS (2015). Revealing the sequence and resulting cellular morphology of receptor-ligand interactions during *Plasmodium falciparum* invasion of erythrocytes. *PLoS Pathog* 11, e1004670.

Wellems TE (2002). *Plasmodium* chloroquine resistance and the search for a replacement antimalarial drug. *Science* 298, 124-126.

White N (1999). Antimalarial drug resistance and combination chemotherapy. *Philos Trans R Soc Lond Biol Sci* 354, 739-749.

White NJ, Hien TT, Nosten FH (2015). A brief history of Qinghaosu. *Trends Parasitol* 31, 607-610.

Whitehouse C (2002). *Asphodelaceae*. *Flora of Tropical East Africa*. In: Beentje HJ. (Ed.). Balkema Publishers, Roterdam.

WHO (2019). World malaria report 2019. World Health Organization, Geneva.

WHO (2017). World malaria report 2017. Country profile: Ethiopia. World Health Organization, Geneva.

Winter RW, Cornell KA, Johnson LL, Ignatushchenko MV, Hinrichs DJ, Riscoe MK (1996). Potentiation of the antimalarial agent rufigallol. *Antimicrob Agents Chemother* 40, 1408-1411.

Woyessa A, Gebre-Michael T, Ali A, Kebede D (2002). Malaria in Addis Ababa and its environs: assessment of magnitude and distribution. *Ethiopian J Health Dev* 16, 147–155.

Wube AA, Bucar F, Asres K, Gibbons S, Rattray L, Croft SL (2005). Antimalarial compounds from *Kniphofia foliosa* roots. *Phytother Res* 19, 472-476.

Ziegler J, Linck R, Wright DW (2001). Heme aggregation inhibitors: antimalarial drugs targeting an essential biomineralization process. *Curr Med Chem* 8, 171-189.

Appendices

Appendix I: ^{1}H, ^{13}C, DEPT and ESIMS of dianellin

Appendix Ia: ^{1}H NMR spectrum of dianellin, methanol-d_4

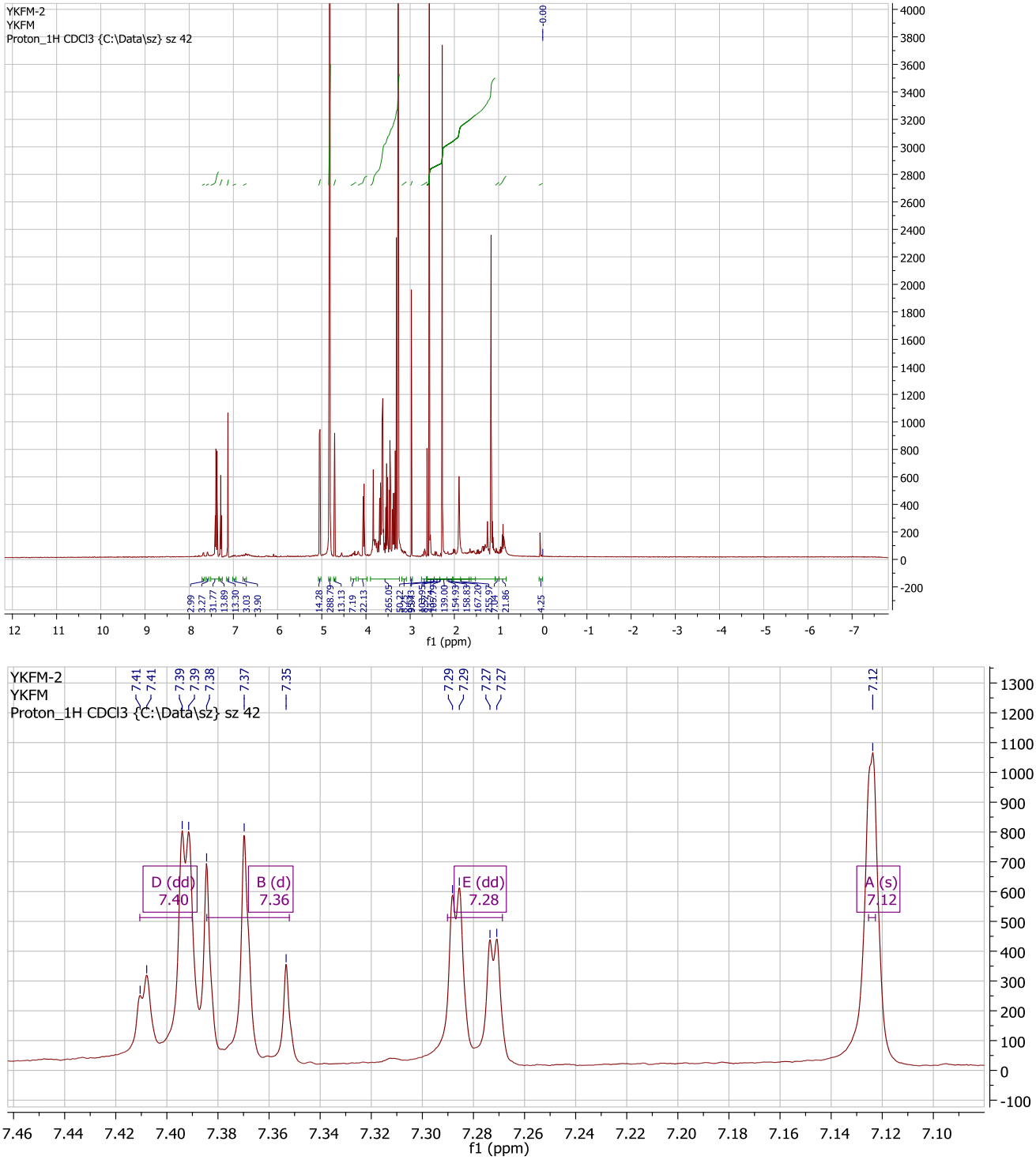

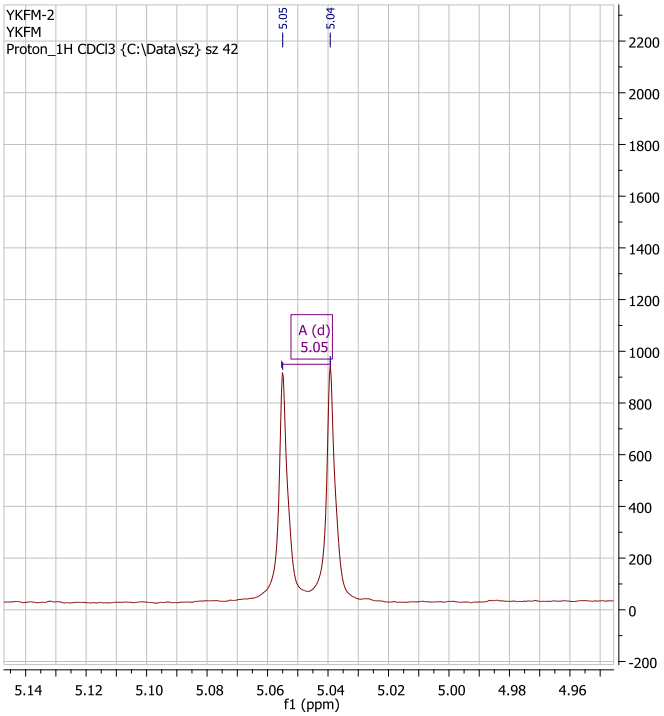
YKFM-2
YKFM
Proton_1H CDCl3 {C:\Data\sz} sz 42
5.05
5.04
A (d)
5.05
f1 (ppm)

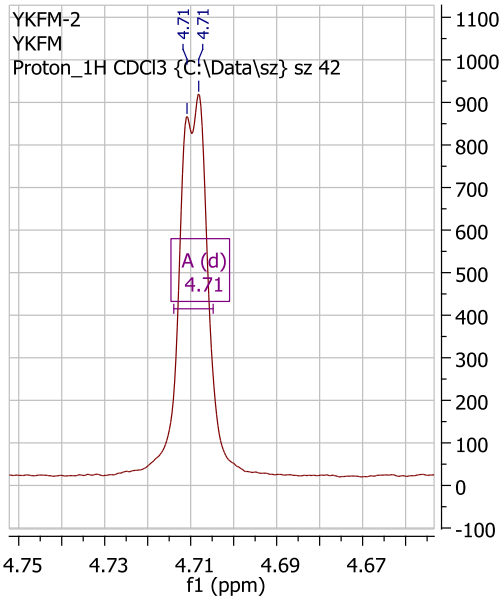
YKFM-2
YKFM
Proton_1H CDCl3 {C:\Data\sz} sz 42
4.71
4.71
A (d)
4.71
f1 (ppm)

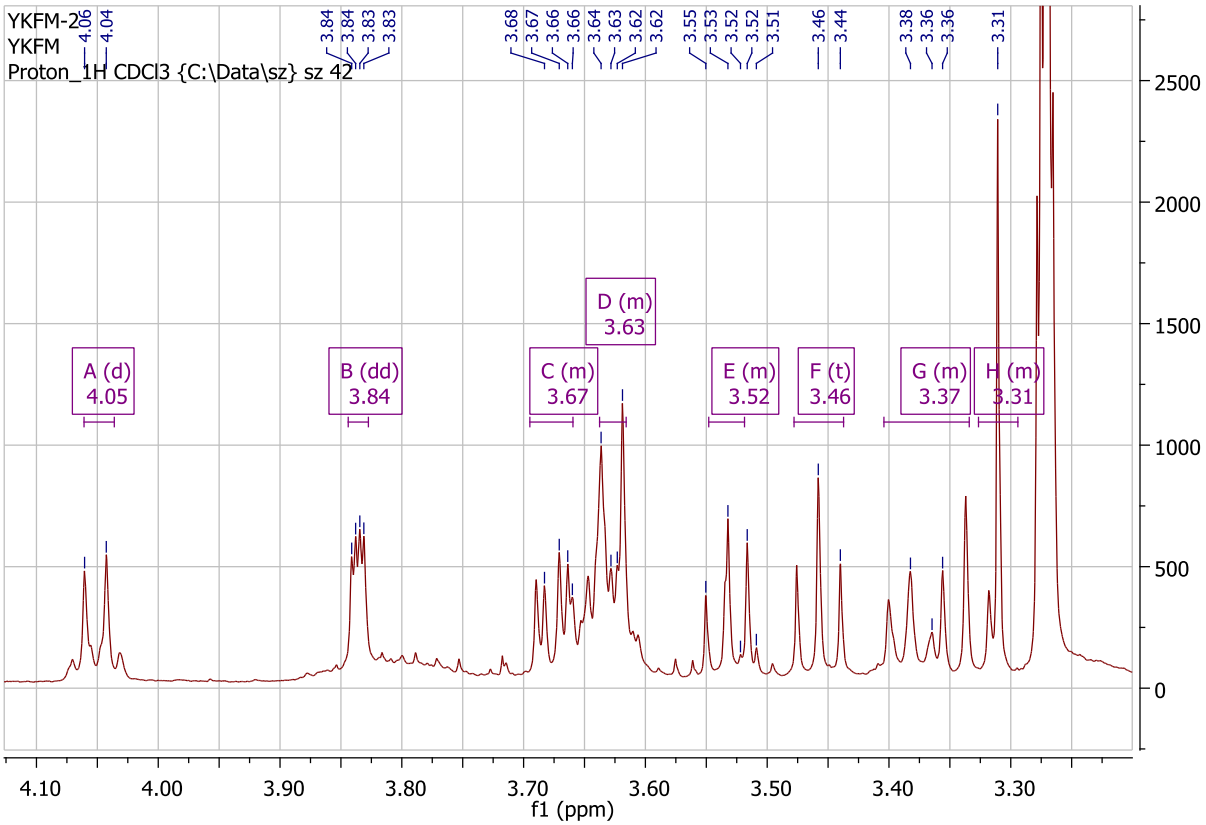
YKFM-2
YKFM
Proton_1H CDCl3 {C:\Data\sz} sz 42
A (d)
4.05
B (dd)
3.84
C (m)
3.67
D (m)
3.63
E (m)
3.52
F (t)
3.46
G (m)
3.37
H (m)
3.31
f1 (ppm)

Appendix Ib: ^{13}C NMR spectrum of dianellin, methanol-d_4

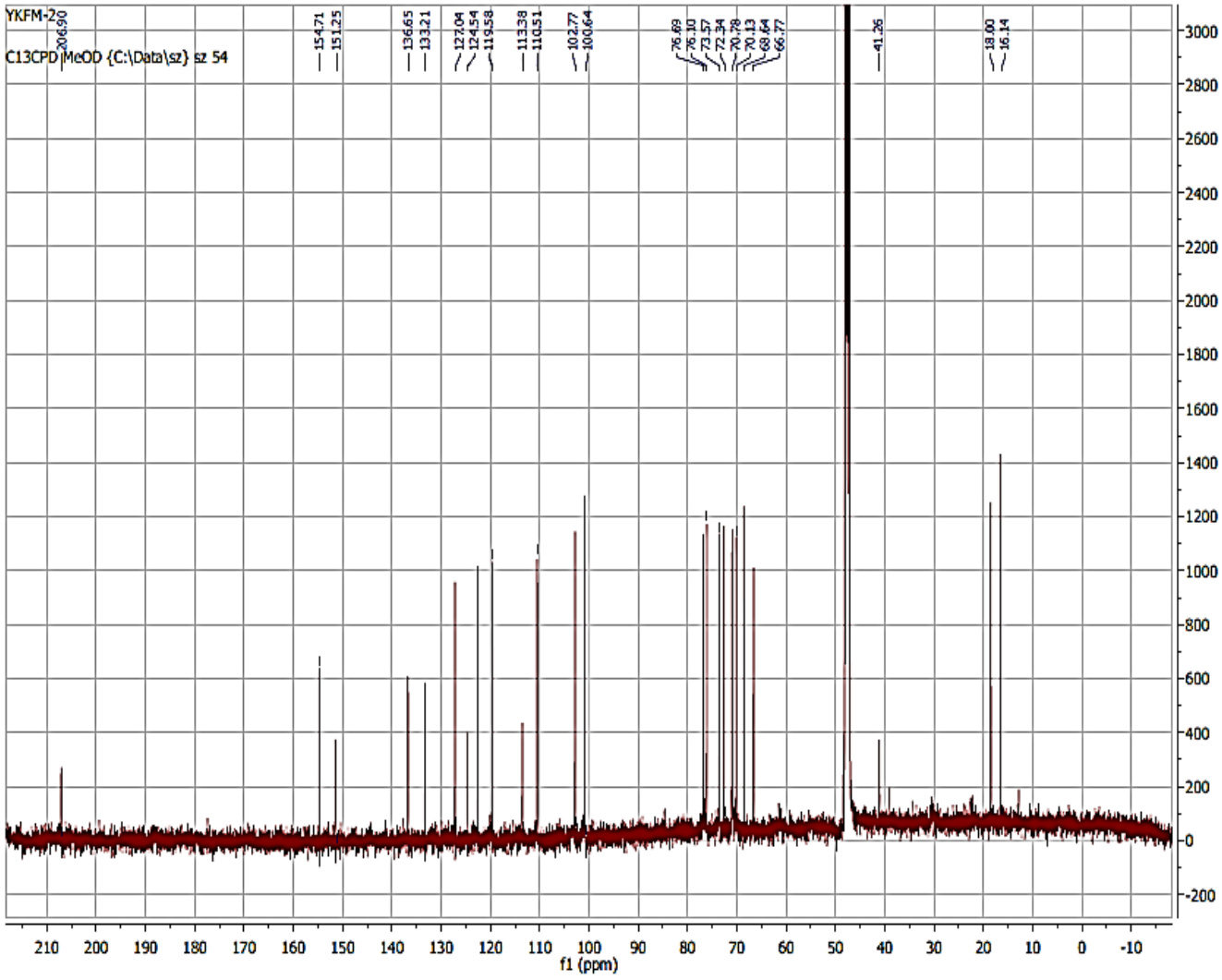

Appendix Ic: DEPT spectrum of dianellin, methanol-d_4

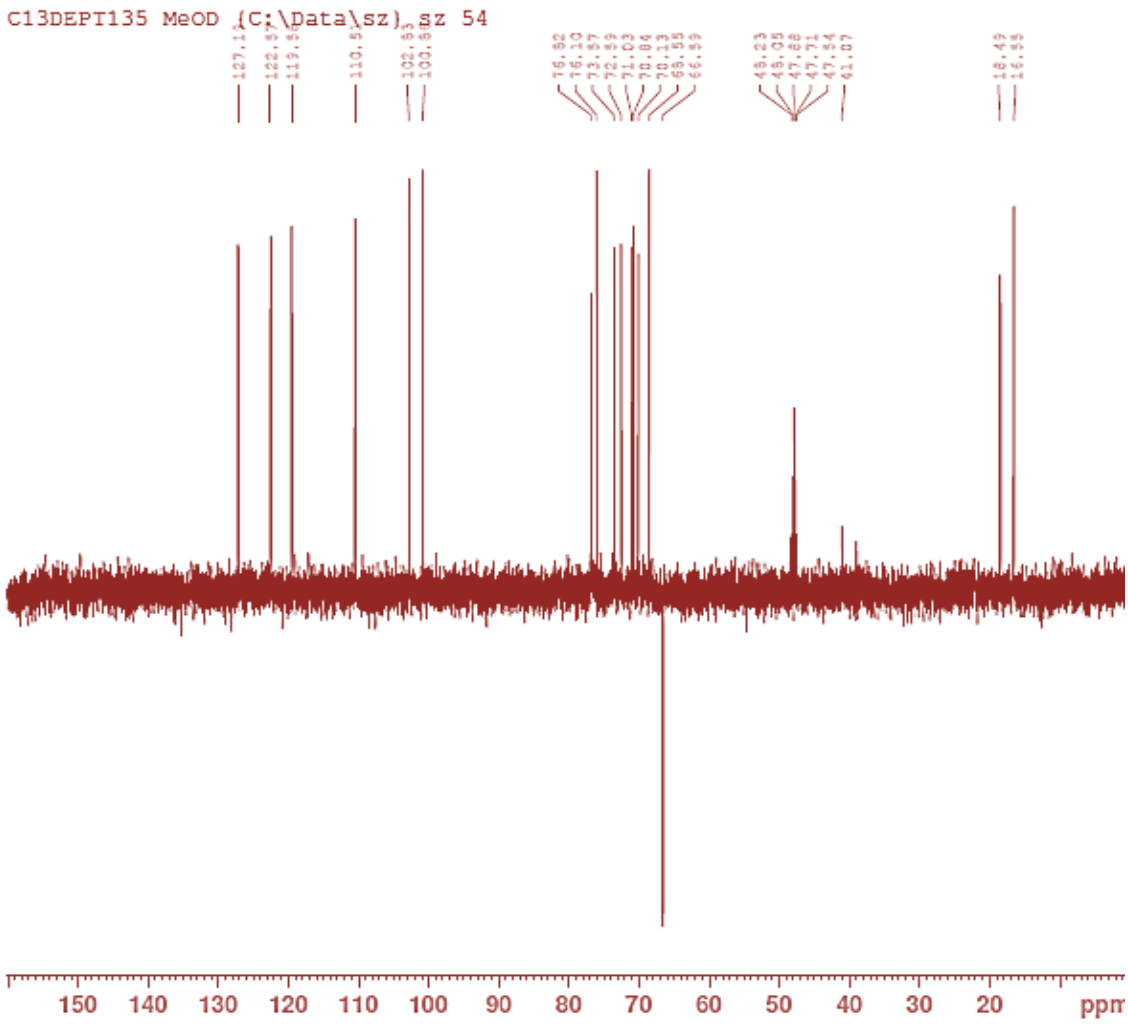

Appendix Id: ESIMS spectrum of dianellin

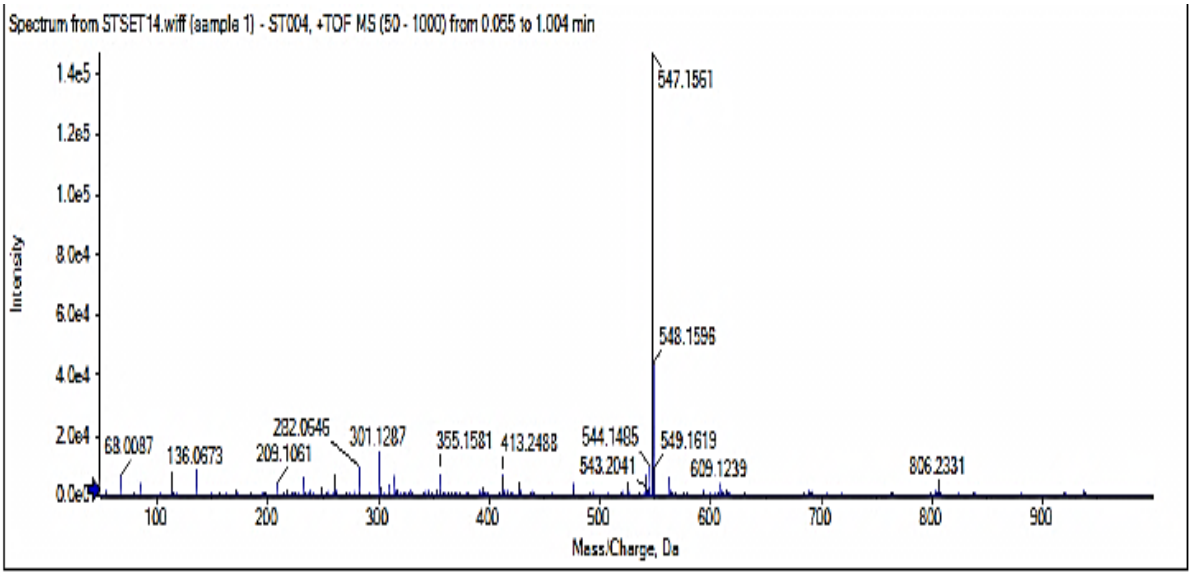

Appendix II: ^{1}H, ^{13}C, DEPT and ESIMS of knipholone isolated from *K. foliosa*

Appendix IIa: ^{1}H NMR spectrum of knipholone, chloroform-*d*

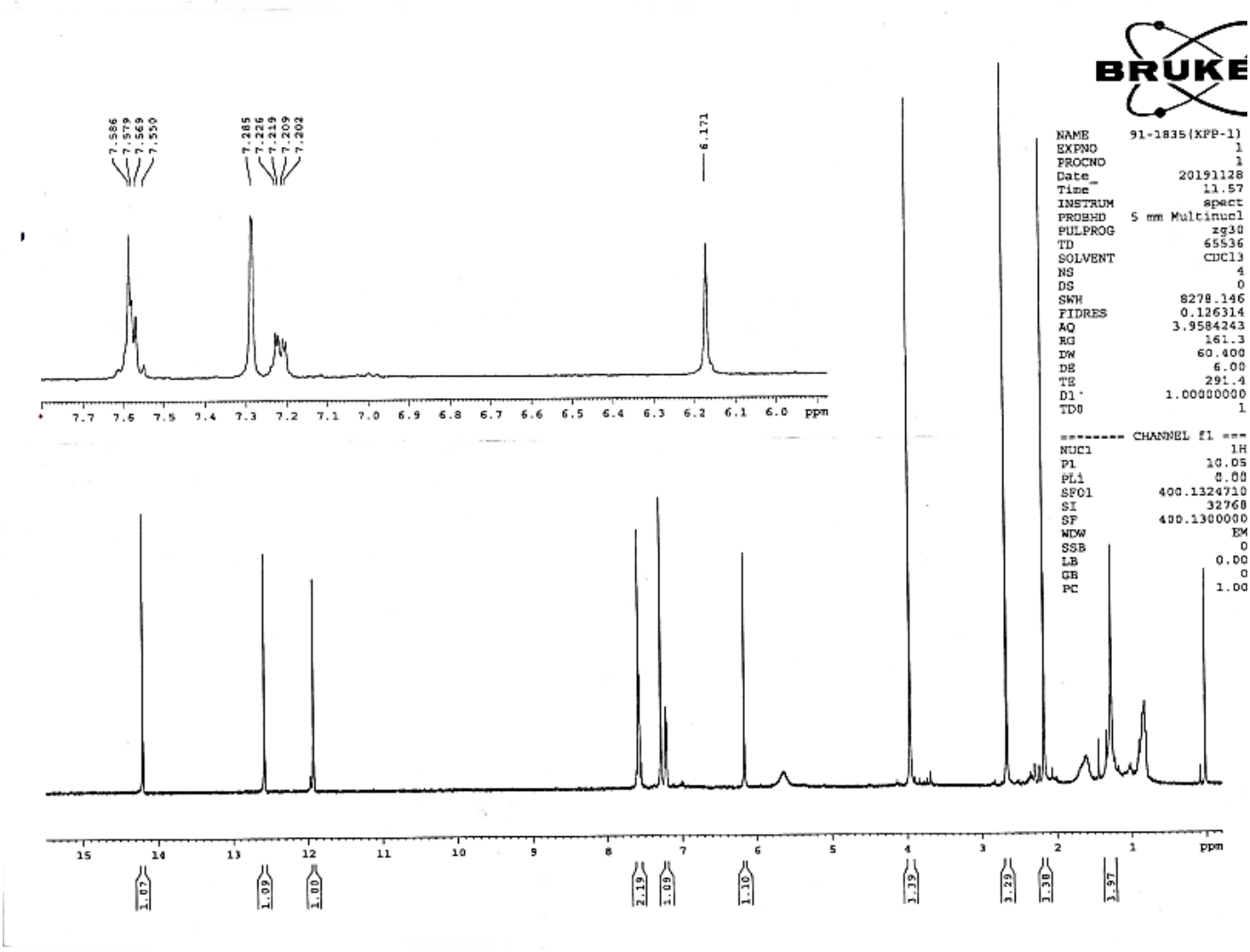

Appendix IIb: ^{13}C NMR spectrum of knipholone, chloroform-*d*

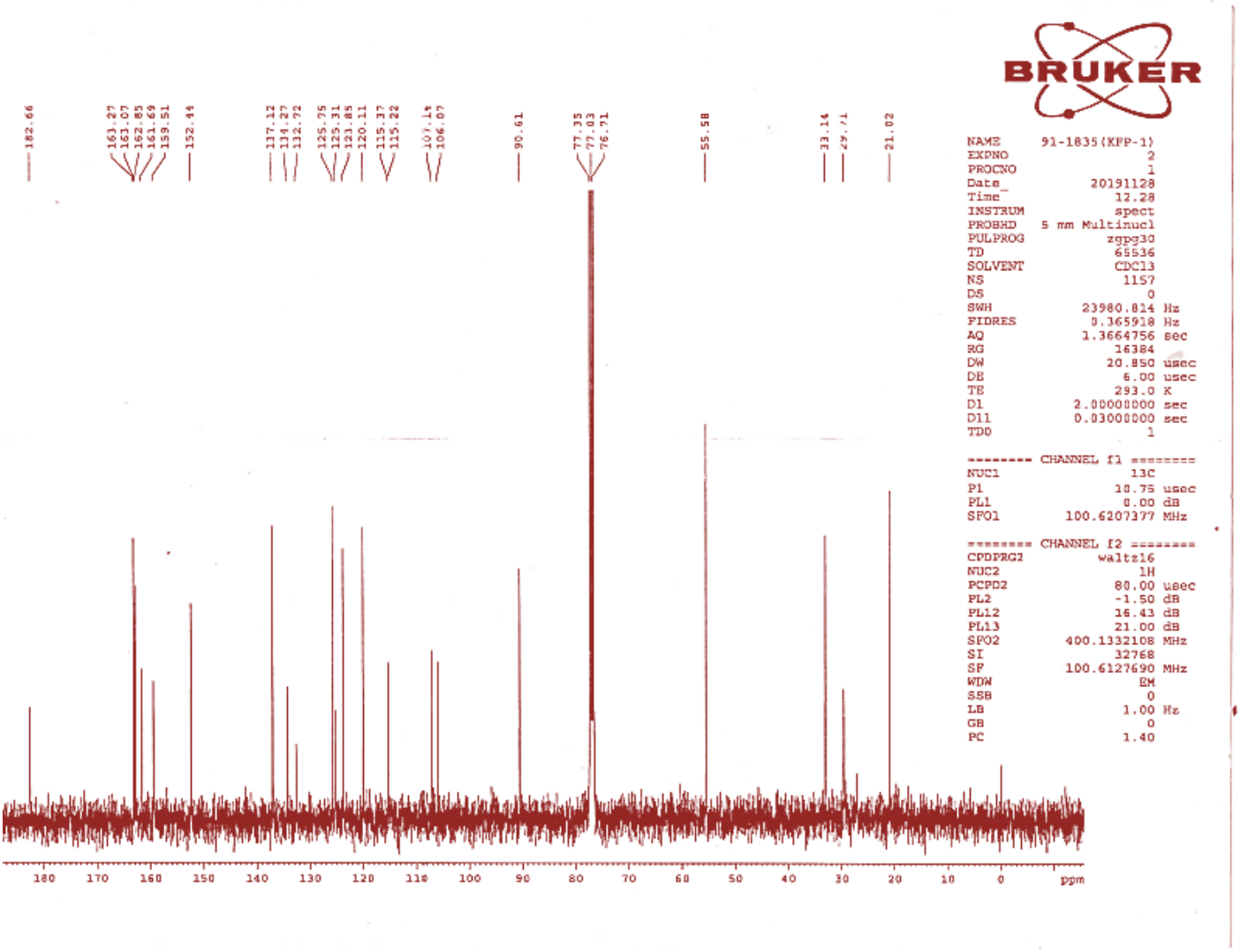

Appendix IIc: DEPT spectrum of knipholone, chloroform-*d*

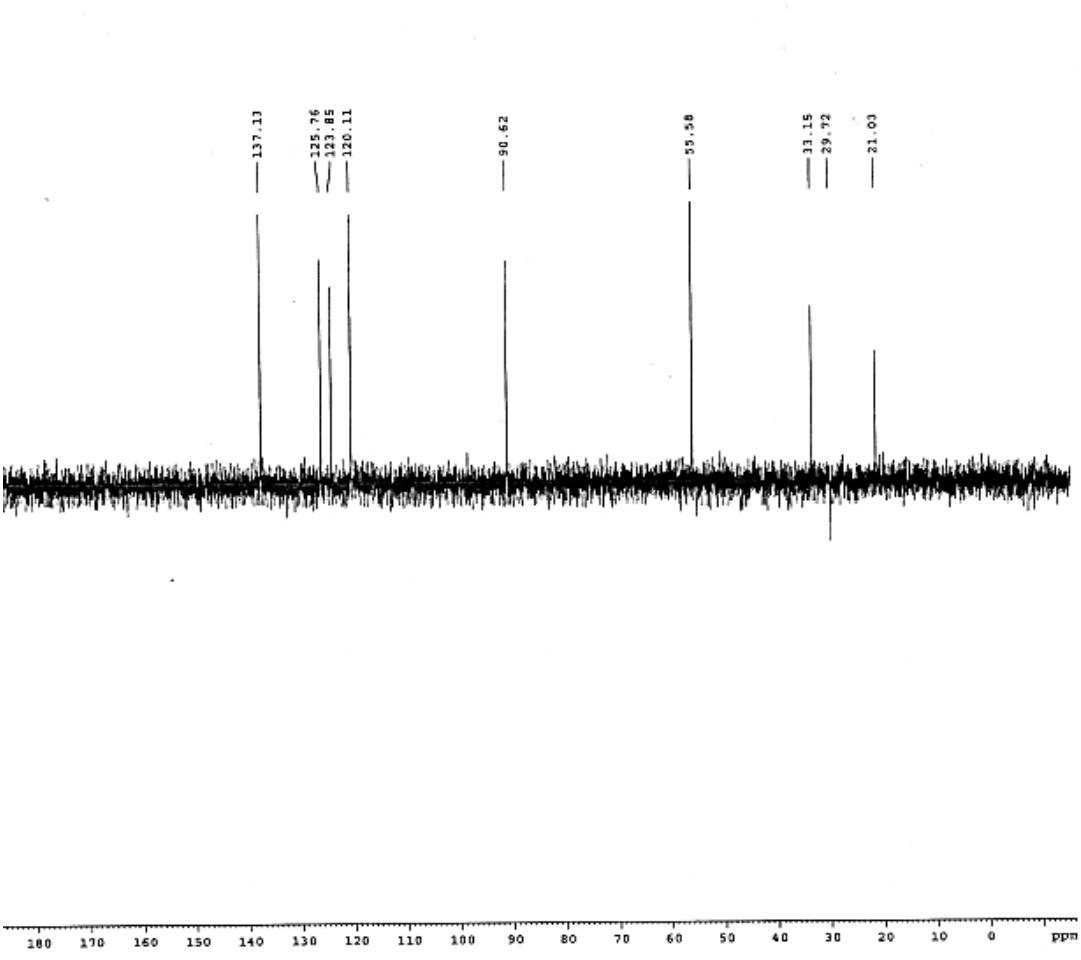

BRUKER

NAME	91-1835(KFP-1)
EXPNO	3
PROCNO	1
Date_	20191128
Time	12.43
INSTRUM	spect
PROBHD	5 mm Multinucl
PULPROG	dept135
TD	65536
SOLVENT	CDCl3
NS	256
DS	0
SWH	23148.148 Hz
FIDRES	0.353213 Hz
AQ	1.4156276 sec
RG	16384
DW	21.600 usec
DE	6.00 usec
TE	293.0 K
CNST2	145.0000000
D1	2.00000000 sec
D2	0.00344828 sec
D12	0.00002000 sec
TD0	1
======== CHANNEL f1 ========	
NUC1	13C
P1	10.75 usec
P2	21.50 usec
PL1	0.00 dB
SFO1	100.6227690 MHz
======== CHANNEL f2 ========	
CPDPRG2	waltz16
NUC2	1H
P3	10.15 usec
P4	20.30 usec
PCPD2	80.00 usec
PL2	-1.50 dB
PL12	16.43 dB
SFO2	400.1332108 MHz
SI	32768
SF	100.6127690 MHz
WDW	EM
SSB	0
LB	1.00 Hz
GB	0
PC	1.40

Appendix IId: Negative mode ESIMS spectrum of knipholone

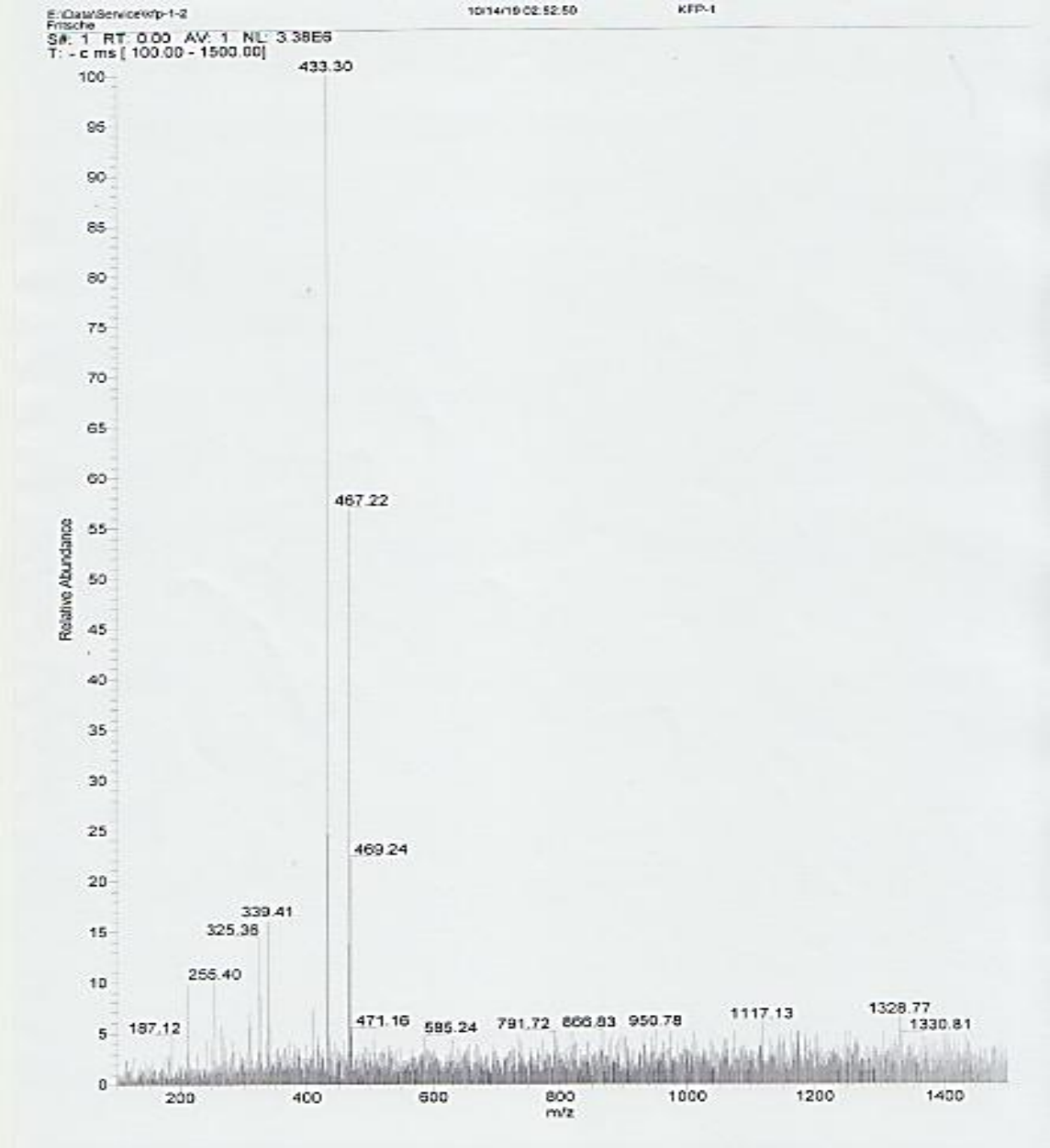

Appendix IId: Positive mode ESIMS spectrum of knipholone

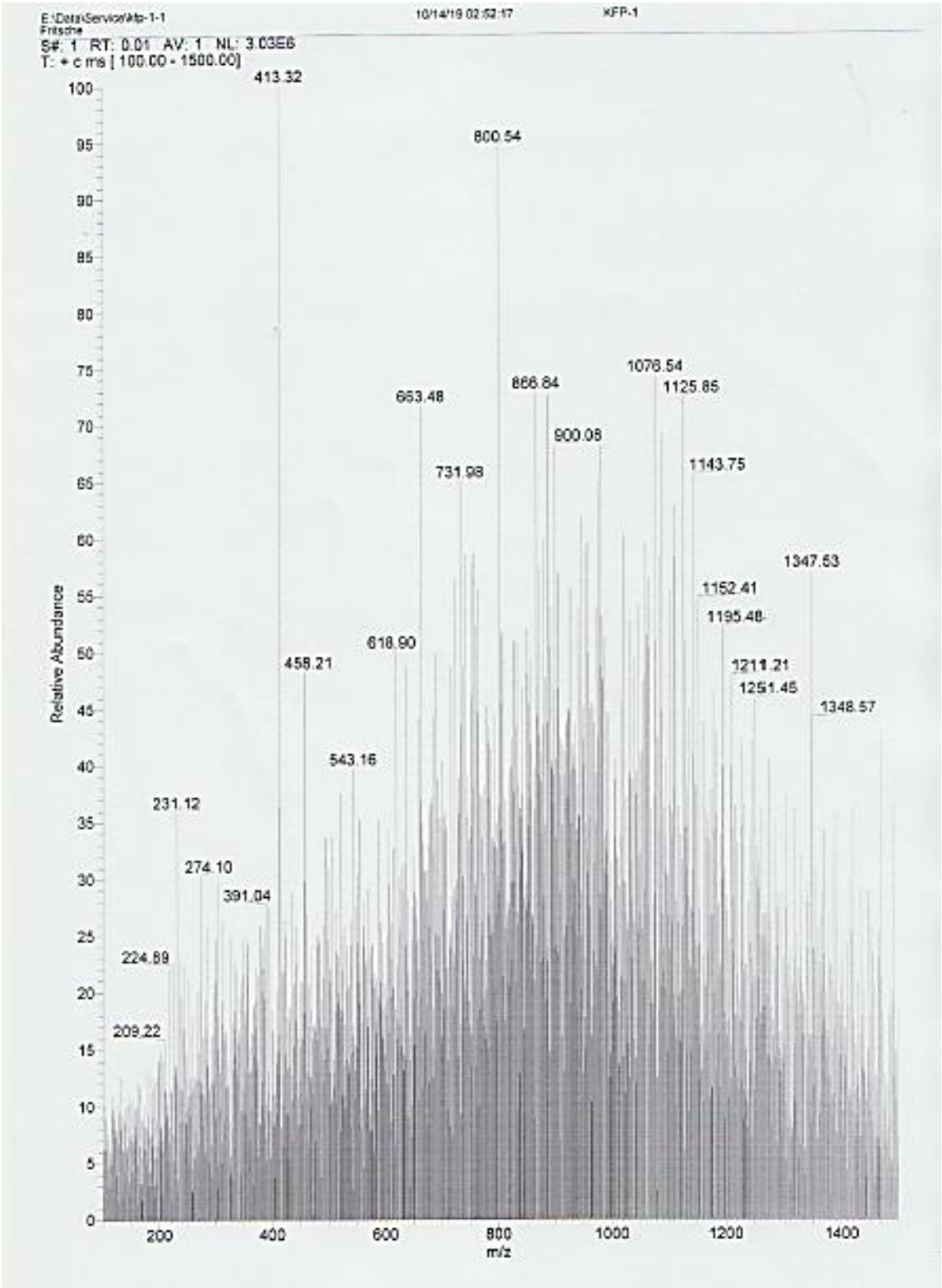

Appendix III: ^{1}H and ESIMS of 10-knipholone gentiobioside

Appendix IIIa: ^{1}H NMR spectrum of 10-kniphole gentiobioside , methanol-d_4

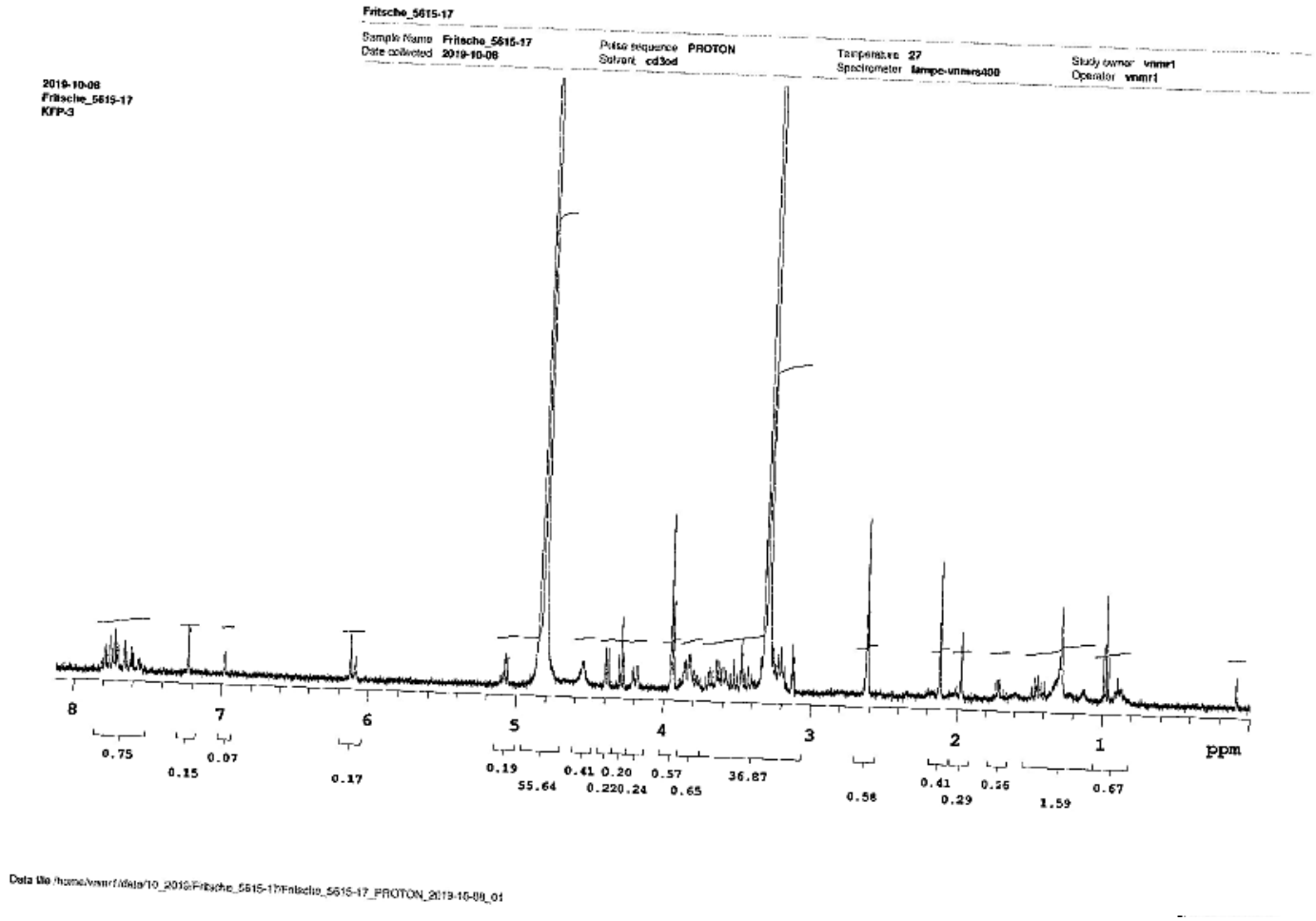

Appendix IIIa: ^{1}H NMR spectrum of 10- knipholone gentiobioside, methanol-d_4

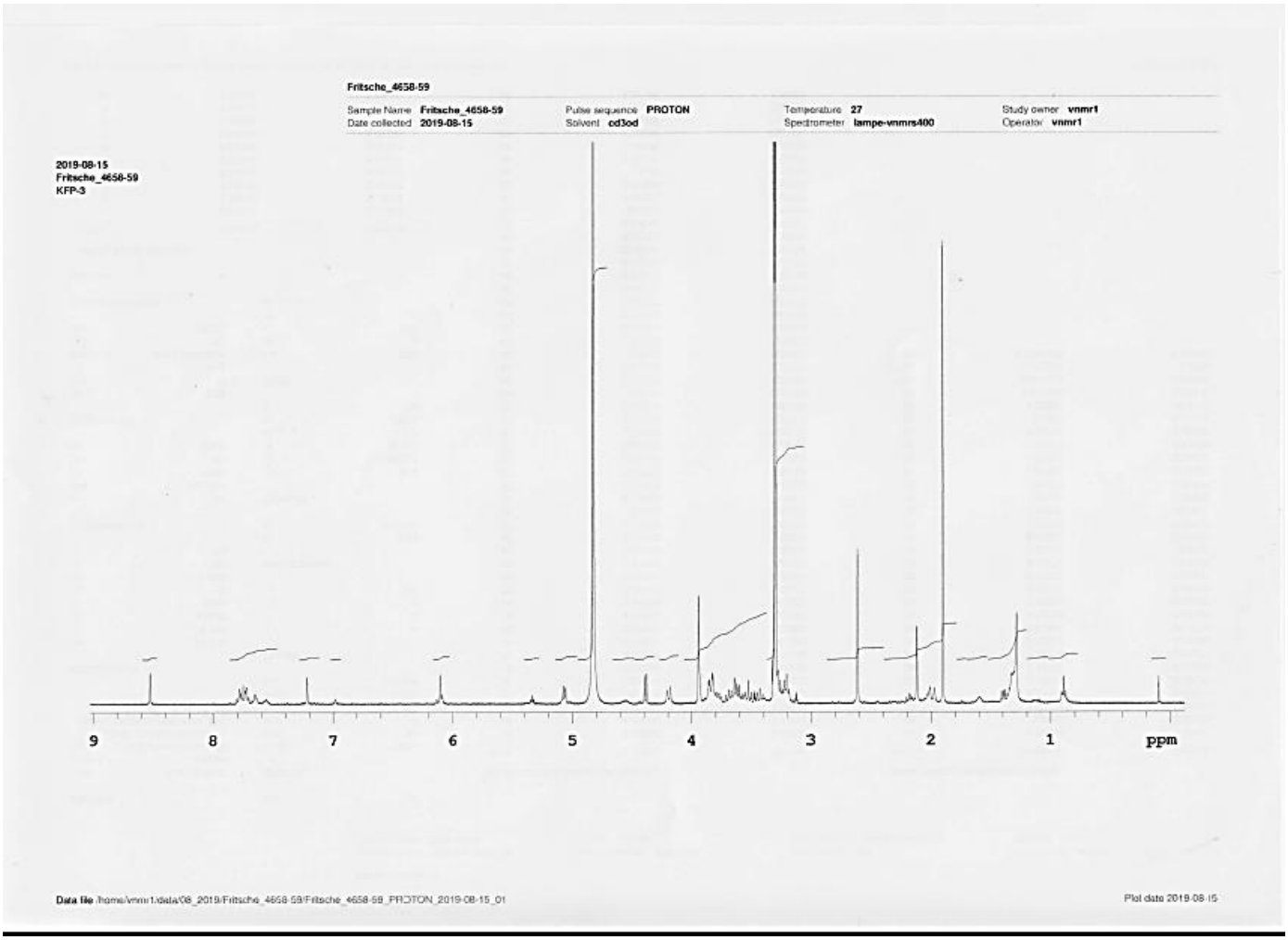

Appendix IIIb: Negative mode ESIMS spectrum of 10- knipholone gentiobioside

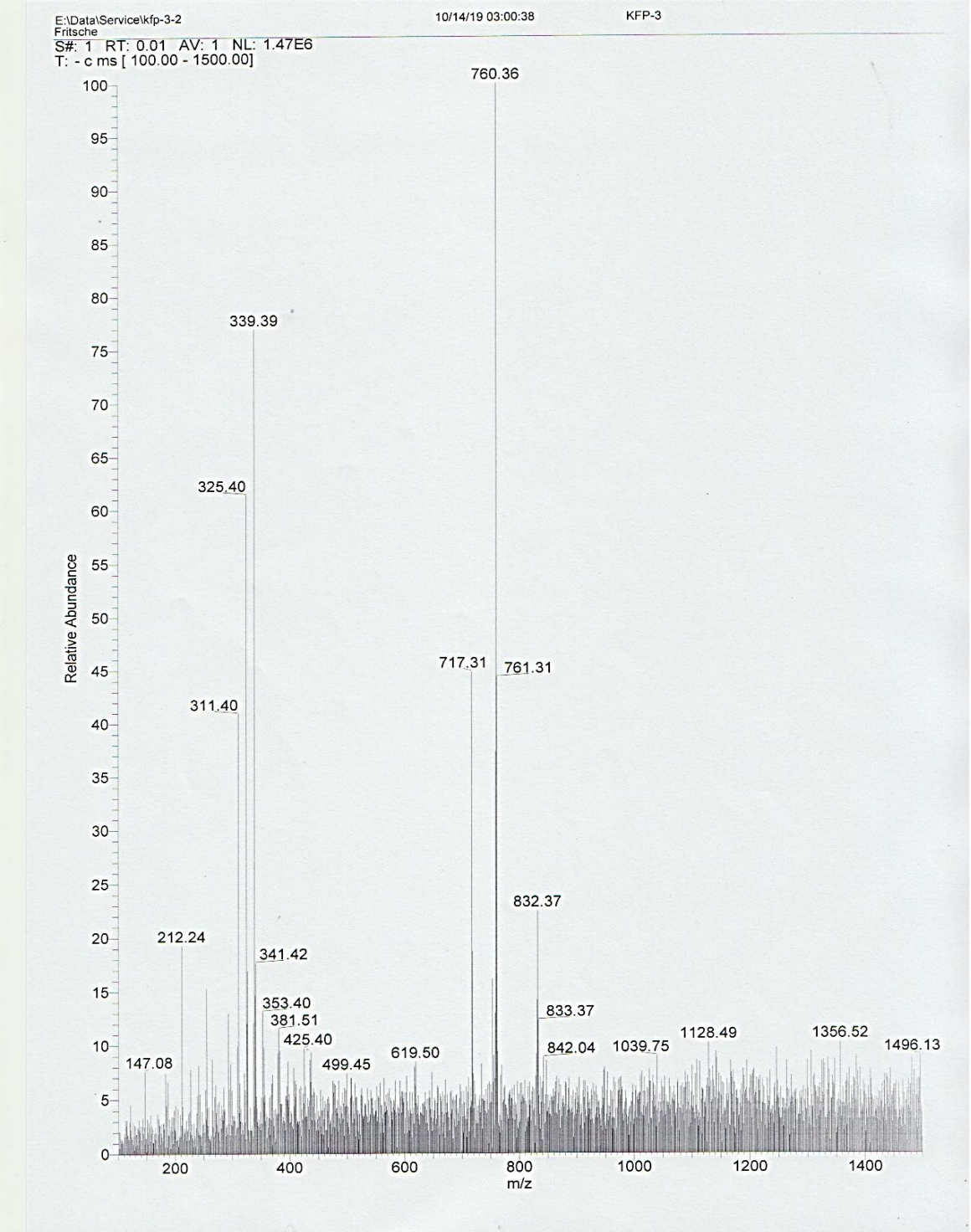

Appendix IIId: Positive mode ESIMS spectrum of 10- knipholone gentiobioside

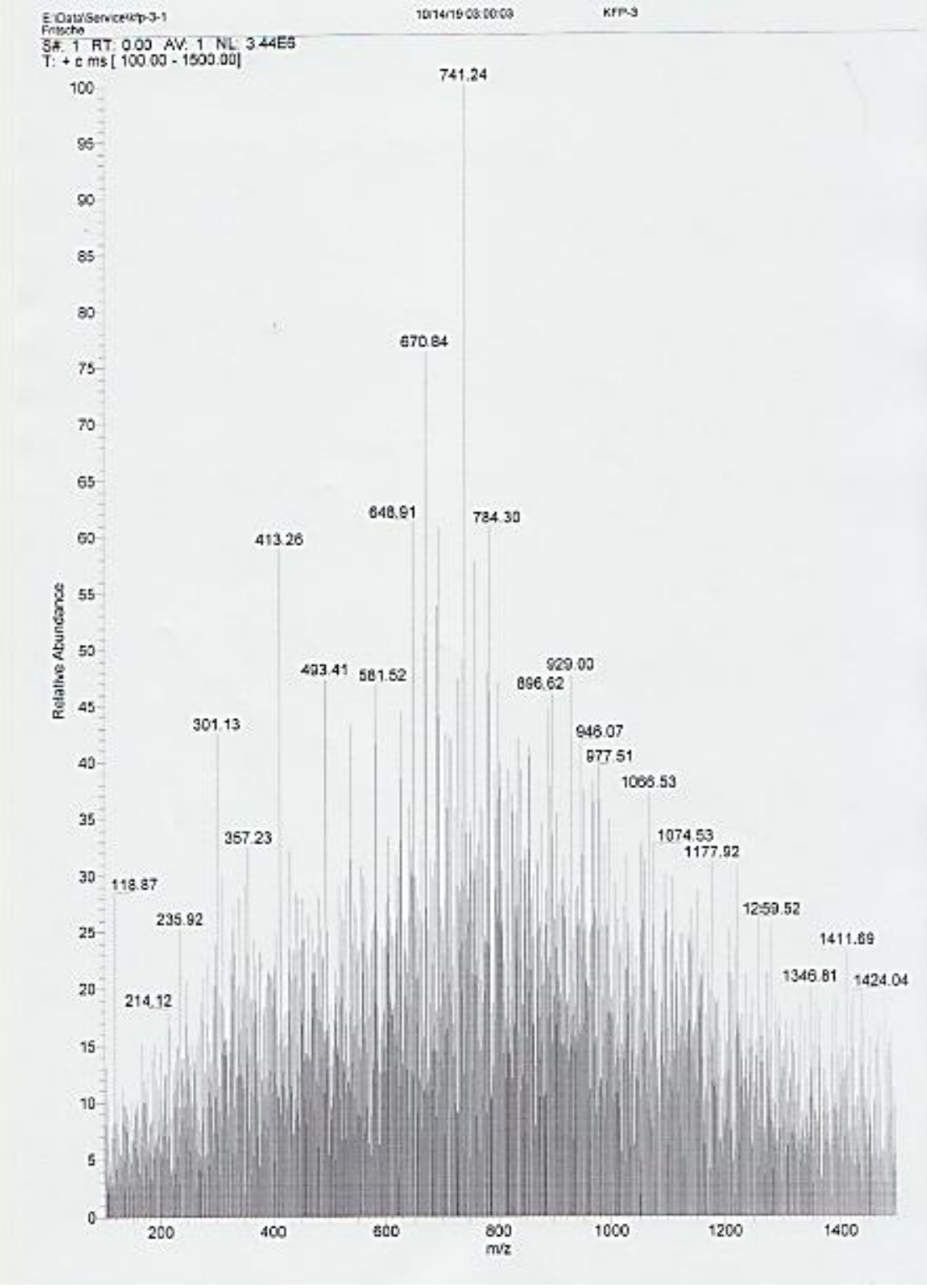

Appendix IV: ^{1}H, ^{13}C, DEPT and ESIMS of 12-hydroxypentadec-9-en-1-yl methyl phthalate

Appendix IVa: ^{1}H NMR spectrum of 12-hydroxypentadec-9-en-1-yl methyl phthalate, chloroform-*d*

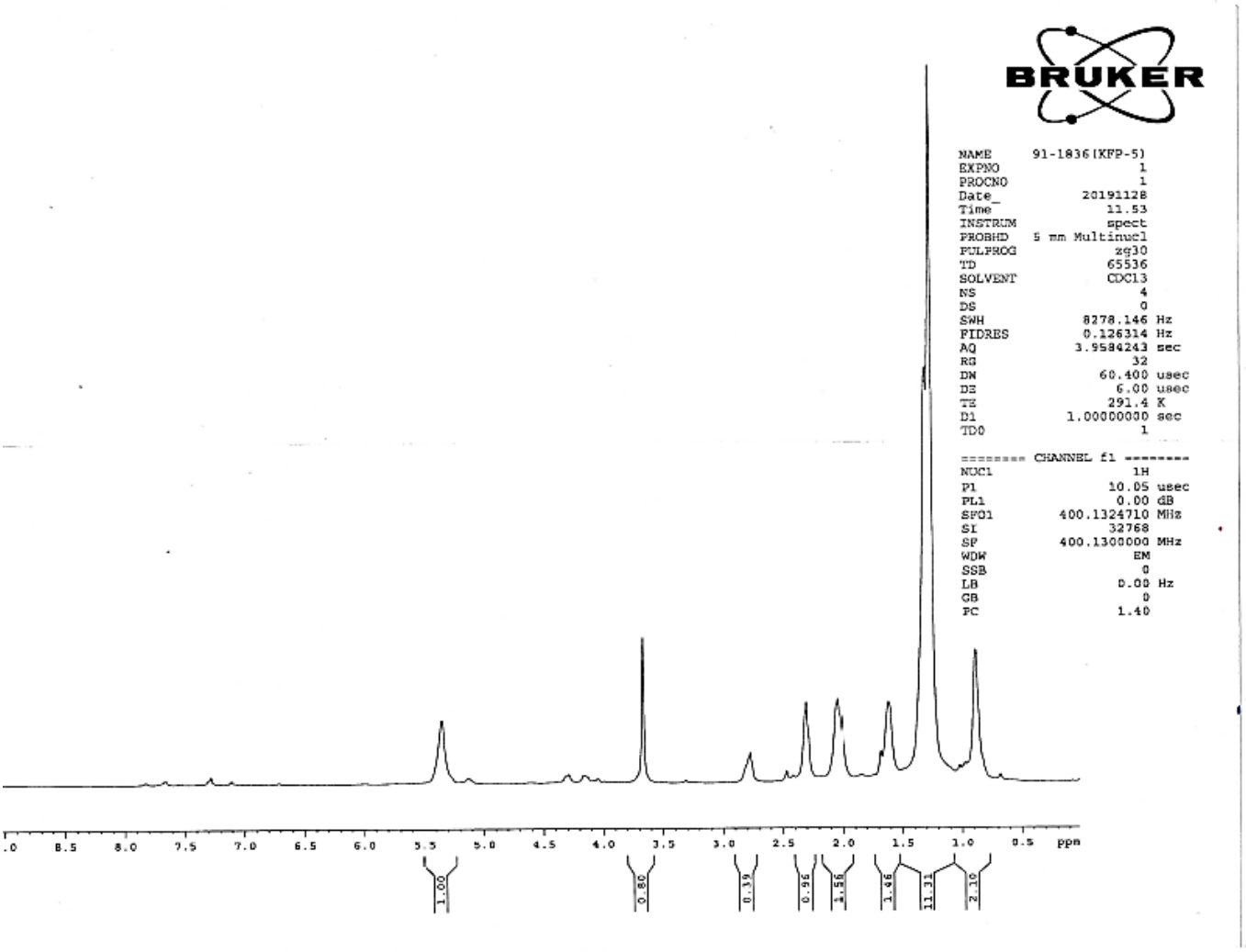

Appendix IVb: ^{13}C NMR spectrum of 12-hydroxypentadec-9-en-1-yl methyl phthalate, chloroform-*d*

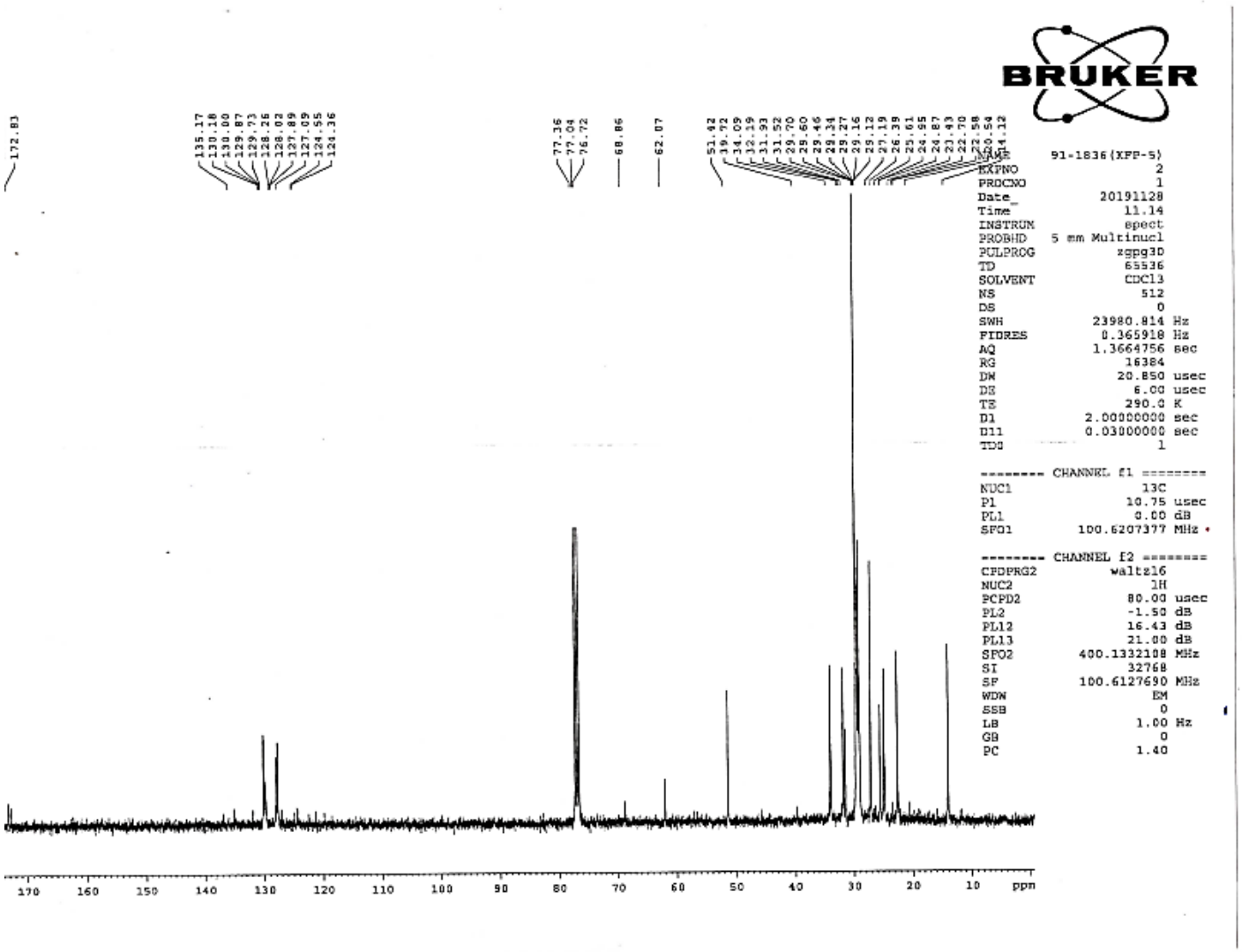

Appendix IVc: DEPT spectrum of 12-hydroxypentadec-9-en-1-yl methyl phthalate, chloroform-*d*

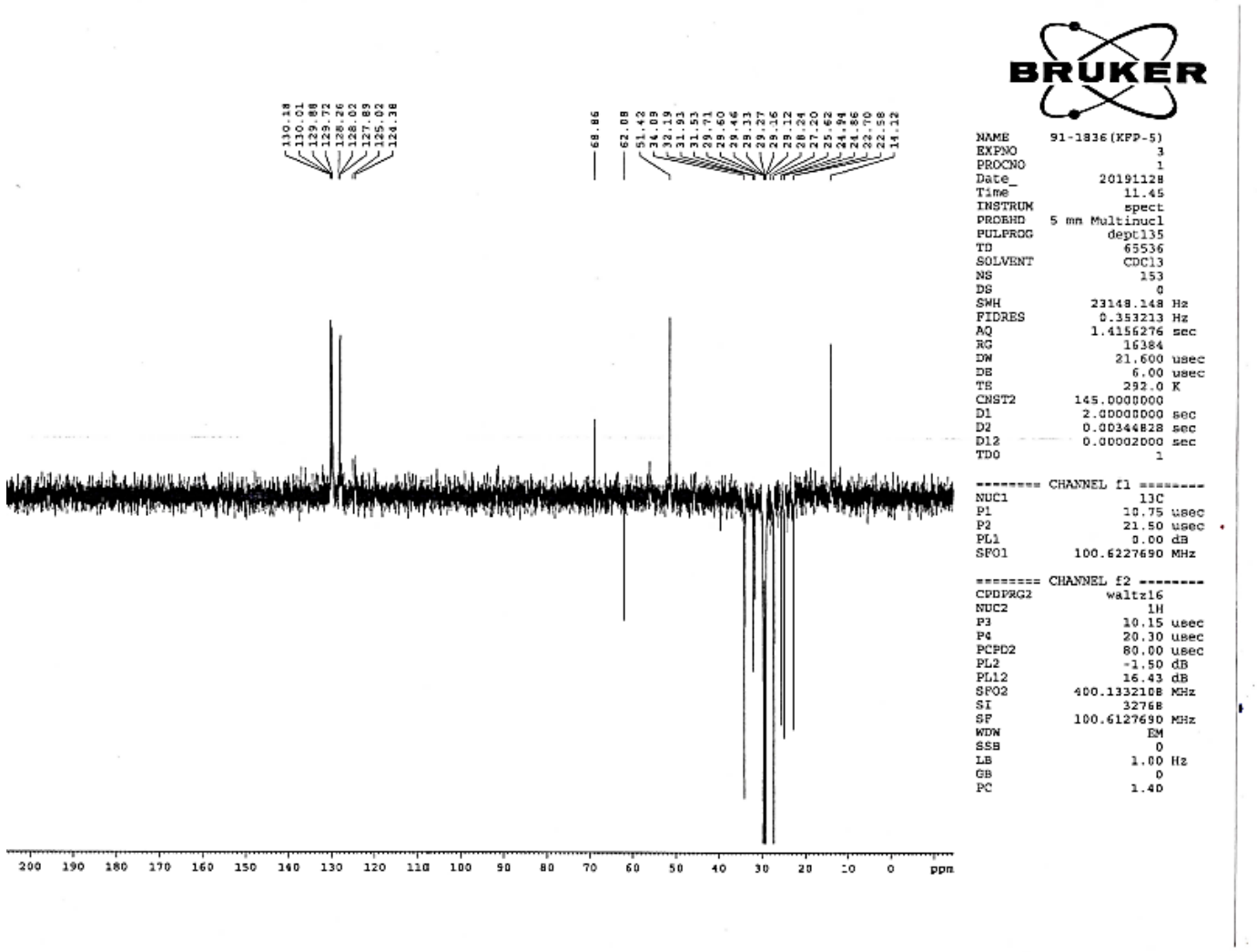

Appendix IVd: ESIMS spectrum of 12-hydroxypentadec-9-en-1-yl methyl phthalate

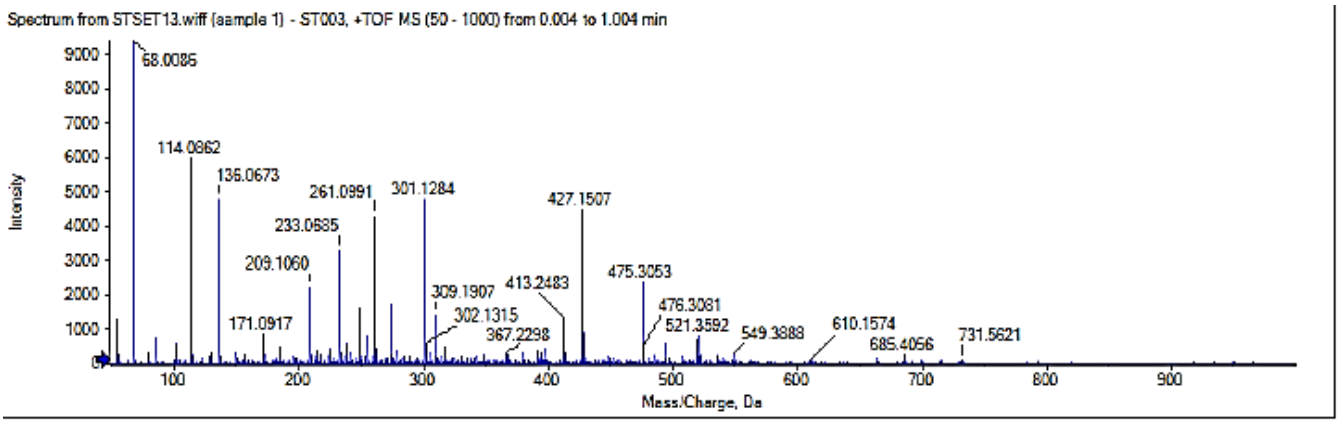

Appendix V: ^{1}H and ESIMS of knipholone isolated from *K. insignis*

Appendix Va: ^{1}H NMR spectrum of knipholone, chloroform-*d*

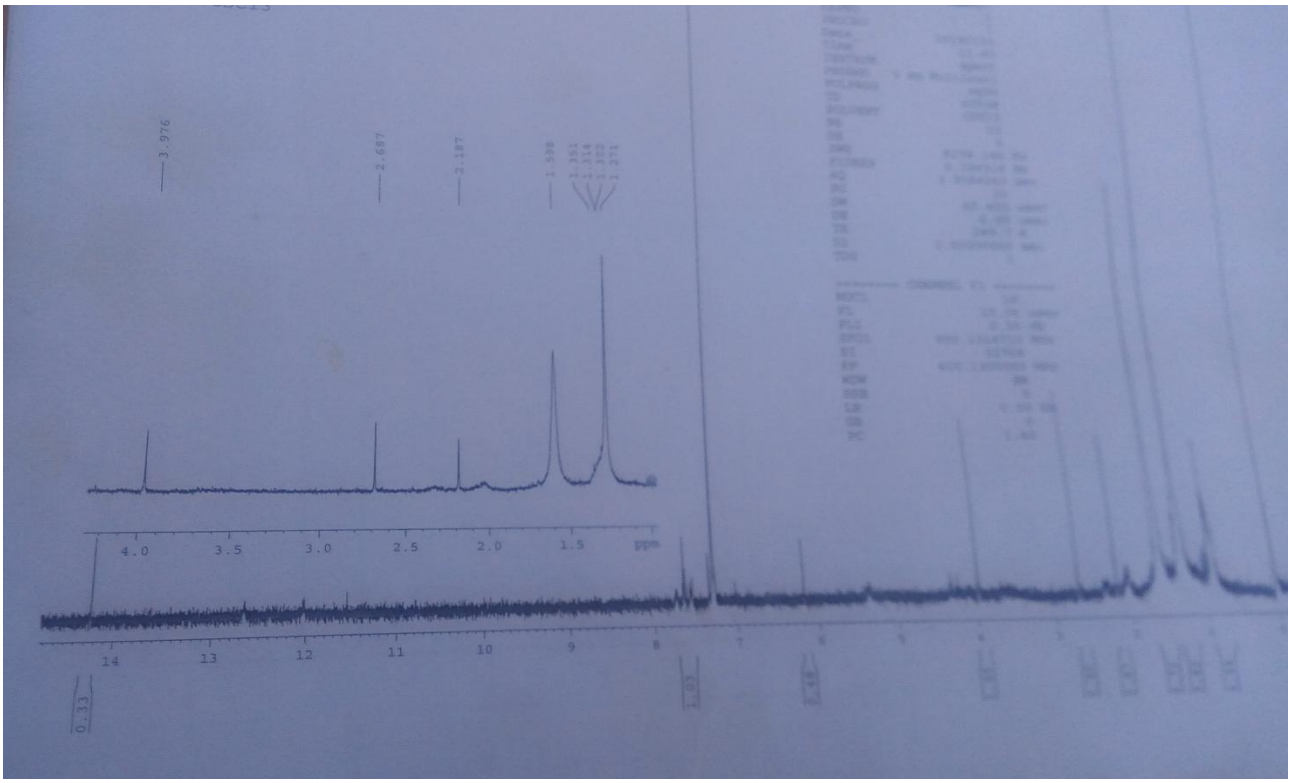

Appendix Vb: ESIMS spectrum of knipholone

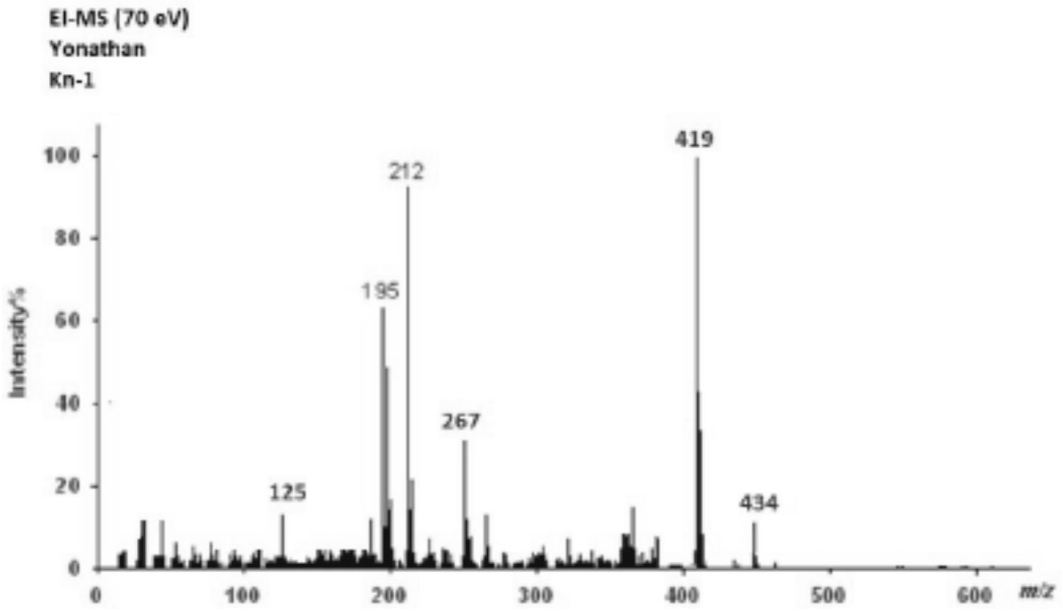

Appendix VI: Molecular docking supplementary figures

A. B.

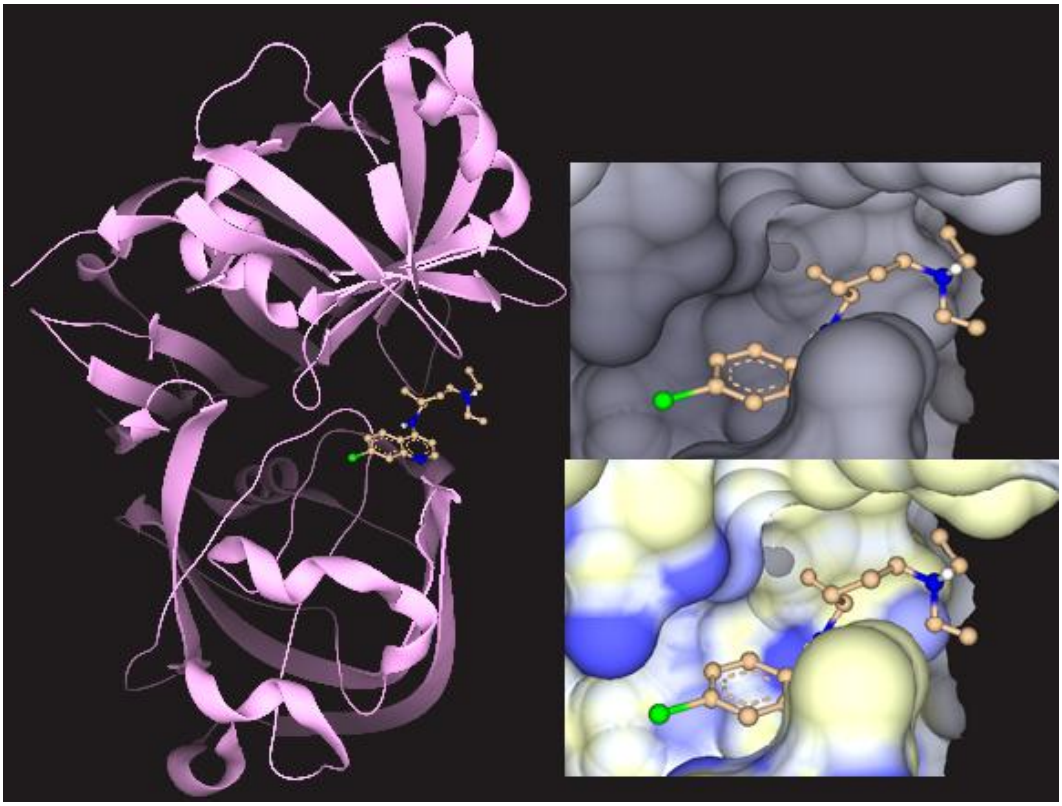

D. E.

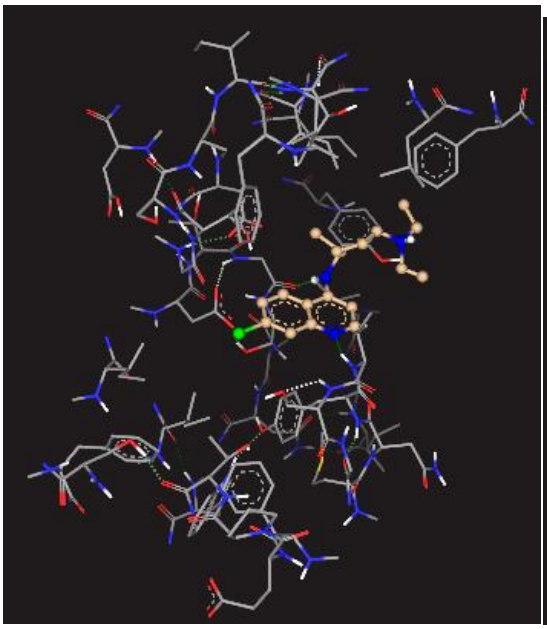

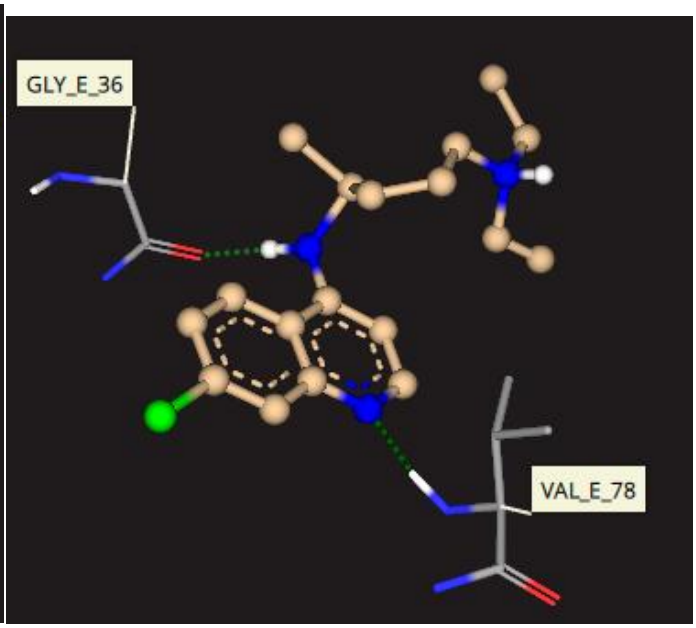

F.

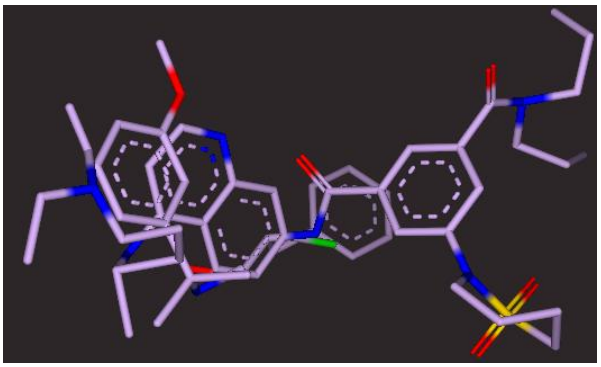

Figure VIa. A) Ribbon diagram of docked chloroquine-plasmepsin II chain E subunit complex. B) Surface representation showing chloroquine in the binding site of plasmepsin II. Chloroquine is shown in ball-stick model. C) Surface representation showing chloroquine in the binding site of plasmepsin II with lipophilicity coloring. White representing hydrophobic pockets and blue representing hydrophilic pockets. Chloroquine is shown in ball-stick model. D) Binding interaction of chloroquine with amino acid residues of plasmepsin II. E) Hydrogen bond interaction of chloroquine with amino acid residues Gly36 and Val78. F) Superimposition of chloroquine with P2FE-400 in the binding site of plasmepsin II.

A. B.

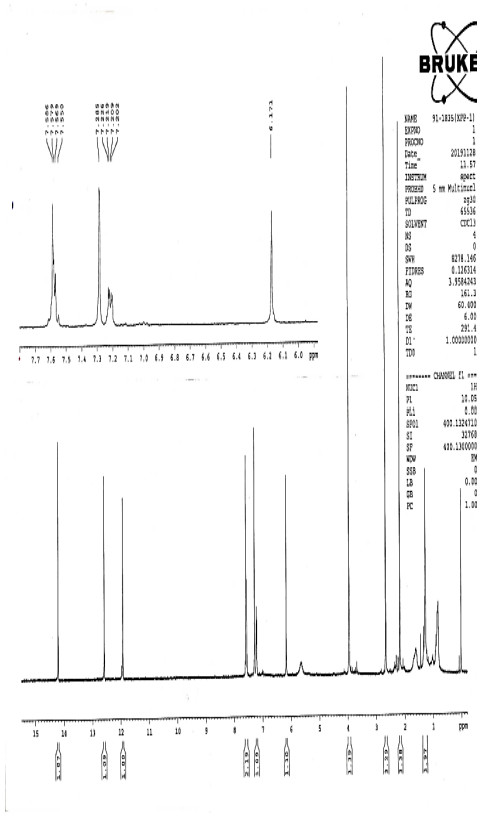

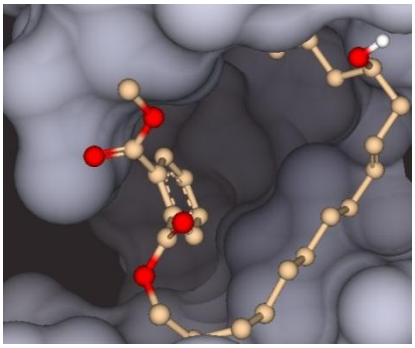

C.

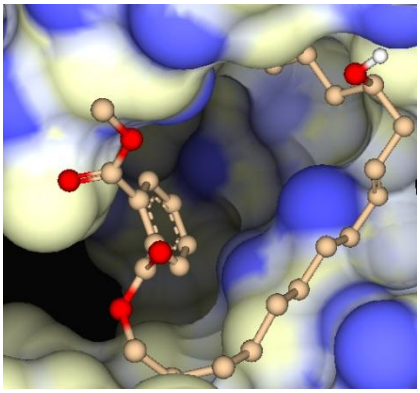

D. E.

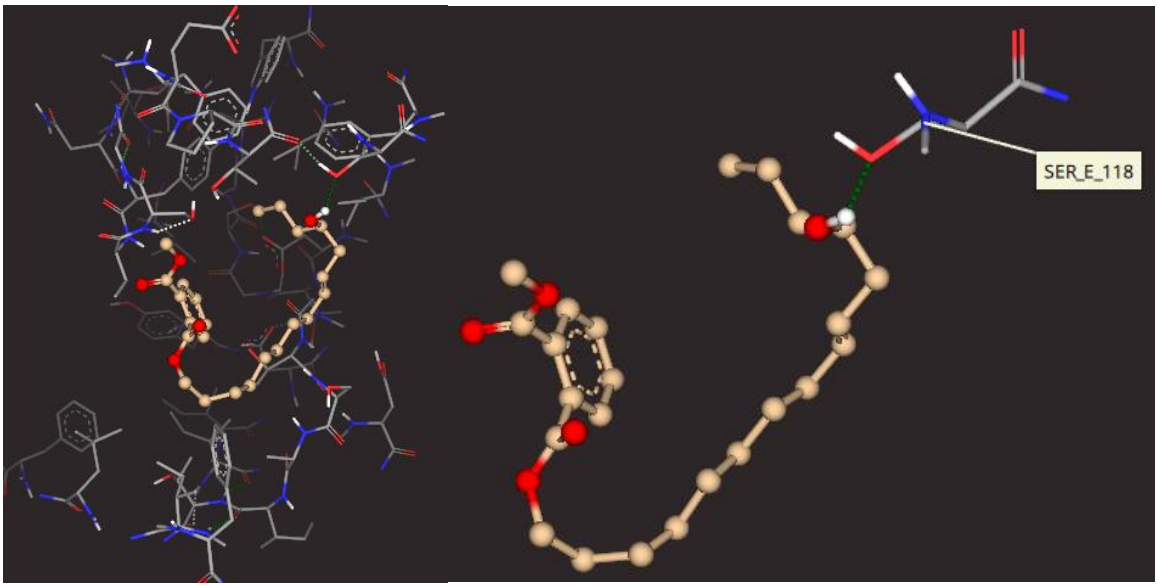

F.

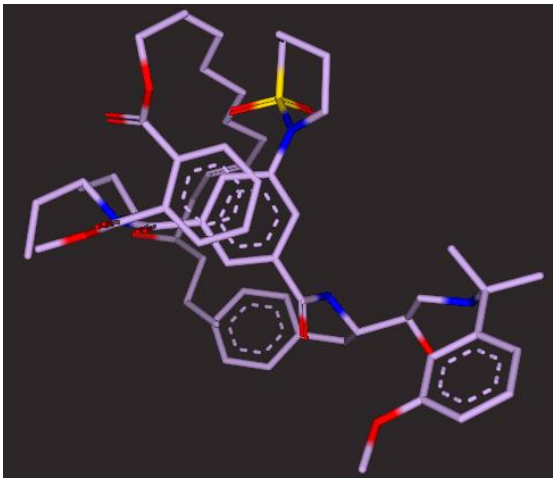

Figure VIb. A) Ribbon diagram of docked KFP-5-plasmepsin II chain E subunit complex. B) Surface representation showing KFP-5 in the binding site of plasmepsin II. KFP-5 is shown in ball-stick model. C) Surface representation showing KFP-5 in the binding site of plasmepsin II with lipophilicity coloring. White representing hydrophobic pockets and blue representing hydrophilic pockets. KFP-5 is shown in ball-stick model. D) Binding interaction of KFP-5 with amino acid residues of plasmepsin II. E) Hydrogen bond interaction of KFP-5 with amino acid residues amino acid residue Ser118. F) Superimposition of KFP-5 with P2FE-400 in the binding site of plasmepsin II.

A. B. C.

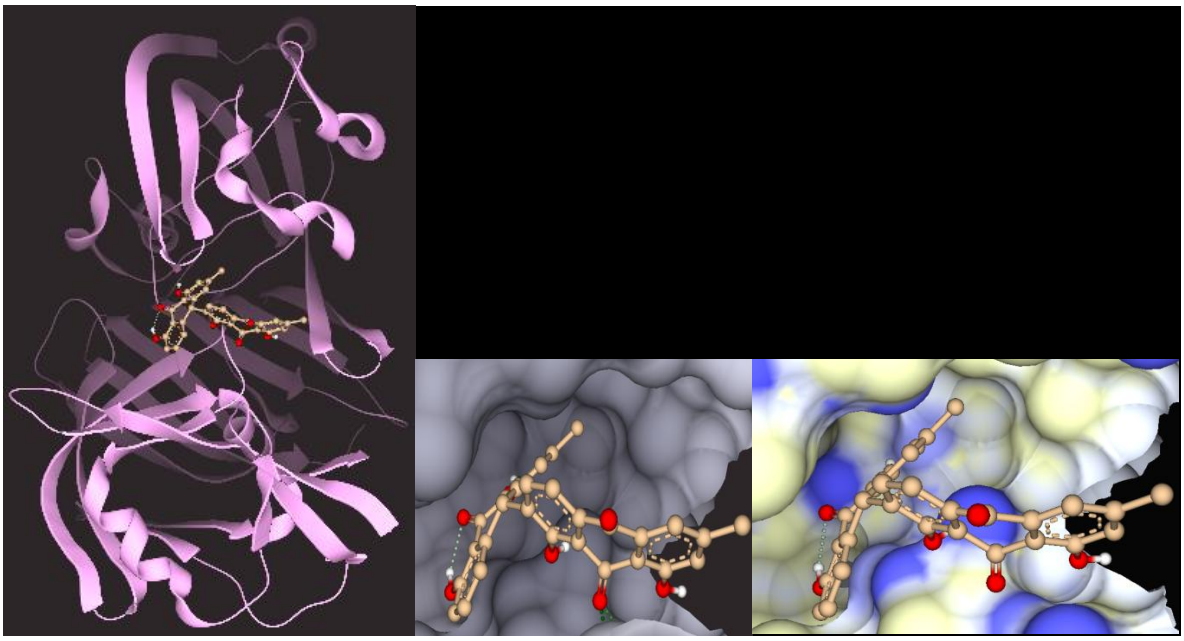

D. E.

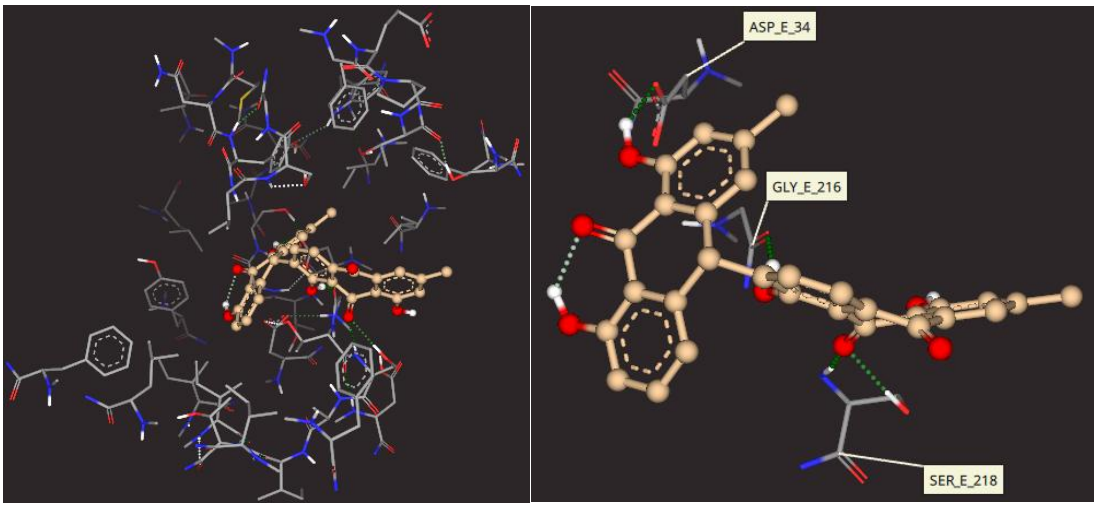

F.

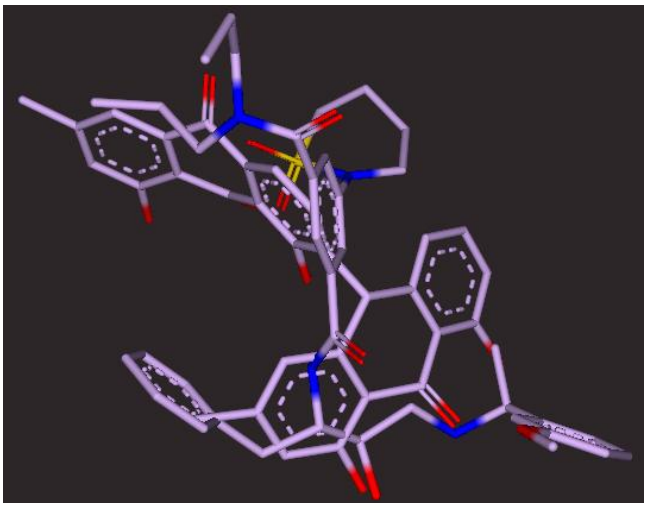

Figure VIc. A) Ribbon diagram of docked anthraquinone-plasmepsin II chain E subunit complex. B) Surface representation showing anthraquinone dimer in the binding site of plasmepsin II. Anthraquinone dimer is shown in ball-stick model. C) Surface representation showing anthraquinone dimer in the binding site of plasmepsin II with lipophilicity coloring. White representing hydrophobic pockets and blue representing hydrophilic pockets. KFP-5 is shown in ball-stick model. D) Binding interaction of anthraquinone dimer with amino acid residues of plasmepsin II. E) Hydrogen bond interaction of anthraquinone dimer with amino acid residues amino acid residue Ser118. F) Superimposition of anthraquinone dimer with P2FE-400 in the binding site of plasmepsin II.

A. B.

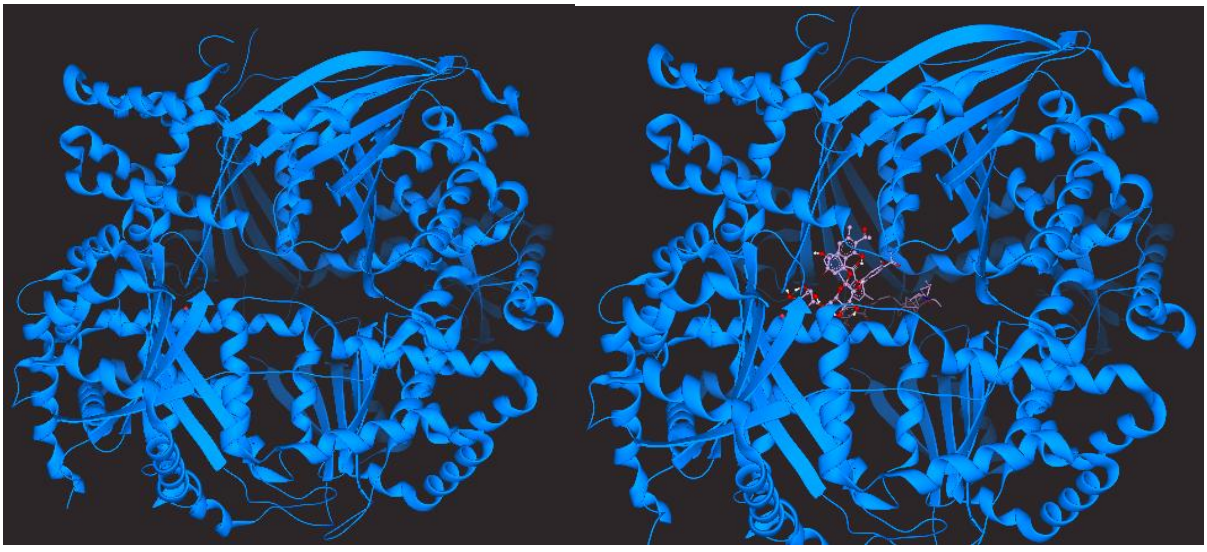

C. D.

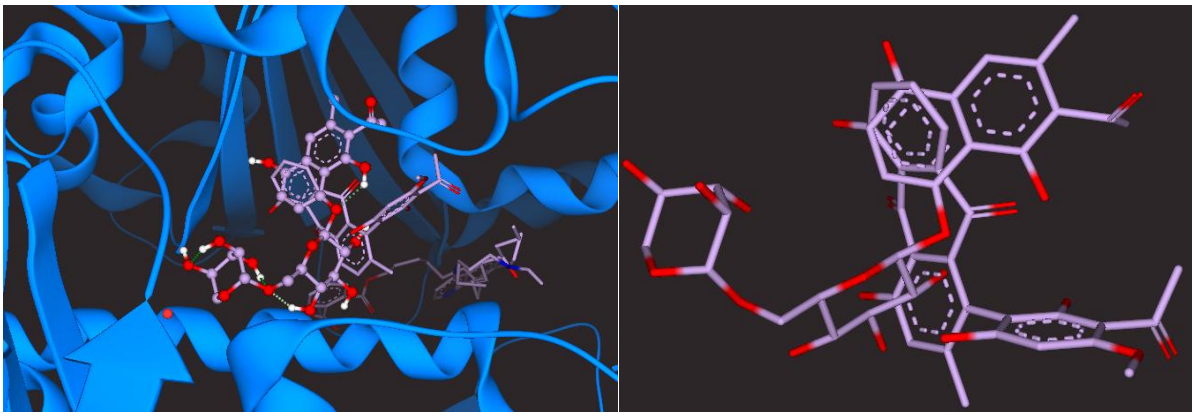

E.

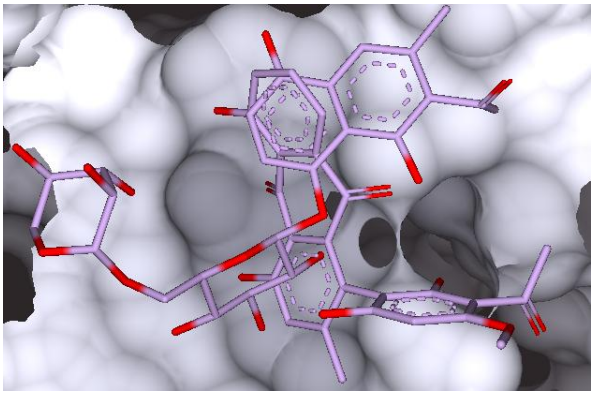

Figure VId. The three-dimensional structure of falcilysin (PDB 3s5h). A) Ribbon diagram of falcilysin (PDB 3s5h). B) Ribbon diagram of the docked compounds-falcilysin complex. Naphthalene derivative1 is shown as balls-sticks, while all other compounds are shown as solid lines C) A close-up view of diagram B. D) Superimposition of knipholone with naphthalene derivative1 in the binding site of falcilysin. E) Surface representation showing the docked compounds in the binding site of falcilysin

A. B.

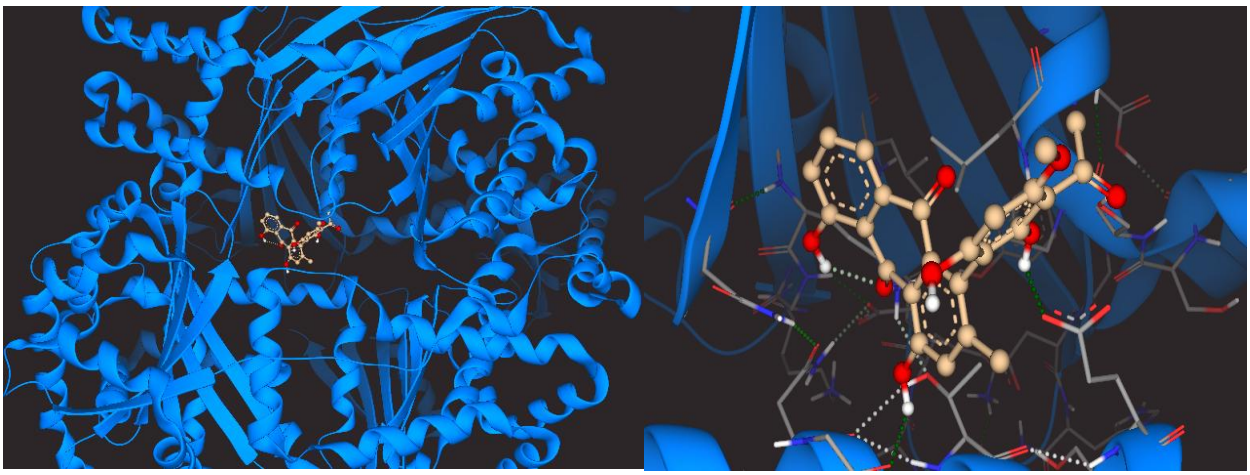

C. D.

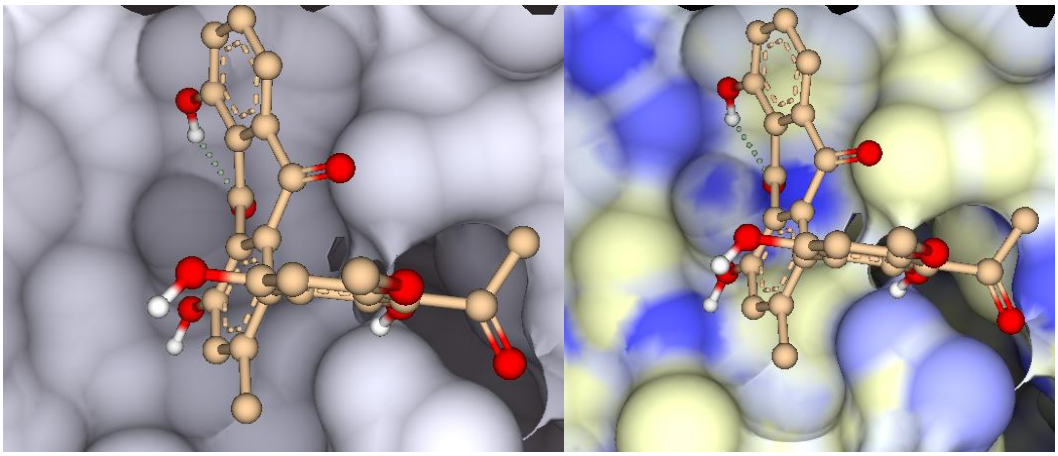

E. F.

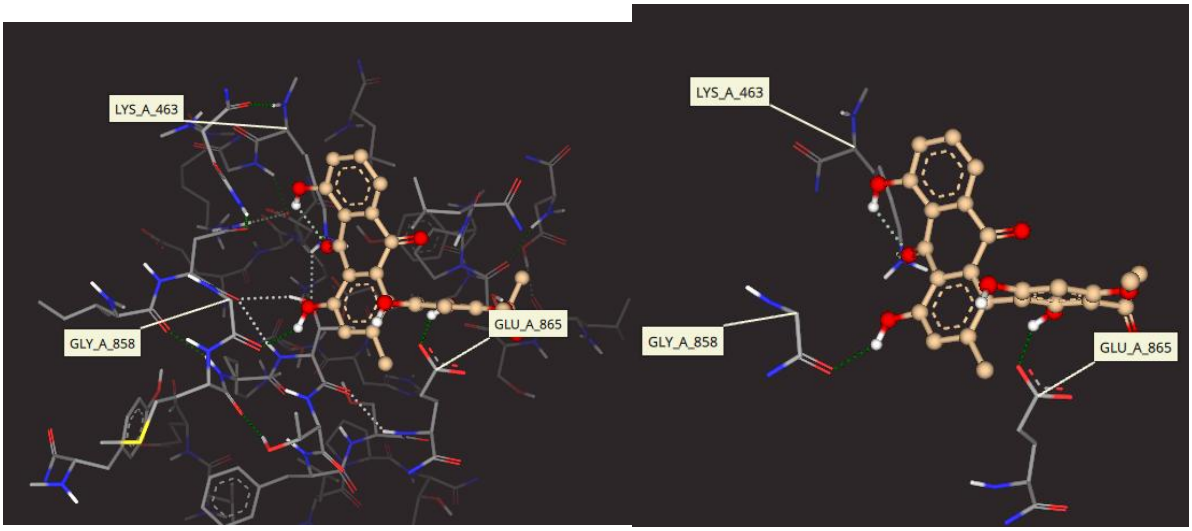

Figure VIe. A) Ribbon diagram of docked knipholone-falcilysin complex. knipholone is shown in ball-stick model. B) A close-up view of diagram A. C) Surface representation showing knipholone in the binding site of falcilysin. Knipholone is shown in ball-stick model. D) Surface representation showing knipholone in the binding site of plasmepsin II (PDB 4cku) with lipophilicity coloring. White representing hydrophobic pockets and blue representing hydrophilic pockets. Knipholone is shown in ball-stick model. E) Binding interaction of knipholone with amino acid residues of falcilysin. F) Hydrogen bond interaction of knipholone with amino acid residues amino acid residue Lys463, Gly858 and Glu865.

A. B.

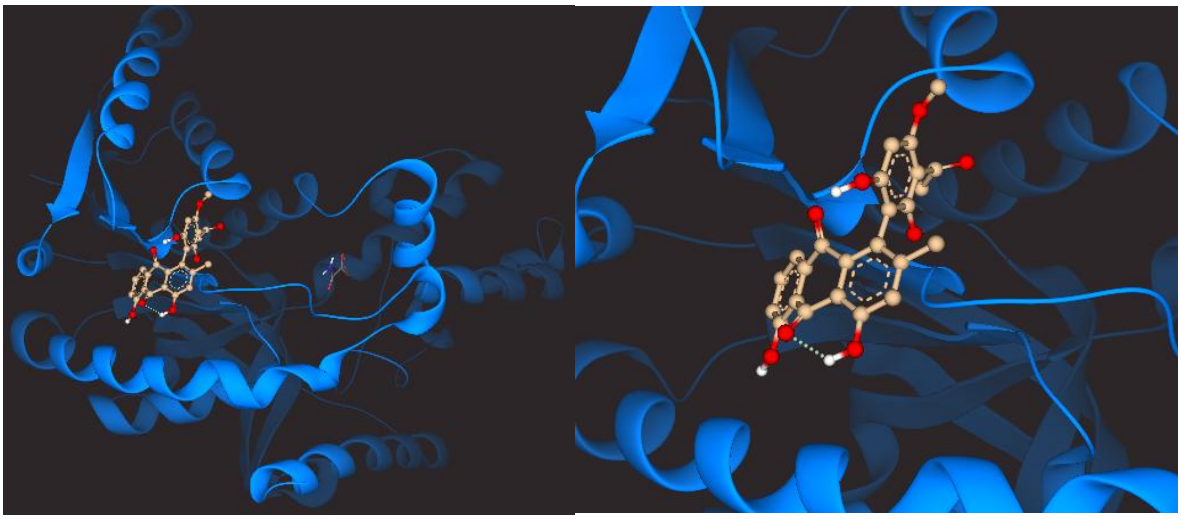

C. D.

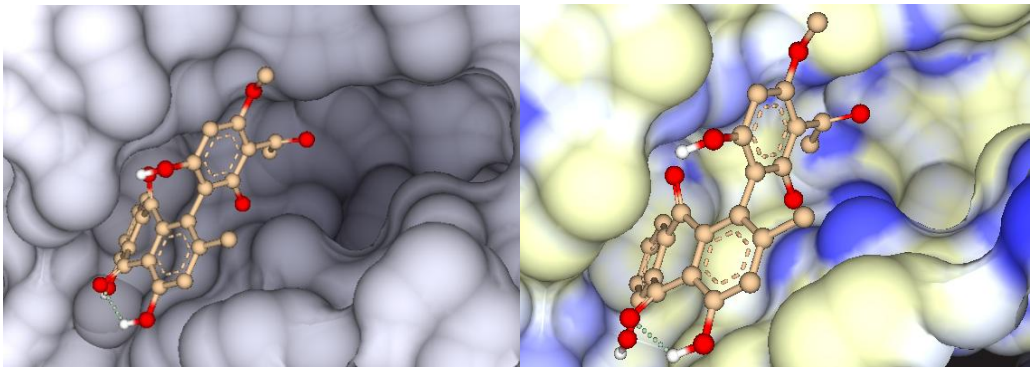

E. F.

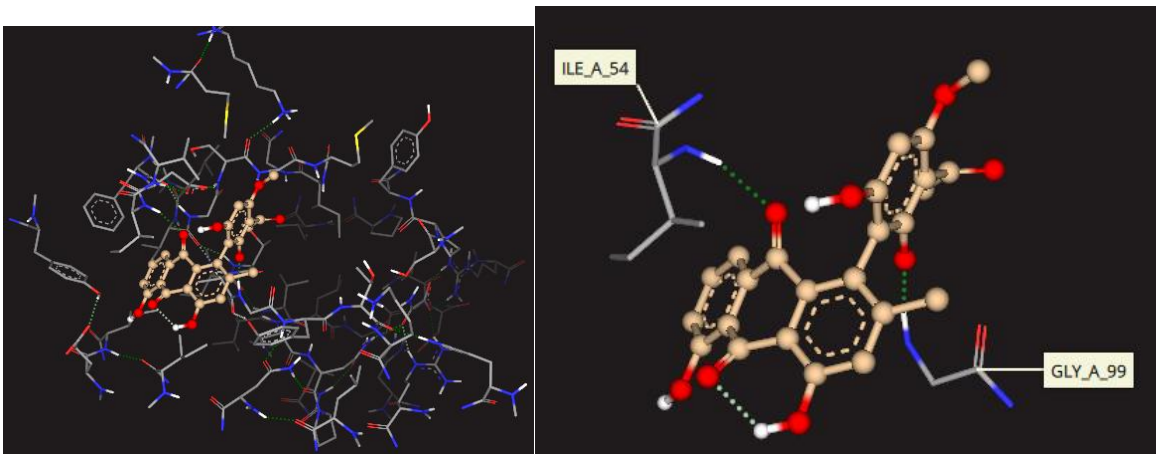

Figure VIf. A) Ribbon diagram of docked knipholone- pfLDH complex. Knipholone is shown in ball-stick model. B) A close-up view of diagram A. C) Surface representation showing knipholone in the binding site of pfLDH. Knipholone is shown in ball-stick model. D) Surface representation showing knipholone in the binding site of pfLDH with lipophilicity coloring. White representing hydrophobic pockets and blue representing hydrophilic pockets. Knipholone

is shown in ball-stick model. E) Binding interaction of knipholone with amino acid residues of pfLDH. F) Hydrogen bond interaction of knipholone with amino acid residues amino acid residue Ile54 and Gly99.

A.

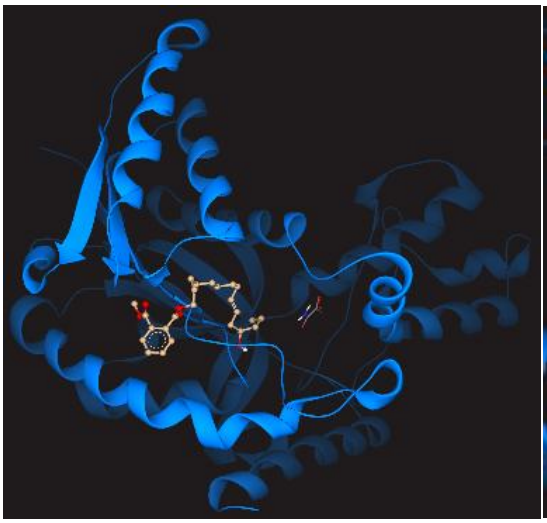

B.

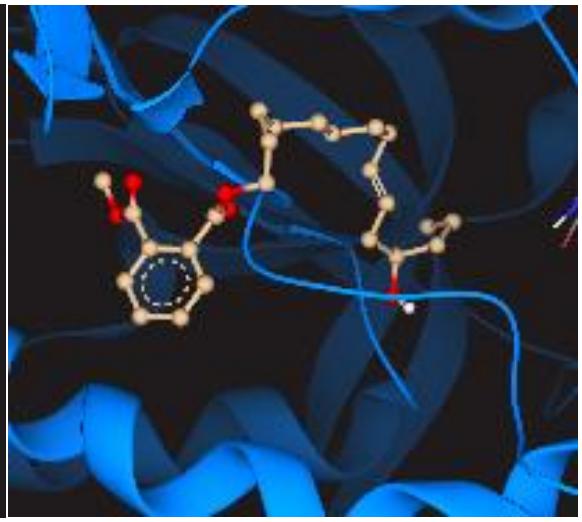

C.

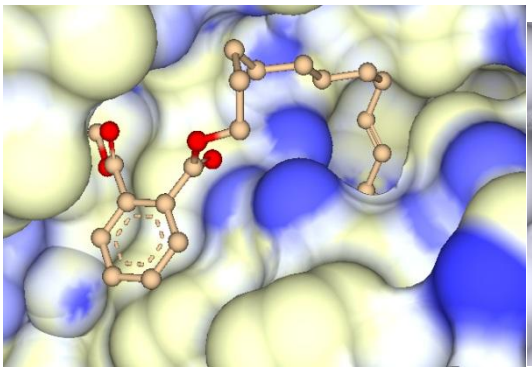

D.

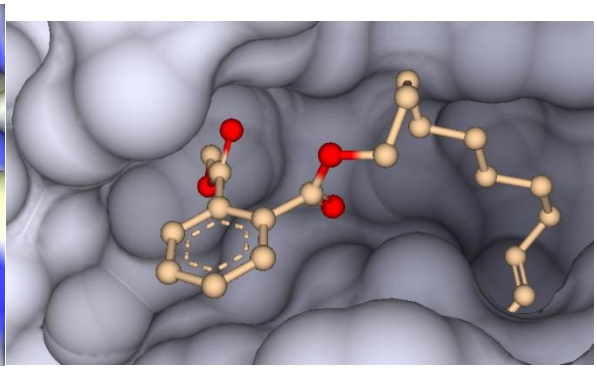

E.

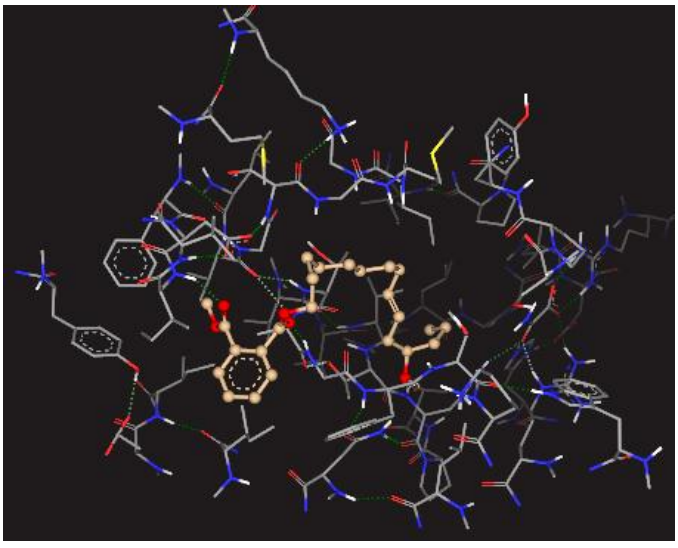

F.

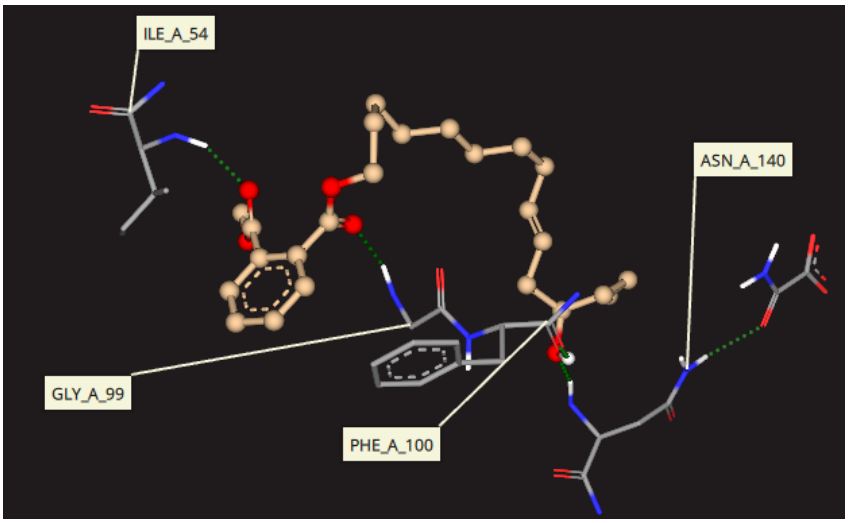

G.

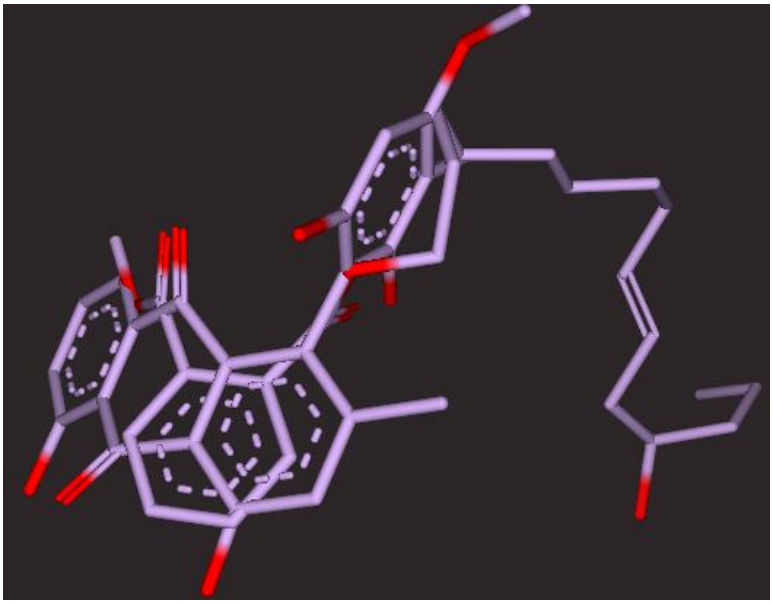

Figure VIg. A) Ribbon diagram of docked KFP-5-pfLDH complex. KFP-5 is shown in ball-stick model. B) A close-up view of diagram A. C) Surface representation showing KFP-5 in the binding site of pfLDH. KFP-5 is shown in ball-stick model. D) Surface representation showing KFP-5 in the binding site of pfLDH with lipophilicity coloring. White representing hydrophobic pockets and blue representing hydrophilic pockets. KFP-5 is shown in ball-stick model. E) Binding interaction of KFP-5 with amino acid residues of pfLDH. F) Hydrogen bond interaction of knipholone with amino acid residues amino acid residue Ile54, Gly99, Phe100 and Asn140. G) Superimposition of KFP-5 with knipholone in the binding site of pfLDH.

A. B.

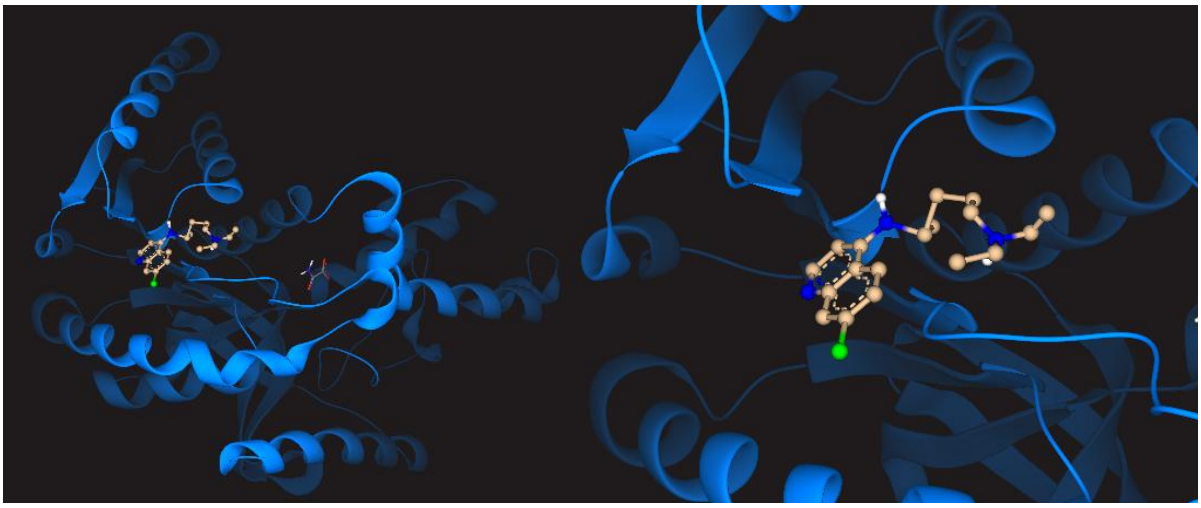

C. D.

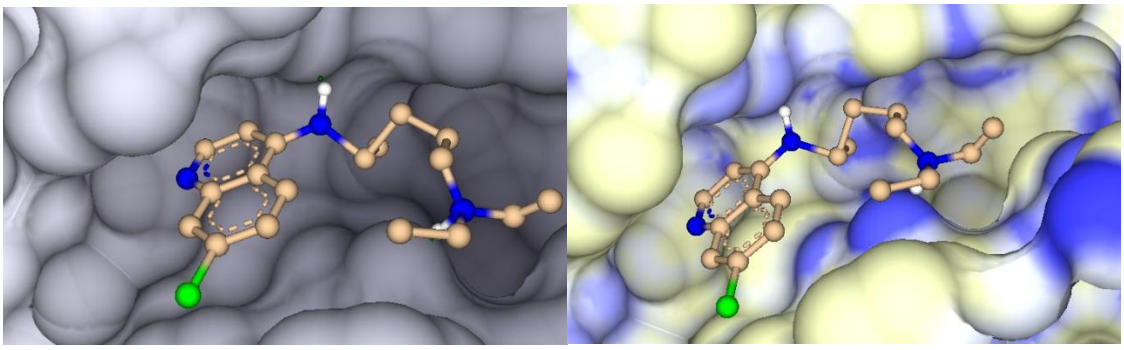

E. F.

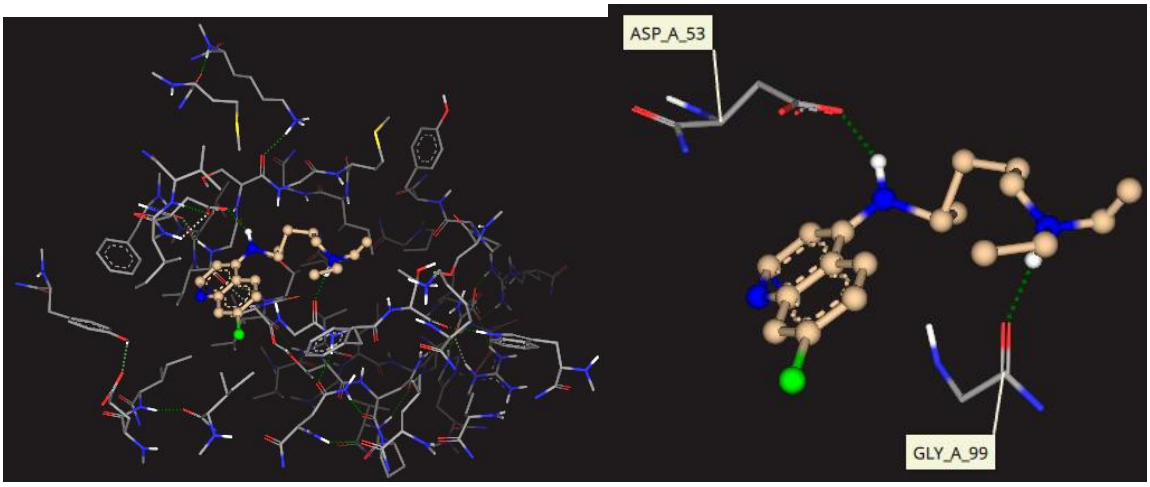

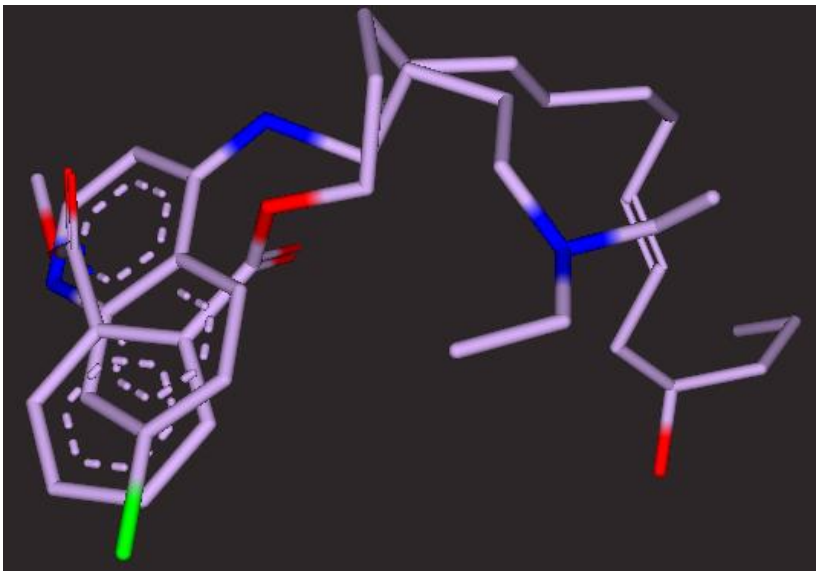

Figure VIh. A) Ribbon diagram of docked chloroquine-pfLDH complex. Chloroquine is shown in ball-stick model. B) A close up view of diagram A. C) Surface representation showing chloroquine in the binding site of pfLDH. Chloroquine is shown in ball-stick model. D) Surface representation showing chloroquine in the binding site of pfLDH with lipophilicity coloring. White representing hydrophobic pockets and blue representing hydrophilic pockets. Chloroquine is shown in ball-stick model. E) Binding interaction of chloroquine with amino acid residues of pfLDH. F) Hydrogen bond interaction of chloroquine with amino acid residues amino acid residue Asn53 and Gly99, Phe100. G) Superimposition of chloroquine with knipholone in the binding site of pfLDH.

A. B.

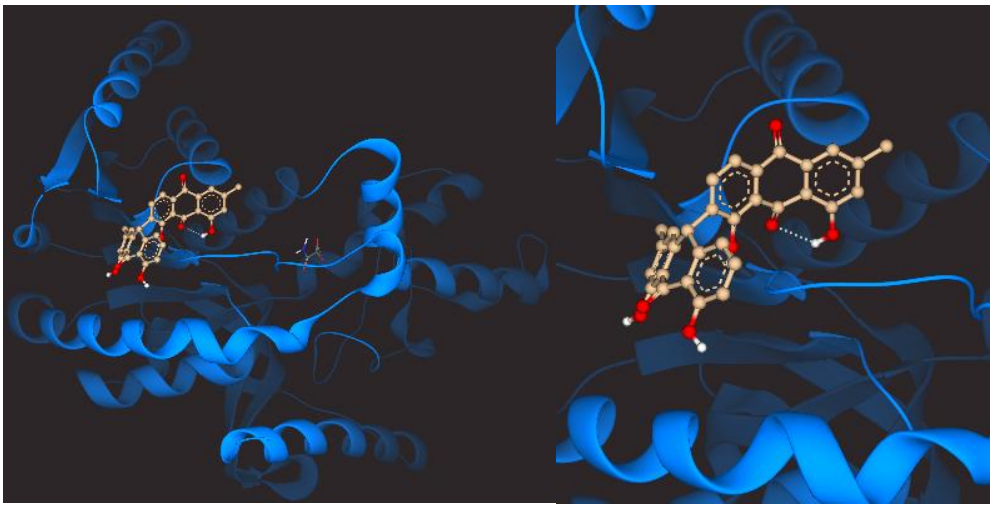

C.

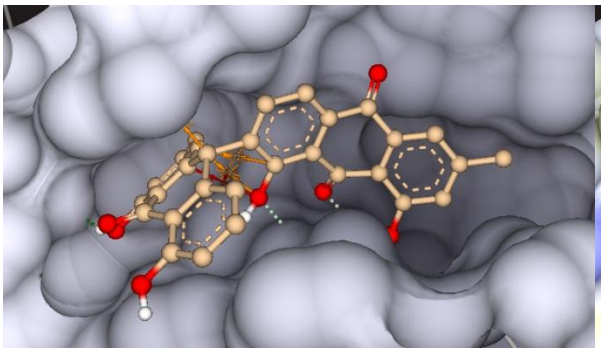

D.

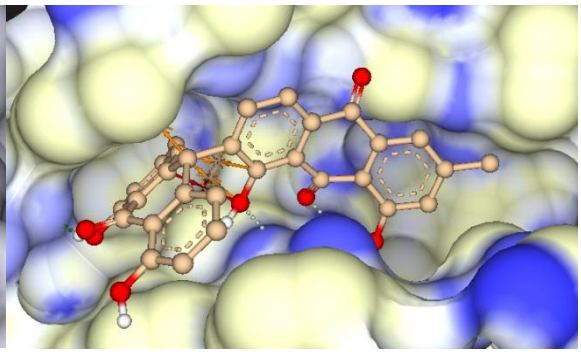

E.

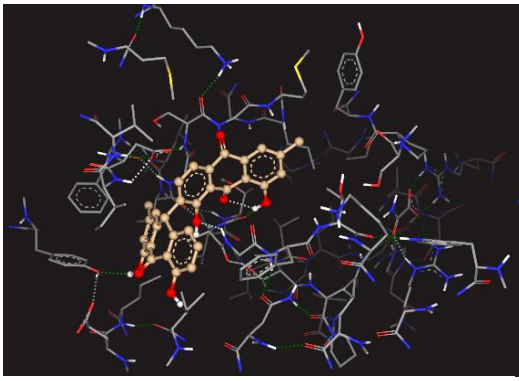

F.

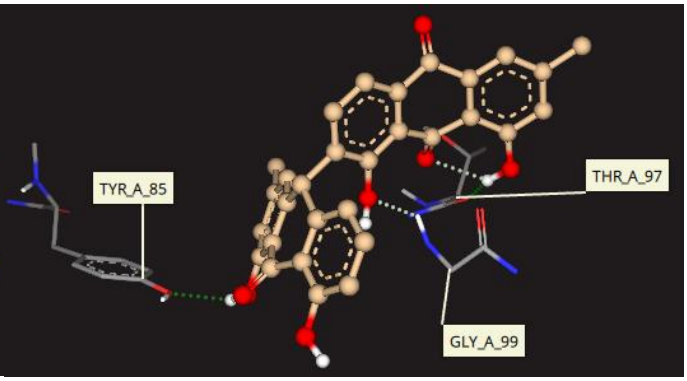

G.

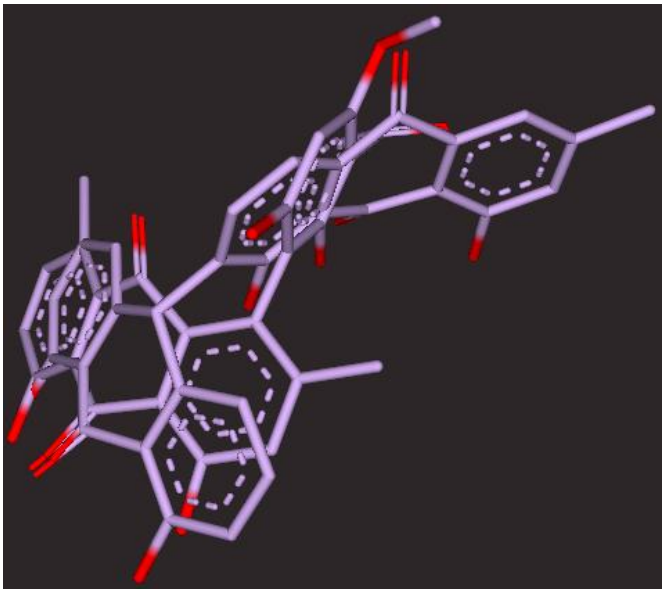

H. I.

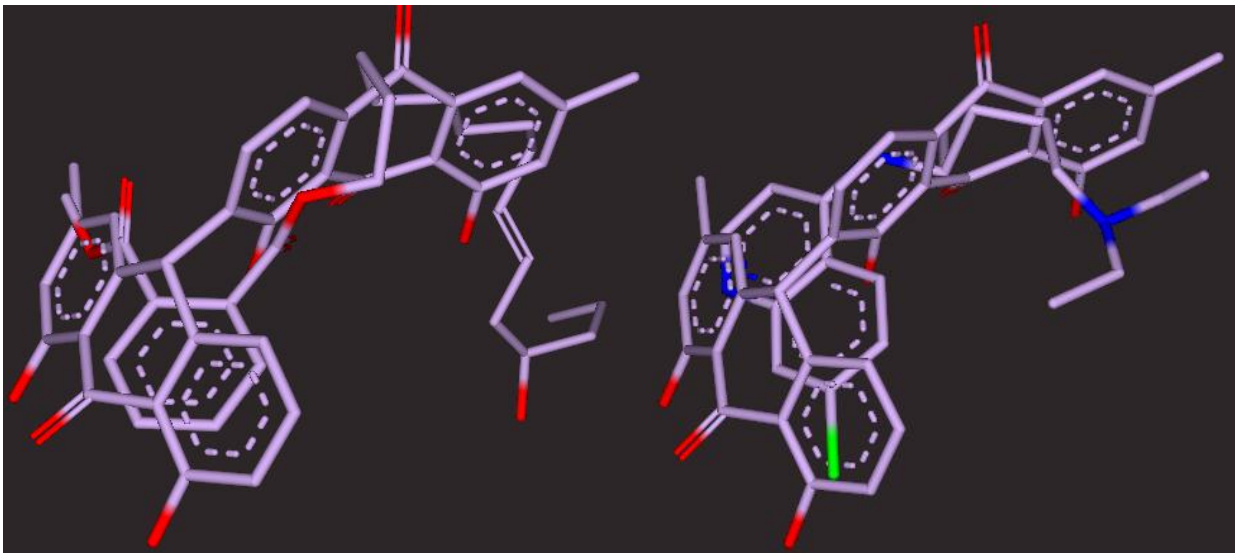

Figure VIi. A) Ribbon diagram of docked anthraquinone-pfLDH complex. Anthraquinone dimer is shown in ball-stick model. B) A close-up view of diagram A. C) Surface representation showing anthraquinone dimer in the binding site of pfLDH. Anthraquinone dimer is shown in ball-stick model. D) Surface representation showing anthraquinone dimer in the binding site of pfLDH with lipophilicity coloring. White representing hydrophobic pockets and blue representing hydrophilic pockets. Anthraquinone dimer is shown in ball-stick model. E) Binding interaction of anthraquinone dimer with amino acid residues of pfLDH. F) Hydrogen bond interaction of anthraquinone dimer with amino acid residues amino acid residue Tyr85, Gly99 and Thr97. G) Superimposition of anthraquinone dimer with knipholone in the binding site of pfLDH. H) Superimposition of anthraquinone dimer with KFP-5 in the binding site of pfLDH. I) Superimposition of anthraquinone dimer with chloroquine in the binding site of pfLDH.

Appendix VII: A paper published ftom this thesis

Yonatan Alebachew, Daniel Bisrat, Solomon Tadesse, Kaleab Asres. *In vivo* anti-malarial activity of the hydroalcoholic extract of rhizomes of *Kniphofia foliosa* and its constituents. Malaria Journal. 2021;20:3.